LIDAR DERIVED MODELS AND NDVI TRENDS INDICATE VEGETATION THRESHOLD RESPONSE TO HYDROCLIMATIC DRIVERS ACROSS THE PEACE ATHABASCA DELTA

FARNOOSH ASLAMI
Master of Science, University of Mohaghegh Ardabili, 2013

A thesis submitted
in partial fulfilment of the requirements for the degree of

MASTER OF SCIENCE

in

GEOGRAPHY

Department of Geography and Environment
University of Lethbridge
LETHBRIDGE, ALBERTA, CANADA

LIDAR DERIVED MODELS AND NDVI TRENDS INDICATE VEGETATION THRESHOLD RESPONSE TO HYDROCLIMATIC DRIVERS ACROSS THE PEACE ATHABASCA DELTA

FARNOOSH ASLAMI

Date of Defence: December 4, 2023

Dr. Christopher Hopkinson Supervisor	Professor	Ph.D.
Dr. Laura Chasmer Thesis Examination Committee Member	Associate Professor	Ph.D.
Dr. Daniel Peters Thesis Examination Committee Member, Environment and Climate Change Canada, University of Victoria	Research Scientist	Ph.D.
Dr. Craig Mahoney Thesis Examination Committee Member, Government of Alberta, Environment and Parks	Wetland Scientist	Ph.D.
Dr. Craig Coburn Chair, Thesis Examination Committee	Professor and Chair	Ph.D.

ABSTRACT

In northeastern Alberta, Canada, the Peace Athabasca Delta (PAD) is a Ramsar and UNESCO World Heritage-designated wetland complex vital for biodiversity and well-being of the Indigenous communities residing there. In this study, remote sensing techniques were used to understand the changes that have occurred within the PAD over the past four decades. Initially, lidar data was used to quantify vegetation height changes and better understand NDVI (Normalised Difference Vegetation Index) trends across lidar survey sample areas. These findings were then utilized to interpret Landsat-derived vegetation and surface water trends across the entire PAD. Between 1984 and 2022, NDVI trend analysis indicated greening along ecotones surrounding perched basins (shrubification), accompanied by noticeable drying patterns in the surface water trends. Further, a significant drying event spanning 1999 to 2003, appears to have been initiated by the strong 1998 El Niño event. The overall average greening rates pre and post 1999-2003 were 2.1 m/yr. and 3.1 m/yr., respectively. The severe drying during that short interval appears to have altered the rate and patter of vegetation processes across the delta post-2003. The more recent period of 2018 to 2022 was also notable for the observed high levels of inundation. If the PAD's open water and vegetation cover trends continue, surface moisture is generally expected to decrease, with commensurate increases in shrub cover. Meanwhile, certain areas like the southern region around Mamawi Lake, could become wetter due to localised changes in surface drainage. While flooding events are expected to continue to be a regular feature of this landscape, the extent to which the PAD can return to its historically large areas of persistent inundation remains uncertain.

ACKNOWLEDGMENTS

It is a pleasure to express my heartfelt thanks to my supervisor, Dr. Christopher Hopkinson, for his invaluable guidance and unwavering support throughout the challenging journey of my study. This path demanded that I step out of my comfort zone. Without Dr. Hopkinson's patience and instrumental mentorship, I would never have reached this pivotal moment of finalizing my MSc thesis. Thank you, Chris, I owe you a lot!

I extend my heartfelt appreciation to my committee member, Dr. Laura Chasmer, for her unwavering confidence in my abilities and work. Dr. Chasmer graciously shared her extensive knowledge of wetlands with me and patiently provided valuable assistance with my writing. Thank you, Laura, for your support and guidance.

I am also grateful to my committee members, Dr. Daniel Peters and Dr. Craig Mahoney, for their enthusiastic support and valuable insights throughout my MSc.

A very special round of appreciations go to my fantastic friends, and brilliant research collaborators, Ms. Danika King and Dr. Celeste Barnes. I have learned a lot from you both, and I am still learning. Thank you, Danika! Thank you, Celeste!

I would like to express my eternal love and gratitude to my family. My heartfelt thanks go to my dear younger brother, Ashkan, my younger sister, Faranak, my wonderful mother, Farah, and my caring father, Akbar.

Last but not least, I want to dedicate special appreciation to my amazing soul mate and best friend of 15 years, Reza. Throughout the challenging journey of immigration and the completion of this MSc, he has been my unwavering support, providing love, care, and encouragement. Thank you, the Marvelous Mr. Reza, for everything.

To the love of my life, Reza ...

TABLE OF CONTENTS

LIST OF TABLES

Chapter 1

Chapter 2

Chapter 3

LIST OF FIGURES

Chapter 1

Chapter 2

Chapter 3

LIST OF ABBREVIATIONS

ΔCHM	Canopy Height Model change
AVHRR	Advanced Very High Resolution Radiometer
CC	canopy cover
CHM	Canopy Height Model
DEM	Digital Elevation Model
DSM	Digital Surface Model
DUC	Ducks Unlimited Canada
ETM+	Enhanced Thematic Mapper Plus
L2	Level 2
LAI	Leaf Area Index
Lidar	Light detecting and ranging
MK	Mann-Kendall
MK Z	Mann-Kendall significance
MNDWI	Modified Normalized Difference Water Index
MODIS	Moderate Resolution Imaging Spectroradiometer
N	Sample size
NAD83	North American Datum of 1983
NDVI	The Normalized Difference Vegetation Index
NIR	Near Infrared
OLI	Operational Land Imager
OLS	Ordinary Least Square
PAD	Peace Athabasca Delta
PCT 90	90th percentile
RMSE	Root mean square error
Std	Standard Deviation
SWIR	Shortwave Infrared
TM	Thematic Mapper
TS	Theil-Sen
USGS	United States Geological Survey
VI	Vegetation Index
WRI	Water Ratios index

Chapter 1: Boreal Wetland Remote Sensing

1.1 Introduction

The global environment is undergoing unprecedented changes, with climate change and human activities exerting profound impacts on ecosystems worldwide (Leemans et al., 2009). One such region is the Peace Athabasca Delta (PAD), located in northern Alberta, Canada. The PAD is designated a wetland of international importance by the Ramsar and UNESCO World Heritage conventions, underscoring its ecological significance, unique role in providing habitat for diverse species, and contribution to the well-being of human communities (Ramsar Convention, 2016).

Numerous studies note the critical interplay between vegetation dynamics, climate change, and human-induced modifications to ecosystems (Field et al., 2014; Foley et al., 2005; Sala et al., 2000). The Intergovernmental Panel on Climate Change (IPCC) reports highlight the escalating threats posed by climate change, emphasizing the need for a comprehensive study into the impacts on biodiversity and ecosystems (Masson-Delmotte et al., 2021). In the context of the PAD, studying the connections between climate trends and ecosystem response is necessary as a first step in understanding its long-term fate.

Human activities, ranging from resource extraction to land use change, further amplify the challenge faced by dynamic ecosystems (Foley et al., 2005). In the PAD, a region acutely affected by upstream industrial developments (Kelly et al., 2010; Schindler & Donahue, 2006; Timoney, 2013), the study of vegetation trends becomes a linchpin in the broader effort to reconcile human needs with environmental sustainability. This research explores vegetation trends in the PAD using the advanced technologies of airborne lidar and the Landsat mission optical image archive to

contribute to both scientific understanding and policy decisions for preserving the unique ecological balance of the area.

1.1.1 Environmental Characteristics of the Peace Athabasca Delta (PAD)

The PAD covers a complex expanse of boreal forest, wetlands, and lakes (Prowse et al., 2006a; Schindler & Donahue, 2006; Timoney, 2013). The circumpolar Boreal biome, or taiga, is one of the most extensive and significant global biogeoclimatic regions. Encompassing a substantial expanse in North America and Eurasia, it features coniferous forests, woodlands, wetlands, and lakes (Brandt, 2009). Wetlands are areas where water is a defining factor, influencing soil saturation, vegetation and ecological processes (Mitsch & Gosselink, 2015), while lakes refer to open water bodies with a defined basin or depression. Lakes are generally larger bodies of water than wetlands, and they contain water year round (Warner & Rubec, 1997). The PAD is not merely a geographical entity but a dynamic and interconnected system of ecological processes that sustain an array of flora and fauna covering approximately 6,000 square kilometers (Timoney, 2013).

The environmental attributes of the PAD are intricately molded by the dynamic interplay of its hydrological patterns and diverse vegetation (Timoney, 2009). The delta experiences seasonal variations in water levels, influenced by factors such as snowmelt, precipitation, and upstream activities. These fluctuations create a mosaic of habitats, including marshes, shallow lakes, and riparian zones, fostering rich biodiversity and providing crucial breeding grounds for numerous species (Timoney, 2013).

1.1.2 Unique Challenges and Vulnerabilities

The PAD is not immune to the profound changes sweeping across the global environment. As global air temperatures rise and climate patterns shift, the PAD faces unprecedented challenges that threaten its delicate balance. One of the primary concerns is the alteration of hydrological

regimes, a consequence of climate change that directly impacts water levels and flow patterns within the delta (Prowse et al., 2006a).

The region is further impacted by upstream human activities, notably the expansive industrial extraction activities in Alberta's oil sands region (Timoney, 2009). The hydro-ecological balance of the PAD faces disruption due to changes in water quality, habitat fragmentation, and the introduction of pollutants linked to various human activities, including petroleum, forestry, and agricultural activities (Timoney, 2009). These alterations not only jeopardize the ecological equilibrium of the delta but also pose challenges to its overall biotic health and resilience as a complex interconnected system. Furthermore, river regulation and management practices play a crucial role in influencing the PAD's hydrological variations in space and time (Beltaos & Peters, 2023; Peters & Prowse, 2001; Timoney, 2021), thus potentially compounding or interacting with the threats posed by anthropogenic land use activities.

Climatic changes in the Boreal zone have resulted in changes to forest and wetland ecosystems, including transition to shrubs; tree mortality, etc. The transition from open/moss wetlands to shrubs can increase ecosystem productivity (Sim et al., 2019), however, this can also accelerate the transition to drier ecosystems (Lemay et al., 2018). These ecotonal changes underscore the complex interplay between climate variations and ecosystem responses, emphasizing the need for a nuanced understanding to inform effective conservation and management strategies. Ecotonal change refers to shifts or alterations in the transition zones between distinct ecological communities (Hupy & Yansa, 2009). Drivers of ecotonal change include shifts in climate patterns, habitat fragmentation, land-use changes, and alterations in ecological disturbance regimes. Climate change, in particular, can influence the geographic distribution of ecotones as air temperature and precipitation patterns shift (Evans & Brown, 2017;

Hupy & Yansa, 2009). Human activities such as urbanization, deforestation, and agricultural expansion can disrupt natural ecotones, leading to ecological shifts and changes in biodiversity (Goldblum & Rigg, 2010).

The ecotonal changes observed in Boreal ecosystems as a response to climatic shifts or human activities can exhibit varying patterns - either as permanent alterations or cyclical transformations (Valk, 2005). Some ecotonal changes may result in persistent shifts in vegetation and ecosystem composition, establishing a new equilibrium under the influence of evolving climatic conditions. In contrast, other changes may follow cyclical patterns, responding to periodic fluctuations in environmental factors (Valk, 2005). Understanding the dynamics of these changes, whether long-lasting or cyclical, is essential for predicting long-term ecological impacts and implementing adaptive conservation strategies.

The combined impact of climate change and human activities presents a complex set of challenges for the PAD, concurrently affecting the Indigenous community residing in Fort Chipewyan, who are intricately connected to the delta's flora and fauna, and for spiritual and cultural practices. The resulting changes impact the accessibility of local food sources, which are critical to the sustenance of Indigenous communities, and carry substantial social and economic repercussions for the entire region where communities exist and ecosystems provide important services (Chapin et al., 2004).

1.2 Literature Review

1.2.1 Boreal Wetlands

According to Mitsch and Gosselink (2015), the official definition of wetlands in Canada is: "Land that is saturated with water long enough to promote wetland or aquatic processes as indicated by poorly drained soils, hydrophytic vegetation and various kinds of biological activity

which are adapted to a wet environment." Canada possesses approximately 1.29 million square kilometers of wetlands, encompassing 13% of the country's land area, which is nearly a quarter of the global wetland reserves that remain today (Warner & Rubec, 1997). The vegetation within these wetlands includes various species of sedges, sphagnum mosses, and specialized wetland trees like black spruce and tamarack, providing essential habitats for numerous wildlife species (Smith et al., 2007).

Wetlands exhibit significant productivity and contribute to a wide array of ecosystem benefits. On a local level, wetlands offer provisions, including food and fiber, as well as serve as a natural filter for contaminants, sediment reservoirs, and a buffer against flooding. They also provide essential wildlife habitats, recreational spaces, and aesthetic value. At a larger scale, landscapes abundant with wetlands contribute to the regulation of regional climates and play a crucial role in providing habitat for migratory species, both within continents and across continents (Gallant, 2015). Additionally, Boreal wetlands play a pivotal role in the carbon cycle, functioning as significant carbon sinks within the Boreal landscape (Canadell et al., 2004).

The exploitation of resources like oil, gas, peat, minerals, hydropower, and trees has brought a variety of landscape changes in Boreal wetlands (Schindler & Donahue, 2006). Also, one of the highest warming rates is reported in this zone, heavily influencing Boreal wetlands (Bonsal & Kochtubajda, 2009). Climate change has exerted significant pressure on the hydrological and geomorphological aspects of Boreal ecosystems, leading to notable alterations. Wetlands are particularly sensitive as they exist between aquatic and terrestrial ecosystems and are therefore dependent on vertical and horizontal variations in groundwater table and surface water extent. In Boreal wetlands, and the PAD in particular, the formation, expansion, and melting of river ice are crucial phases in the hydrological cycle that can cause flooding (Beltaos et al., 2006). Flooding

plays a critical role in sustaining riparian ecosystems adjacent to rivers. It revitalizes early successional plant communities, fostering a diverse array of wildlife (Schindler & Smol, 2006). Additionally, snow accumulation plays a vital role in the hydro system of these areas (Newton et al., 2016). Declining snowpacks and earlier snowmelt in mountainous watersheds are reducing the average annual streamflow and causing earlier peak runoff during the year (Pi et al., 2021). Concurrently, permafrost thaw and seasonal freeze-thaw processes are altering the significance of surface and groundwater flows in these ecosystems (Chasmer & Hopkinson, 2017; Connon et al., 2014; Pi et al., 2021).

Boreal wetlands are shaped and sustained by relatively cool climates, where precipitation exceeds evapotranspiration most years (Chasmer et al., 2020a). Nonetheless, contemporary climate changes have the potential to drive these ecosystems towards heightened terrestrialization rates (Chasmer & Hopkinson, 2017). Wetland self-regulation is tightly interconnected with local hydro-climatology, particularly factors like precipitation, evapotranspiration, soil water storage, and groundwater recharge. Consequently, even slight alterations in water balance can yield substantial effects on wetlands, particularly in regions where potential evapotranspiration surpasses precipitation or during periods characterized by extended dry climatic cycles relative to wet ones (Mwale et al., 2009). All these changes have led to different phenology for plants (extended growing season), faster growth, and changes in vegetation forms (e.g. grassy tundra to shrublands or bigger and denser shrubs) in Boreal ecosystems, consequently affecting the regional climate, hydrology, and carbon cycle (Mekonnen et al., 2018; Myers-Smith & Hik, 2018).

1.2.2 Previous Studies on Vegetation Trends in the PAD and Boreal Landscapes

A comprehensive and up-to-date analysis of vegetation trends in the PAD is currently lacking. The earliest vegetation study using Landsat images over the PAD dates back to 1979 (Wickware

& Howarth, 1981; Wickware, 1979), which was a three-year change detection analysis to evaluate the capabilities of Landsat data in mapping the PAD's habitats. Later, Timoney (2006) used vintage air photos from 1927 to 2001 (not perfectly overlapped) to evaluate the ranges and types of land cover in the PAD and reported no unusual changes in post-Bennett Dam relative to pre-Bennett Dam changes. They mentioned that evaluating changes, both trends, and patterns, in this delta are scale-dependent. Timoney and Argus (2006) and Timoney (2008a) studied field transects in the PAD between 1993 and 2001 to find the temporal response of five common willow species to flooding and drying and the factors influencing the area. They reported that willow cover decreased as a result of flooding in the mid-to-late 1990s. The development of woody wetland communities, wildfires, and a general decline in the spatial coverage of open water and marsh areas are signs of a drying trend (Timoney, 2013). Continuing these trends may lead to the drying of isolated basins in the PAD and replace hydrophytic vegetation species with land species (such as grasses and willows) over time. Recently, Peters et al. (2020) used Sentinel 2B imagery acquired on 19 September 2019 and lidar in September 2013 to represent vegetation structure over the PAD. After employing cluster analysis (K-means), they grouped a few input variables into meaningful clusters to describe the vertical and horizontal structure of the ground features.

On the contrary, there are many research studies demonstrating how vegetation has been changing in similar ecosystems across Canada or similar landscapes. For example, Sánchez-Pinillos et al. (2022) analyzed data from 6876 permanent plots that were spread across most of the Canadian Boreal zone to evaluate how recurrent, low-intensity droughts impacted forest mortality. Their findings demonstrated that the frequent occurrence of low-intensity dry conditions had a more pronounced impact on forest mortality compared to the severity of the driest conditions within the plot. Conversely, in mixed forests containing broadleaf species, successive dry

conditions had a minimal impact on forest mortality (Sánchez-Pinillos et al., 2022). Mack et al. (2021) reported that severe fire-induced shifts in dominant plant species compensated for increased combustion of soil carbon over decades in Alaskan Boreal forests, transitioning tree dominance from slow-growing black spruce to fast-growing deciduous broadleaf trees.

Berner and Goetz (2022) also found that greening (increased spectral vegetation index) was more prevalent than browning (decreased spectral vegetation index) in the northern Eurasia and North America and was predominantly observed in cold sparsely treed regions with high soil nitrogen and moderate summer warming. Meanwhile, browning was more common in the warmest peripheries of the Boreal forest and major forest types (e.g., evergreen conifer forests), particularly in densely treed areas experiencing warmer and drier summers (Berner et al., 2020).

Given the diverse responses of species to climatic change, certain species are expected to increase in abundance while others will likely decrease. Consequently, ecosystems will undergo changes in their structural composition. Over time, certain species might be displaced to higher latitudes or elevations. Additionally, rare species characterized by small ranges may become susceptible to local or even global extinction (Melillo et al., 1990). An increase in shrub cover is anticipated to accelerate Arctic warming by reducing land surface albedo and increasing evapotranspiration (Fraser et al., 2014a). Taller shrubs effectively trap snow, resulting in increased winter ground temperatures, and nutrient mineralization, causing a positive feedback loop that encourages more shrub expansion. Herbivore populations may be affected by changes in plant composition caused by shrub shading (Fraser et al., 2014a).

Air temperature plays a key role in shaping species distribution worldwide, as it significantly influences the majority of biological processes (Dusenge et al., 2019). In response to rising air temperatures, photosynthesis and plant plus microbial respiration typically show an upward trend.

However, at elevated air temperatures, respiration often becomes the dominant process (Melillo et al., 1990). Consequently, climate change could conceivably trigger a phase of net carbon release from the land into the atmosphere. Enhanced soil water availability is expected to promote plant growth in arid ecosystems and increase carbon storage in cool and moist environments such as lowland tundra. On the other hand, water stress could become a leading factor in tree mortality (Melillo et al., 1990).

1.3 Research Methodology

1.3.1 The Study Area

In northeastern Alberta, Canada, the PAD is designated a wetland of international importance by the Ramsar and UNESCO World Heritage conventions, underscoring its ecological significance, unique role in providing habitat for diverse species, and contribution to the well-being of human communities (RamsarConvention, 2016). Today 80% of the PAD lies within the Wood Buffalo National Park (Figure 1.1). The residents in and around Fort Chipewyan, nestled on the northwest shore of Lake Athabasca, have historically relied on the lake and its tributaries for travel and sustenance through fishing, hunting, trapping, and gathering medicinal plants. The Hylton (2023) interview with local Indigenous community members revealed that they have witnessed the impact of warming winters, gradually eroding their ice roads and their solitary connection to the outside world. They have grappled with increasingly frequent and intense wildfires, with their village of Fort Chipewyan shrouded in smoke for weeks on end. Furthermore, they have experienced an unsettling decline in water levels and the deteriorating health of both their community and surrounding wildlife (Hylton, 2023). These adversities can be attributed to multiple human-induced factors: climate change, alterations to river flow regime due to damming, and notably, Fort Chipewyan's vulnerable position downstream of the Alberta oilsands.

The PAD is approximately half covered in water and is a dynamic mosaic of lakes, rivers, ponds, marshes, peatlands, meadows, and shrubby wetlands, as well as forests and dry grasslands in the higher ground (Timoney, 2013). Timoney (2013) approximately classified the delta into four zones of vegetation, including "Forest", "Thicket and Savannah", "Marsh and Meadow" and "Open Water" (aquatic), along an elevation and moisture gradient, starting with forests at the highest elevations and moving down to thickets and savannahs, marshes and meadows, and aquatic vegetation at the lowest elevations (Table 1.1).

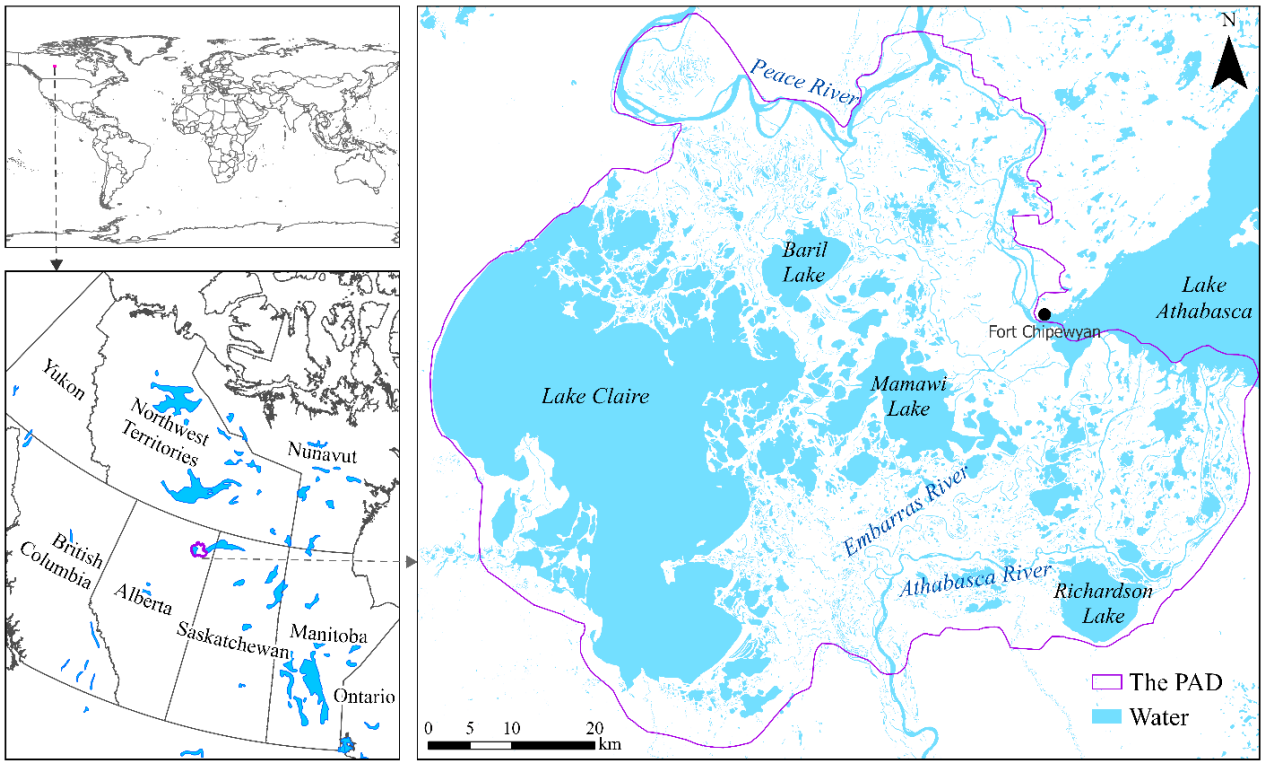

Figure 1.1. The Peace Athabasca Delta location (water maps from CanVec[1] , 2023).

[1] Topographic Data of Canada - CanVec Series - Open Government Portal

Table 1.1. Typical landforms in the delta [(Timoney, 2013), page 79].

Vegetation Class	Typical water Regime	Landforms	Typical Elevation (m asl)	Dominant Soil
Aquatic	Permanently flooded, >50 cm deep	Open and restricted basins and channels	<209	Rego Gleysol
Marsh and Meadow	Standing water ≥ 3 years in 10, <50 cm deep, water table at or above surface	Wetter restricted basins, shores of open-drainage basins, abandoned channels, lowest levees	209-210	Variety of Gleysols, Regosols
Savannah and Thicket	Standing water < 3 years in 10, <50 cm deep, water table at or below surface	Drier perched basins and plains, low to intermediate levees	210-212	Variety of Gleysols, Regosols
Forest	Rarely flooded (if so, duration < 1 week)	Terraces, highest levees	>212	Cumulic Regosol

Situated at the confluence of the Peace and Athabasca River Deltas, along with several smaller deltas at the western terminus of Lake Athabasca, the PAD ecosystem constitutes a complex deltaic formation (Timoney & Lee, 2016), including open, semi-restricted, and restricted based on their level of hydraulic connection with the primary flow system (Peters et al., 2021; Timoney, 2021). During periods of moderately high water, semi-restricted basins are intermittently or seasonally connected. Restricted basins often only receive river water replenishment during extremely high water levels. Such water levels in the PAD cannot be produced by open water (summer) floods; instead, ice jams on the Peace, Slave, or Athabasca Rivers and the resulting flooding are required to replenish these constrained basins (Timoney, 2013).

The PAD consistently receives substantial inflows of water and sediment from the Athabasca River. On occasion, during ice-jam floods and instances of extreme flow, it also receives water from the Peace River. Moreover, the presence of beaver dams, higher-than-usual precipitation, wind seiches, and the occurrence of spring and summer floods all contribute to the replenishment of water within the floodplain basins (Timoney, 2021).

The PAD has complex hydrology due to its low relief and distributary channels (Töyrä et al., 2003; Wolfe et al., 2006b), which are affected by climate change, flow regulation (W. A. C. Bennett dam on the Peace River), Oilsands developments, and land-use changes (Hall et al., 2012; Pietroniro et al., 2006; Prowse et al., 2006b). The northern section of the PAD, which is most connected to the Peace River, is the area where the drying of the PAD is the source of most concern. The most important anthropogenic development impacting the PAD was the construction of the W. A. C. Bennett dam (named after the former Premier of British Columbia (BC), William Andrew Cecil) on the Peace River, BC, in 1968. Site C of this project received approval from the Government of British Colombia in December 2014, and is planned to be online in 2024, with completion by 2025[1]. While the dam impacts downstream hydrology, Timoney (2021) showed that even though regulation has not changed the frequency or intensity of spring floods nor the recharging of perched basins, it has had a significant impact on the seasonal runoff distribution, which has reduced summertime flows on the Peace River. Regulation also has led to higher average river flows throughout the late fall and early winter freeze-up period (Lamontagne et al., 2021; Timoney, 2021).

Moreover, the industrial developments upstream of the delta, such as Alberta's oilsands (Hall et al., 2012) and the potential for contamination from polycyclic aromatic hydrocarbons (Kurek et al., 2013) create more environmental concerns. Just upstream of the PAD, in tributaries of the Lower Athabasca River, oil sands mining (open pit and in situ) is taking place. This causes landscape changes and requires the abstraction of small amounts of water from the mainstem for bitumen processing (Peters et al., 2021). Additionally, regional meteorological records indicate a

[1] Project Overview | Site C (sitecproject.com)

definite warming trend from the 1900s to the present century, however, there is no discernible upward or downward trend in precipitation data (Timoney, 2013).

1.3.2 Remote Sensing

Conventional mapping methods involve extensive on-site data collection and can be expensive and time-consuming, especially when dealing with remote or inaccessible locations (Chasmer et al., 2020b). Traditional mapping methods face challenges in Boreal wetland regions due to their remote and inaccessible nature, dense vegetation, seasonal variability, hydrological dynamics, scale considerations, and the need for accurate integration of diverse datasets (Chasmer et al., 2020b).

As an alternative, remote sensing technologies provide a means for monitoring of the Earth's surface, which enables comprehensive mapping of wetland and forest areas, as well as their ecotone transitions in space and time (Chasmer et al., 2020b). It involves the use of sensors, typically mounted on satellites, aircraft, or drones, to capture data about the Earth's surface and atmosphere. Remote sensing enables the acquisition of various types of information, including imagery, temperature, and spectral data (Campbell & Wynne, 2011).

The sensors onboard these platforms capture electromagnetic radiation, such as visible light, infrared, or microwaves, emitted or reflected by the Earth's surface. This data is then processed to generate valuable information about the target area. Remote sensing techniques are pivotal for Earth observation, with passive and active methods offering distinct advantages and drawbacks. Passive sensors can be cost-effective and provide a wide range of imaging options across the electromagnetic spectrum but due to the need for an external light or energy source (i.e. the sun in the case of passive multispectral sensing), physical obstructions and shadows (e.g. due to vegetation canopies or clouds), and imaging at night pose major constraints. Active sensors

generate their own source of illumination, so can avoid some of the operational or occlusion-based limits of passive sensors, though they can be more complex and costly due to the need to transmit powerful signals. The choice depends on specific application needs, considering factors such as cost, environmental conditions, and the desired level of spectral or geometric information. The integration of active and passive imaging offers a comprehensive approach to Earth observation (Campbell & Wynne, 2011).

Building upon the capabilities of passive remote sensing, specialized programs like NASA's Landsat enhance our ability to glean precise and detailed information about the Earth's surface. The multi-platform and -sensor Landsat mission has provided a comprehensive archive of satellite imagery since its launch in the early 1970s (USGS, 2021). This long-standing mission contributes invaluable data for applications ranging from environmental monitoring to land use planning.

On the other hand, lidar, which stands for Light Detection and Ranging, an active remote sensing system, represents a modern technology that utilizes laser light to measure distances with high accuracy. Lidar systems, which can be mounted on drones, aircraft, or satellites, emit laser pulses towards the target of interest and capture the reflected signals. This technology provides high-resolution three-dimensional structural data, often in point cloud form, and over recent decades has revolutionised terrain mapping, forestry assessments, and urban planning (Wehr & Lohr, 1999).

1.3.2.1 Landsat Imagery and Trend Analysis

The initiation of the United States Geological Survey (USGS) repository of Landsat imagery granted unrestricted access to high-quality, ready-to-analyze imagery with exceptional spectral and geometric precision (Hermosilla et al., 2018). This database offers a suitable spatial and temporal

resolution for the portrayal of natural as well as human-induced alterations in terrestrial landscapes (Griffiths et al., 2013; Roy et al., 2016; White et al., 2015).

The Landsat program, initiated by the United States Geological Survey (USGS) and NASA, has been a cornerstone in Earth observation since its inception. It comprises a series of Earth-observing satellites equipped with advanced sensors, contributing to a wealth of global data that spans several decades. Landsat sensors capture data in various spectral bands, including visible, near-infrared, and thermal infrared, enabling detailed analysis of land cover, vegetation health, and surface temperature. The evolution of sensors, from the Thematic Mapper (TM) to the Enhanced Thematic Mapper Plus (ETM+) and the latest Operational Land Imager (OLI) and Thermal Infrared Sensor (TIRS) on Landsat 8, has expanded the spectral range and improved the spatial and radiometric capabilities.

Multi-spectral remotely sensed image stacks of images are the most common approaches for detecting changes (Fraser et al., 2014b). Vegetation index (VI) trend analysis is one of the most common approaches in assessing changes and trends through time. A VI, which is produced from the spectral transformation and or ratio of two or more bands of satellite data sensitive to plant biomass and vigor, is a measure of the relative density and health condition (greenness) of the vegetation. The Normalized Difference Vegetation Index (NDVI), the most commonly used VI, can be derived from most multi-spectral sensors (Tucker, 1979). A positive trend in NDVI over timed (also frequently referred to as "greening") can denote an increase in vegetation height, leaf cover, biomass, or abundance in total vegetation growth, whereas a negative trend in NDVI over time (also known as "browning") is typically interpreted as decreased quantities of vegetation or growth rate (Kumar et al., 2022; Myers-Smith et al., 2020; Pan et al., 2018). There is much research linking NDVI to vegetation productivity in the Boreal ecosystems (Hope et al., 1993; Olthof et al.,

2008; Raynolds et al., 2012; Riedel et al., 2005). There are many studies that have attributed apparent greening and browning to environmental drivers and processes, particularly warming trends (Myers-Smith et al., 2020; Wang & Friedl, 2019).

As wetlands are characterized by their dynamic hydrological processes and significant fluctuations in water availability (Valk, 2005), monitoring changes in water bodies is essential for understanding their ecological dynamics. Numerous sophisticated remote sensing spectral indices are available for mapping and monitoring water and moisture content (see the review in Bijeesh and Narasimhamurthy (2020)). The effectiveness of these indices varied depending on the specific scene, sensor, and prevailing climatic conditions (Bijeesh & Narasimhamurthy, 2020). The Modified Normalized Difference Water Index (MNDWI) is a common spectral index to detect and map water and its change (Xu, 2006). However, the spectral indices might be ineffective when turbid water pixels are present in the image. In such cases, the classification of a pixel as a non-water pixel may occur even when it is actually a water pixel (Guo et al., 2017). In these cases, more sophisticated techniques to assess water quality may be required (see the review by Chawla et al. (2020)).

NDVI and MNDWI trend analysis relies on high-quality data, which necessitates that the primary imagery should be free of noise, saturation, clouds, and shadows. In many Boreal environments, obtaining a cloud-free time series of multi-spectral images like Landsat can be challenging. However, image compositing has demonstrated its advantages as a technique for reducing data volume, especially when dealing with dense coarse and medium spatial image time series (Flood, 2013; Robinson et al., 2017). It enables the creation of the highest-quality observations with little to no cloud or cloud shadows. There are several approaches for creating a composite, including Mean (Robinson et al., 2017), Focal Mean or Median (Gumma et al., 2020;

Oliphant et al., 2019; Teluguntla et al., 2018), Medoid (Flood, 2013), Maximum NDVI (Ruefenacht, 2016), and Score System for Best Available Pixel (Griffiths et al., 2013; White et al., 2014). A detailed explanation of each of the mentioned methods can be found in Chapter 2. Qiu et al. (2023) indicate that each composite algorithm possesses unique characteristics, and no single algorithm can surpass all others in terms of performance across all locations and composite periods. Therefore, the most appropriate best available pixel compositing algorithm is likely somewhat location- and application-dependent, thus requiring some initial investigative work to choose the approach most suited to the study.

This study utilizes Landsat imagery spanning from 1984 to 2022 to conduct a comprehensive trend analysis of vegetation across the PAD. Detailed information on the data, processing methods, and outcomes is provided in Chapters 2 and 3.

1.3.2.2 Lidar and Canopy Changes

Unlike passive remote sensing, lidar uses an active satellite/airborne/in-situ sensor, to collect vegetation, topographic, and sometimes bathymetric information. Lidar measures distances by calculating the time between transmitting and receiving laser signals (Hopkinson et al., 2004). Using either or both discrete return and full waveform laser scanners (Figure 1.2) (Salas, 2021), typical lidar mapping systems emit pulses of energy to determine distances based on the round trip travel time between emitted and reflected signal amplitudes (Dong & Chen, 2017; Hopkinson et al., 2001; Lefsky et al., 2002; Wehr & Lohr, 1999).

Discrete return lidar provides a point cloud with discrete position and elevation coordinate values, whereas full waveform lidar captures the full signal response, offering a more detailed representation of the environment. However, processing full waveform lidar data can be more

computationally intensive due to the continuous nature of the waveform, while discrete return lidar data is generally simpler to process (Dassot et al., 2011).

As an active sensor technology, lidar offers the advantage of being able to collect data during both daytime and nighttime, as it is not reliant on passive solar illumination. However, as it relies on laser light within or close to the visible spectrum, ranging performance can be compromised by atmospheric effects such as heavy fog, smoke, or excessive moisture like rain, snow, and clouds obstructing the path between the laser system and the object. Lidar's unique ability to send small laser pulses through canopy gaps allows it to accurately sample canopy structure and terrain surface elevation along the path of the laser pulse (Wehr & Lohr, 1999).

Common lidar systems emit laser pulses in Near Infrared (NIR) (1064 nm) or Shortwave Infrared (SWIR) (1550nm) for topographic mapping (Baltsavias, 1999). For bathymetric mapping, blue-green lasers (532 nm) are used due to enhanced water penetration (Wehr & Lohr, 1999). When the laser pulse from a multi-return system interacts with a tree canopy, the first return is generally assumed to originate from the top of the tree or the point where the emitted laser pulse first encounters the tree canopy. The last return may interact with the ground beneath the tree, though the ability to map the ground is largely contingent on the density of the vegetated canopy. Intermediate returns, such as the second, third, or fourth returns, are likely caused by tree branches and understory vegetation positioned between the top of the canopy and the ground (Li et al., 2021b).

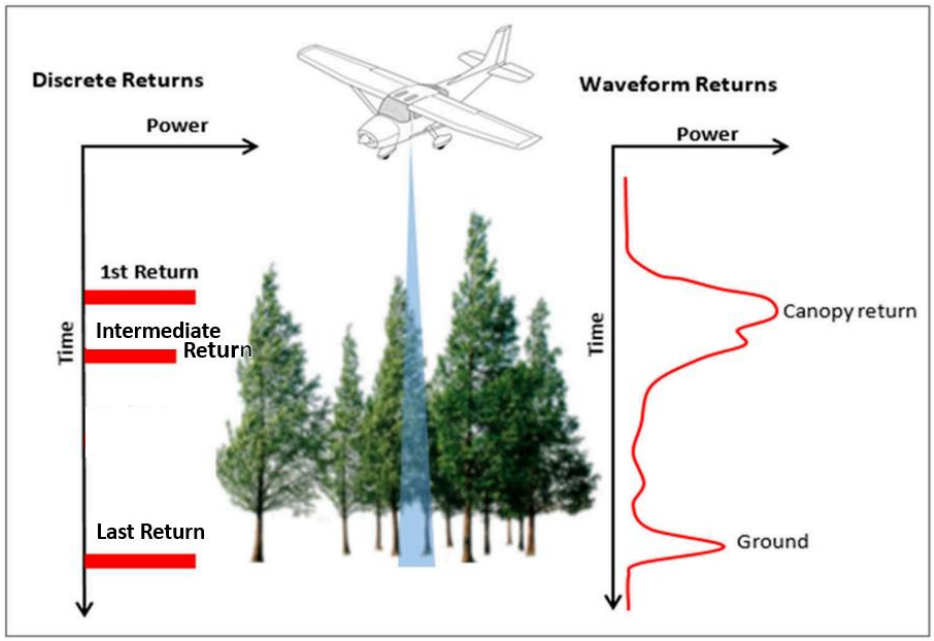

Figure 1.2. Discrete vs waveform returns in lidar (adapted from Salas (2021)). Early discrete lidar systems struggled with data sampling density, high costs, and a need to choose between first or last return logic. Circa 1999-2000, commercial systems introduced multiple returns per emitted pulse, providing both canopy and terrain surface information. Discrete return systems can potentially slightly bias canopy heights if crown apices are missed or if the upper foliage area presents a small target area (Hopkinson, 2007). On the other hand, lidar return signal waveforms can provide a more detailed representation of forest canopy structure throughout the full vertical profile.

A compilation of these discrete return lidar points is referred to as a lidar point cloud (Figure 1.3). Lidar point cloud data can also undergo a process of point-level "classification." This involves labeling each point based on the type of object it reflected off. For instance, if a pulse reflects off a tree branch, it might be categorized as "vegetation." Similarly, if the pulse reflects off the ground, it can be classified as "ground." Classifying lidar point clouds involves an additional processing step. Utilizing all data or both classes of "ground" and "vegetation," we can generate a Digital Surface Model (DSM) of the local upper surface. The "ground" class provides the basis for creating a Digital Elevation Model (DEM) of the terrain. By subtracting the DEM from the DSM in a vegetated area, we can produce a Canopy Height Model (CHM), which describes the spatial

variation in vegetation heights. When multiple lidar datasets are recorded at different points in time, these datasets can be utilized for time-series change analysis, enabling the detection of changes that have occurred over the observed period. However, when employing two distinct lidar technologies from different time periods for change detection, it is advisable to account for variations in sample density and sensor variations, which can necessitate adjustments to ensure accurate and reliable comparative analyses (Hopkinson et al., 2016).

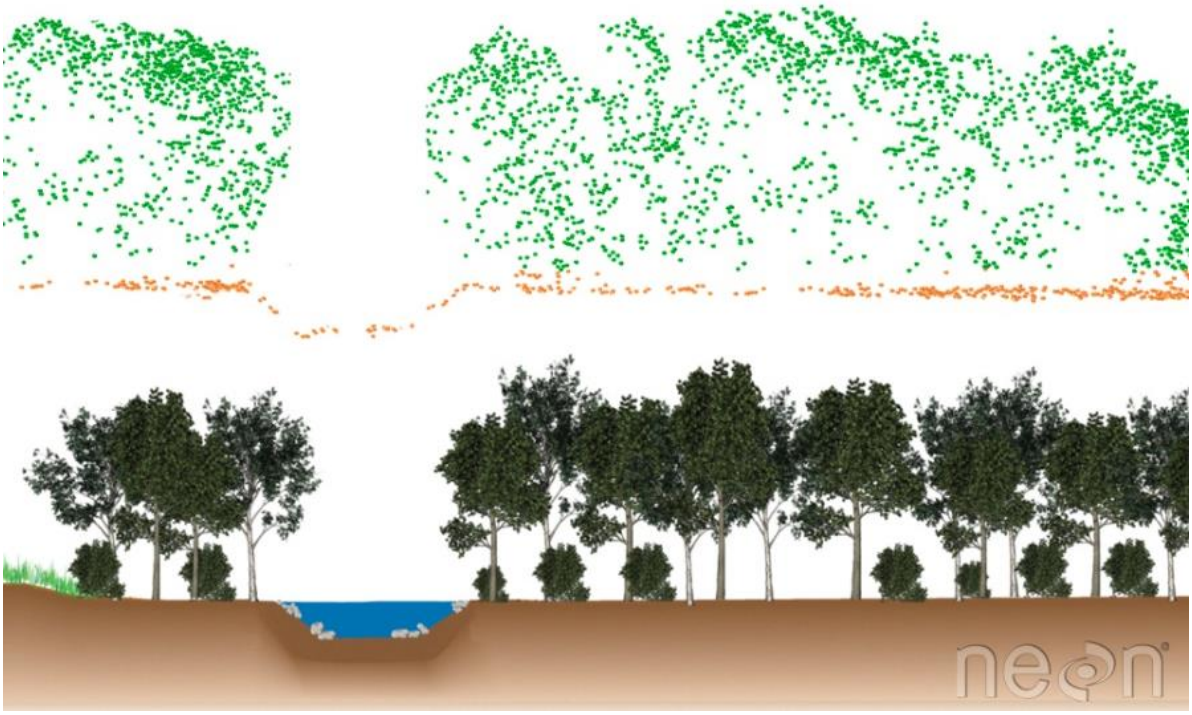

Figure 1.3. Cross-section displaying lidar point cloud data (above) and the corresponding landscape profile (below). Graphic credit: Leah A. Wasser[1].

Lidar is gaining popularity for a range of bio-geophysical applications, such as wetland ecosystems (Chasmer et al., 2020b; Lang & McCarty, 2009; Luo et al., 2015) or water surface mapping (Hopkinson et al., 2011; Huang et al., 2014; Lang et al., 2012). This technology enables

[1] https://www.earthdatascience.org/courses/use-data-open-source-python/data-stories/what-is-lidar-data/

researchers to assess various parameters such as canopy height, vertical structure, Leaf Area Index (LAI), and biomass, which are critical for understanding ecosystem health and dynamics (Chasmer et al., 2016; He et al., 2013; Hopkinson & Chasmer, 2009; Wang & Fang, 2020). In this study, we utilized lidar survey data from overlapping areas in 2000, 2016, and 2018. Comprehensive details of the data collection, processing, and analysis are presented in Chapter 2.

1.4 Knowledge Gaps and Research Objectives

Vegetation changes and trends in space and time provide indicators of broader hydro-ecological health and function within wetland systems. A search of recent literature into the vegetation dynamics of the PAD reveals that limited field observation ground truth data has been collected and no comprehensive spatially extensive multi-decadal vegetation trend analysis has been performed across the whole PAD. Therefore, the over-arching goal of this research is to quantify the range, direction, and mechanism of vegetation changes in the PAD using remote sensing technology.

The first purpose of this research is to improve our understanding of 18 years of Landsat-derived NDVI variations in greening and browning through the utilization of 3 overlapping lidar data sampling campaigns (2000 and 2016/2018). In Chapter 2, lidar data are used to explore the links between spectral information derived from Landsat to variations in canopy height and cover. The objective is to gain a deeper comprehension of the factors influencing the spatial and temporal fluctuations in NDVI within Boreal wetland ecosystems and land cover types. Analyzing the response of lidar CHM change and correlating it with NDVI trends enables us to derive more insightful conclusions from the NDVI trends. We investigate the presence of any pixel-level relationships or correlations between the two datasets, as well as any correspondence in spatial patterns of change along ecotones between land cover types.

Higher positive NDVI values have been long interpreted as healthy vegetation, but it is unknown how different types of vegetation cover (willows, bushes, forest, etc.), particularly across a wetland with variable soil and vegetation characteristics, are represented in NDVI values. In this chapter, one hypothesis tested is that there has been a significant greening trend due to an expansion of shrub and tree growth over the PAD between 2000 and 2018. Although a total correspondence between NDVI greening/browning trends and bitemporal CHM increases/decreases is not expected, establishing where and under what conditions CHM and NDVI patterns coincide or differ will provide insights into the driving mechanisms that underlie changes in NDVI within complex boreal wetland landscapes.

Upon acquiring a better understanding of the processes underlying NDVI trends across lidar-sampled regions of the PAD, the next goal (Chapter 3) is to examine the spatially continuous trends in vegetation and surface water across the entire PAD from 1984 to 2022. A thorough trend and time series analysis of the NDVI and MNDWI is conducted, and the patterns are stratified into discrete time periods and by landcover, to better understand the interactions and any feedbacks between vegetation, surface water and external climatological drivers.

1.5 Significance of Research and Outcomes

This study aims to enhance our understanding of environmental changes and drivers within the PAD. By scrutinizing key aspects of the region's hydro-ecology, such as vegetation trends and hydrological patterns, the research aims to reveal connections between climate, hydrology, and landcover response. Through this understanding, the study endeavors to contribute valuable insights into the complex dynamics shaping the PAD's ecosystem and potential future trajectory. The identification of trends and potential drivers of change can support more informed and targeted environmental management strategies.

In addition, a better understanding of the vegetation structural influences on NDVI trends within different wetland landcover types has value well beyond the PAD. Given landscape change is pervasive across many remote regions of the world, and in northern to Arctic environments in particular, a better understanding of NDVI (and similar indices) is crucial in interpreting the underlying processes and rates of change across these dynamic regions.

1.6 Thesis Structure

This introductory chapter established the context, significance, and objectives of the study based on a literature review of existing knowledge on Boreal ecosystems, the PAD, previous studies on vegetation trends in the Boreal ecosystems and relevant remote sensing topics. The major objectives and outcomes of the study are presented in journal paper formats, in chapters 2 and 3. The concluding chapter, chapter 4, summarizes key contributions, outlines implications for environmental sustainability, and suggests avenues for future research.

Chapter 2: Comparing Satellite NDVI and Bi-Temporal Airborne Lidar Canopy Height to Examine Boreal Wetland Vegetation Changes Within the Peace Athabasca Delta

Abstract

In northeastern Alberta, Canada, the Peace Athabasca Delta (PAD) is a wetland complex designated by the Ramsar and UNESCO World Heritage conventions as a wetland area of global importance. A range of hydro-climatic drivers and land surface ecosystem changes over the PAD during the past century have been reported by indigenous communities residing in the delta and researchers. To enhance our understanding of the PAD's evolving landscape, we used lidar data to better interpret the Landsat-derived NDVI and MNDWI trends from 2000 to 2018. Comparing lidar-derived canopy models with NDVIs showed a moderate correlation across some landcovers, including shrub swamps ($R^2 = 0.46$). The results from the lidar analysis reveal an overall growth of vegetation taller than 1 m, resulting in increased canopy heights across lidar surveyed areas. Despite this finding, ecotonal vegetation expansion into wetlands in the survey areas was constrained to marsh riparian areas and river banks/levees coordinated with what we observed in Landsat-derived NDVI. The 11% of the survey area showed ecotonal expansion which around 5% of this area observed over shrub swamps and 1% over hardwood swamps. These changes are indicative of patterns of shrubification due to the drying of wetlands in the PAD during the study period. We also studied the drying trend on shallow open water using the MNDWI trends. We observed the disappearance of some ponds after 2000 and the shrinkage of many more small shallow open water surfaces during the study period. Although NDVI trends also showed generally the same greening patterns as ecotonal expansion, in most cases, NDVI trends illustrated larger areas of greening than was evidenced by ecotonal canopy advance using lidar. However, for the

areas sampled, both CHM and NDVI change methods produced similar estimates of vegetated ecotone expansion of ~3.1 m/yr. and ~2.4 m/yr., respectively.

Keywords Lidar, Peace Athabasca Delta, Landsat, Canopy, Trend Analysis, Image Composite

2.1 Introduction

Wetlands cover 13% of Canada, 1.29 million km^2, representing nearly a quarter of the world's total wetlands (Canadian Environmental Sustainability Indicators, 2016). Despite providing vital ecosystem services like carbon storage, flood suppression, water quality improvement, and habitat support, wetland areas have decreased due to human activities such as agriculture, urban development, and resource extraction (Chae et al., 2015; Chasmer et al., 2020a; Davidson, 2014; Hu et al., 2017). Boreal wetlands, characterized by cold climates and typically associated with boreal forests, are prevalent in northern regions of Canada. Climate changes and intensified land use have altered plant phenology, growth rates, and vegetation forms, such as the expansion of shrubs in boreal ecosystems (Abib et al., 2019; Kompanizare et al., 2018; Mekonnen et al., 2018; Myers-Smith & Hik, 2018; Rooney et al., 2012). This shift impacts water and carbon cycles and accelerates warming by reducing land surface albedo, increasing evapotranspiration (Chapin et al., 2005), and trapping snow (Connon et al., 2021), resulting in positive feedbacks that encourage further shrub expansion.

Mapping boreal wetlands is crucial to understand their dynamics. Remote sensing is necessary for large-scale mapping, as it offers the precision and efficiency required to capture the complexity of these ecosystems, surpassing the limitations of traditional methods in handling extensive spatial coverage and dynamic changes. The use of these technologies provides evidence for changes in the area and extent of different land cover types (Fraser et al., 2011; Fraser et al., 2014a), as well as trend analysis using vegetation indices to evaluate gradual or abrupt changes and trajectories

through time (Wulder et al., 2018). There is an extensive body of literature that compares the passive optical Normalized Difference Vegetation Index (NDVI) (Tucker, 1979) to biomass and vegetation productivity across northern regions (Hope et al., 1993; Olthof et al., 2008; Raynolds et al., 2012; Riedel et al., 2005) and globally (Eastman et al., 2013; Ichii et al., 2002; Liu et al., 2015).

Olthof et al. (2008) reported increasing Landsat and Advanced Very High-Resolution Radiometer (AVHRR)-derived NDVI trends, commonly referred to as 'greening' because vegetation appears to be more productive with increasing positive NDVI trends, in Yukon and Quebec, which were attributed to shrubification and vascular plant growth. A similar significant greening trend (85% of land surface) over the western Canadian Arctic between 1984 and 2011 in the majority of vegetation types (Fraser et al., 2014b). Fraser et al. (2011) also found a consistent trend of positive NDVI increase in four national parks in Canada (Wapusk, Ivvavik, Torngat Mountains, and Sirmilik), associated with warming air temperature. Here shrub and herbaceous vegetation replaced bare/unvegetated land surfaces.

Ju and Masek (2016) showed notable greening in the tundra of western Alaska, the north coast of Canada, Quebec, and Labrador, but reported 'browning' (negative NDVI trend) in the boreal forest of eastern Alaska. A similar NDVI browning trend over floodplains, lowlands, and uplands in Alaska between 1986-2009 was reported by Baird et al. (2012), who also concluded that only recently burned areas experienced significant positive trends in mean NDVI, whereas wetlands showed no discernible trend. McManus et al. (2012) found that different vegetation types did not exhibit comparable greening patterns, suggesting that forested areas were less likely to demonstrate significant NDVI trends, while graminoid tundra and low shrub contributed most significantly to observed greening trends.

Determining trends in vegetation NDVI over time requires high quality data with little influence from extraneous influences, such as haze, which could appear to be vegetation changes when they are not. For some areas, such as the Peace Athabasca Delta (PAD) wetland complex, clouds are commonplace, so acquiring a cloud-free multi-year time-series of optical image coverage is difficult. However, such challenges can be addressed using image compositing techniques that reduce time-series data volumes to create the best available observation with no or minimum cloud and cloud shadows for a desired temporal increment (White et al., 2014). To implement this, one point can be chosen within a collection of points in n-dimensional space, to represent the pixel group. In the case of Landsat images, the points represent different observations of a given pixel on different dates, and the n dimensions are the different spectral bands of the image. In the compositing approach, a single date is chosen per pixel for the final composite. The pixel spectral values for that date represent the season or year of interest (Flood, 2013). There are several approaches for creating a composite NDVI, including Mean (Robinson et al., 2017), Focal Mean or Median (Gumma et al., 2020; Oliphant et al., 2019; Teluguntla et al., 2018), Medoid (Flood, 2013), Maximum (Ruefenacht, 2016), and the Score System for Best Available Pixel (Griffiths et al., 2013; White et al., 2014).

Robinson et al. (2017) used the mean pixel approach to create a time series NDVI for the United States. However, Flood (2013) suggested that simple approaches such as the mean of all observations are likely not ideal due to outliers from atmospheric effects and bi-directional reflectance distribution function adjustments, as well as imperfections in cloud/shadow masking procedures. The univariate median represents a potential improvement over the mean due to its resistance to outliers (Oliphant et al., 2019; Ruefenacht, 2016). The Medoid approach, which selects the point that minimizes the sum of the distances to all other points, has the outlier

resistance characteristics of the univariate median and can be applied to multi-variate data such as reflective bands of Landsat (Flood, 2013). In the Maximum NDVI method, the maximum NDVI for all scenes is determined and then the pixel with all its bands from the corresponding scene is included in the final composite (Ruefenacht, 2016). Flood (2013) suggests that using the maximum NDVI provides a time-series that favours vegetation conditions with high greenness, and this might not be appropriate for all applications; e.g. this approach has the potential to reduce the contrast between trees and grasslands. However, several studies have successfully used this approach (Erasmi et al., 2021; Huang et al., 2017; Xu, 2021; Yang et al., 2019). Another approach uses a score-based system of four scores for each pixel, including sensor score, day-of-year score, cloud/cloud shadow or distance to cloud score, and opacity score (Griffiths et al., 2013). The total scores for each pixel are summed, and the image composite chooses the pixel with the highest score (White et al., 2014). To the best of the authors' knowledge, the only studies that have thus far compared the relative performance of the above-noted approaches are (Ruefenacht, 2016) and (Qiu et al., 2023). Qiu et al. (2023) indicate that each composite algorithm possesses unique characteristics, and no single algorithm can surpass all others in terms of performance across all locations and composite periods. Therefore, the most appropriate best available pixel compositing algorithm is likely somewhat location- and application-dependent, thus requiring some initial investigative work to choose the approach most suited to the study.

The earliest vegetation change detection and habitat mapping study using Landsat imagery over the PAD was carried out in the 1970s (Wickware & Howarth, 1981; Wickware, 1979). Later, Timoney (2006) used vintage air photos from 1927 to 2001 to evaluate the ranges and types of land cover in the PAD, reporting no unusual changes that could be associated with the operations of the Bennett Dam. Timoney and Argus (2006) and Timoney (2008a) studied field transects in the

PAD between 1993 and 2001 to examine the temporal response of five common willow species to flooding and drying. They reported that willow cover decreased as a result of flooding in the mid-to-late 1990s. Recently, Peters et al. (2020) used Sentinel2B imagery acquired on 19 September 2019 and lidar data acquired in September 2013 to represent vegetation structure over the PAD. After employing cluster analysis (K-means), they grouped input variables into meaningful clusters to describe the vertical and horizontal structure of the ground features. Timoney (2013) found increases in woody wetland communities, wildfires, and decreases in the overall open water and marsh areas representing evidence of a drying trend. However, Timoney (2021) emphasized that the ecological impacts of all mentioned components have remained poorly documented.

Given the range of hydro-climatic and anthropogenic factors influencing the PAD region and upstream hydrology, there is an over-arching need to quantify the spatial variation and trajectory of vegetation changes, to better understand the cumulative effects of these changes. However, due to limited field observation data, no comprehensive or spatially continuous vegetation trend analyses have been completed over the PAD. This is important because it provides valuable insights into the ecological health and resilience of this critical ecosystem.

The Landsat image archive from 1984 onwards offers an opportunity to assess vegetation distributions and trends but a lack of spatial or temporal representation of ground truth data limits what is achievable with confidence. Consequently, this study aims to explore the use of bitemporal lidar (2000 and 2016/2018) across sample areas within the PAD as an aid to interpreting vascular vegetation changes that are evident within the Landsat NDVI record over the same period.

High positive NDVI values are generally interpreted as healthy vegetation (Martinez & Labib, 2023; Morawitz et al., 2006). However, it is unknown how or if NDVI values and NDVI trends consistently represent changes in biomass or growth conditions across distinct boreal wetland

landcovers (e.g. marshes, shrubs, forests). Understanding NDVI and its correlation (or not) with vegetation height for wetland land cover classes in the PAD will help in interpreting NDVI and NDVI trends across the deltaic wetland environment and other similar northern landscapes.

Lidar data characterizes three-dimensional terrain and vegetation structure and has become a popular tool for forest, wetland, and riparian vegetation studies (Bolton et al., 2018; Chasmer et al., 2020b; Hopkinson et al., 2004; Montgomery et al., 2019). In this study, lidar canopy height and height/cover change data will assist in interpreting observed NDVI and NDVI trends across different PAD landcover classes. Given that NDVI is an index of green leafy foliage cover, and canopy height is an index of biomass, an initial expectation is that for some landcovers, there will be a positive correlation between Landsat-derived NDVI and the lidar-derived Canopy Height Model (CHM). However, as foliage cover and vegetation height are not the same quantity, correlations between these variables (or their changes/trends) are expected to vary with vegetation structural attributes (Zhou & Yin, 2014). While it is not anticipated that the NDVI greening or browning trends will perfectly align with the increasing or decreasing trends in lidar-derived products, examining areas where CHM and NDVI patterns converge or diverge will offer valuable insights into dynamic vegetation patterns and the driving forces behind them. This comparative analysis of changes in both datasets will contribute to the characterization of NDVI in relation to bitemporal CHM fluctuations. Hence, the primary aim of this study is to determine how and where NDVI corresponds to canopy heights, as well as how alterations in canopy height manifest in NDVI trends. The first hypothesis is that there is some relationship between NDVI and CHM that varies with landcover classes. The second hypothesis is to observe a significant greening trend associated with shrub and taller canopy expansion over the PAD between 2000 and 2018.

2.2 Study Area

In northeastern Alberta, Canada, the PAD is a wetland complex that has been designated by the Ramsar and UNESCO World Heritage conventions as a wetland area of global importance due to its status as one of the largest freshwater deltas globally, its biological diversity, and the presence of a thriving wild bison population. About 80% of the PAD lies within the Wood Buffalo National Park. Aside from riverine and groundwater exchanges, the PAD wetland areas gain water largely from overbank flooding during spring ice jams and precipitation, while losing water largely through evapotranspiration (Timoney, 2013). Examination of hydroclimatic data indicates an increase in air temperature over recent decades, while no significant alteration was observed in precipitation levels during the latter part of the 20th century (Peters et al., 2006a). The development of woody wetland communities and a general decline in the spatial coverage of open water and marsh areas, combined with recent wildfires are considered to be indicative of a drying trend (Timoney, 2013).

The location and boundary of the PAD are shown in Figure 2.1a. Of all Alberta's natural subregions, the delta has the lowest elevation and lowest relief. It is located within a wide topographical lowland that is surrounded by rocky outcrops from the Precambrian Shield. Local relief on the deltaic and alluvial plains is approximately 11 m, from 209 m asl on the plain to 220 m asl on high terraces of the Peace and Athabasca Rivers (Timoney, 2013). Because of the low relief and abundance of tall willow spp. shrubs and various species of trees, visibility at ground-level can be limited. Landforms across the PAD include active deltas, distributary channels, and levees, lakes, ponds, and mudflats. There are also non-deltaic landforms, covering <10% of the area. These include bedrock outcrops, raised beaches, eolian features, peatlands, and alluvial terraces (Timoney, 2013). According to Ducks Unlimited Canada (2020) landcover classification,

the majority of the survey areas are comprised of shrub swamps, emergent marshes, and meadow marshes (Figure 2.1).

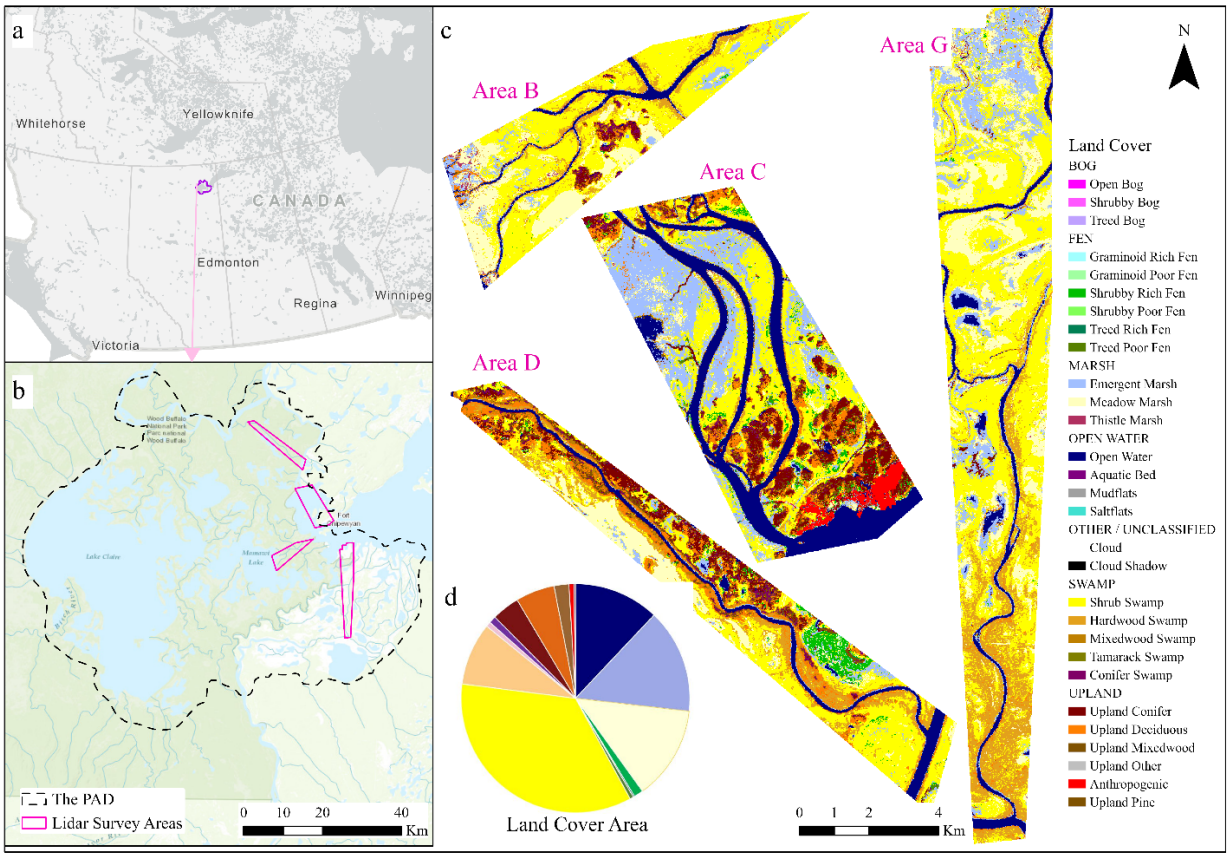

Figure 2.1. a) The Peace Athabasca Delta (PAD) location in Alberta, Canada (inset); b) lidar survey areas; c) landcover classes Ducks Unlimited Canada (DUC) (Ducks Unlimited Canada, 2020) over survey areas [Survey areas B, C, and D are in the Peace Delta, which is affected by regulation, and survey area G is located in the Athabasca delta, which is less affected by flow regulation], d) area of DUC landcover classes.

Although part of the western Canadian boreal forest, the delta's unique flora results from specific requirements, such as permanent standing water and fertile, silty soils with changing hydroperiods, producing a wetland flora typical of the northern prairie grassland region (Timoney, 2013). The dominant or main flora species in various habitat types within the site include seedling stages of *Carex* spp., *Calamagrostis* spp., or shrubs in mudflats, sedges in sedge meadows,

Calamagrostis canadensis in grass meadows, tall shrubs, Balsam poplar *Populus balsamifera,* and birch *Betula* spp. in deciduous forest and white and black spruce *Picea glauca* and *Picea mariana* coniferous forest (Timoney, 2013).

The PAD's lakes and wetland basins are classified into three categories: open, semi-restricted, and restricted (Peters et al., 2021; Timoney, 2021), with large lakes dominating the open basin area. Semi-restricted basins connect seasonally, while restricted ones receive replenishment during rare high water events from ice jams (Peters et al., 2006b). Shallow lake water balance is influenced by local factors, with potential evapotranspiration rates exceeding precipitation (Peters et al., 2006a). This leads to variable wetland areas, responding to periodic flooding and drawdown cycles, creating a highly productive ecosystem (Peters et al., 2021).

2.3 Data

2.3.1 Landsat Data

Collection 2 processing of the Landsat archive has resulted in numerous improvements from Collection 1, including improved geolocation accuracy, radiometric calibration of Landsat 5 and 8, and various masking capabilities for clouds and water (Masek et al., 2020). This solved several limitations of Landsat Collection 1 data, including the comparability of data between sensors (Chen et al., 2021; Mishra et al., 2016; Potapov et al., 2011; Qiu et al., 2018; Roy et al., 2016). However, based on USGS (2021), all Landsat sensors are intercalibrated in Landsat Collection 2 Tier 1. Therefore, in this study, Landsat Collection 2 level 2 (2000 to 2018 summertime) was used, which is atmospherically corrected and presented as Surface Reflectance products.

2.3.2 Lidar Data

Airborne lidar datasets were acquired in 2000, 2016, and 2018 (Table 2.1). Variations in data acquisition parameters and point density outputs across the lidar datasets are due to the advances

in technology over the last two decades (Hopkinson et al., 2016). Based on the understanding that sensor settings and survey configuration can affect how laser pulses interact with vegetation and therefore, the distribution of returns within vegetation canopies (Hopkinson et al., 2008), only upper canopy surface changes were compared over time. These are more reliably sampled from laser pulse first returns. Lidar canopy height model (CHM) was derived at spatial resolutions lower than the lowest point density dataset to accommodate density variations in the data (e.g. Lim et al. (2008). All lidar data used in this study were collected during the summer growing season between mid June and early August (Table 2.1). Figure 2.1 shows the spatial coverage of lidar survey areas from lidar surveys in 2000, 2016, and 2018 (B, C, D, and G).

Table 2.1. Lidar sensor and survey configurations.

Date	Sensor	Pulse Repetition (kHz)	Sensor Altitude (m a.g.l.)	Scan Rate (Hz)	Scan Angle (°)	Returned Point Density (m^{-2})
17/06/2000	ALTM 1225	25	~1000	Variable, depends on scan angle; e.g., 28 Hz for ± 20° scan	10 to ± 20°	all returns 0.55
04/08/2016	Titan	75	~1000	33	24	all returns 4.13
24/07/2018	Titan	75	~1000	32	25	all returns 6.76

2.3.3 Land Cover Data

Wood Buffalo National Park Enhanced Wetland Classification produced by Ducks Unlimited Canada (DUC) (Ducks Unlimited Canada, 2020) was used because it is highly accurate and was classified for land covers within ~1 year of the 2016 and 2018 lidar datasets. The land cover map was created using Sentinel-2 imagery from August 2017, as well as field data, resulting in a 10m resolution map with >79% overall accuracy. In this study, the areas that overlapped with lidar sample areas were extracted and used as base landcover information for lidar and Landsat product comparisons (Figure 2.1b).

2.4 Methods

The main methodological steps are illustrated in Figure 2.2. Canopy structural information was obtained from summertime lidar data. Landsat images from 2000 to 2018 were used for lidar canopy height and NDVI comparisons through time.

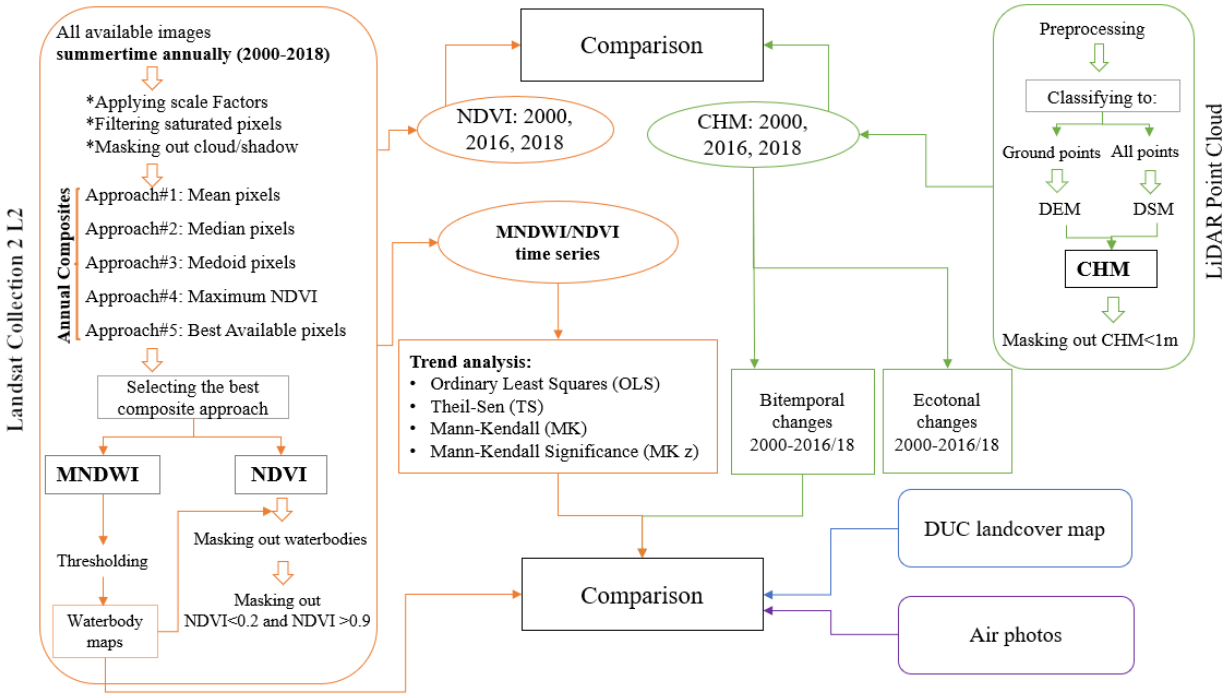

Figure 2.2. The workflow of the study. L2 (Level 2); Best Available Pixels (BAP) method; NDVI (Normalized Difference Vegetation Index); MNDWI (Modified Normalized Difference Index); DEM (Digital Elevation Model); DSM (Digital Surface Model); CHM (Canopy Height Model); DUC (Ducks Unlimited Canada). See text for details.

2.4.1 Landsat Processing

2.4.1.1 Preprocessing

Landsat data preprocessing included: 1) applying fill values and scaling factors (USGS, 2021); 2) removing saturated pixels (Crego et al., 2022; Hemati et al., 2021); 3) masking cloud and cloud shadows (Crego et al., 2022); and 4) coordinate reprojection to the lidar data (NAD83 zone 12). To avoid the effects of drying and/or flooding of water bodies in the analyses, all shallow

open water and rivers/streams were masked in the survey areas (e.g. Ju and Masek (2016). After applying a standard water mask (USGS, 2021), we found that this was not effective at identifying water across all pixels. Therefore, we used the Modified Normalized Difference Water Index (MNDWI) and different thresholds to further filter pixels that were not classified in the original water mask. Following multiple tests and careful observations, we determined the optimal threshold range for MNDWI of each year (MNDWI greater than -0.1, 0, and 0.1). MNDWI is defined below in Equation 2.1 (Xu, 2006).

$$MNDWI = (Green - SWIR) / (Green + SWIR) \quad \text{Equation 2.1}$$

2.4.1.2 Annual Landsat Composites

To reduce the impacts of cloud cover in Landsat images over lidar survey areas, image compositing was applied. However, previous studies did not compare the efficacy of various composite approaches. Therefore, we employed several imaging compositing methods to visually identify and select the most accurate one. These included: mean, focal mean or median, medoid, maximum NDVI, and the Best Available Pixels (BAP) system. In all approaches (except the BAP approach), scan line corrector (SLC)-off issues associated with ETM+ data and any between-sensor differences were mitigated by constraining all images for a given year's composite to a single sensor; i.e. all available Collection 2 Landsat 7 imagery from 2000 to 2002, Landsat 5 from 2003 to 2011 and Landsat 8 from 2013 to 2018 (for 2012 there were no data). Only summer imagery (mid June to early September) was used to minimize the effect of vegetation phenology on NDVI. Finally, the NDVI of each annual summer-time Landsat image was created using red and near-infrared bands. The index is grounded in the principle that leaf cell structure reflects NIR strongly due to the absence of absorption by plant pigments. Conversely, chlorophyll pigments effectively absorb red wavelengths used for photosynthesis (Yoder & Waring, 1994). Thus, plants

considered "healthy" with abundant chlorophyll absorb more red and consequently reflect a larger proportion of NIR compared to "less healthy" plants (Stamford et al., 2023; Tucker, 1979). NDVI is calculated by comparing the reflectance in the near-infrared (NIR) and red electromagnetic wavelengths (Tucker, 1979) (Equation 2.2).

NDVI = (Near InfraRed – Red) / (Near Infrared + Red) Equation 2.2

In this study, only land pixels, where NDVI>0.2 were considered to further ensure that water pixels were excluded from the analysis. To avoid NDVI saturation effects, pixels with NDVI > 0.9 were also excluded from the analysis. All Landsat data processing was done in Google Earth Engine (Gorelick et al., 2017), except for creating BAP composite images, which were generated via the approach from Francini (2021).

2.4.1.3 NDVI/MNDWI Trend Analysis

To determine the spatial pattern of vegetation change trend directions and magnitudes, Ordinary Least Square (OLS) slope, Theil-Sen (TS) slope (Sen, 1968; Theil, 1950), and monotonic Mann-Kendall (MK) (Kendall, 1948; Mann, 1945) trend analyses were used. Mann-Kandall significance (MK Z) was used to evaluate the significance of the trends. Positive and negative NDVI trends represent greening and browning, respectively.

It has been demonstrated that linear trend functions or OLS describe trends in NDVI over time (Baird et al., 2012; Fraser et al., 2011; Ju & Masek, 2016; McManus et al., 2012; Sonnenschein et al., 2011). The slope coefficient for an ordinary least squares regression is linear and used to determine the trend of each pixel over time. TS and MK have also been used in trend analysis because these do not need variable assumptions (e.g. normal distribution) (Neeti & Eastman, 2011). TS slope is calculated from the median of slopes between pixel values and pair-wise time steps, which equals n(n-1)/2s slopes (Tran et al., 2019). The outcome often matches that

of the OLS linear trend but is more appropriately applied to short and/or highly variable time series. The TS method can also reject outliers without impacting the slope. The number of erroneous and outlier values that can be rejected without impacting the result is about 29% of the sample size (Eastman, 2015). The monotonic MK trend is a non-linear trend indicator that measures how continuously a trend is increasing or decreasing (Eastman, 2015). The MK is computed by counting the number of values that decrease or increase over time at each pixel. Results range from -1 and +1, where a value of -1 shows that the trend consistently decreases and never increases, a value of +1 shows the opposite, and a value of 0 shows that there is no consistent trend (Eastman, 2015). The MK significance indicates the significance of the trend, known as the MK Z score, but is used frequently as a trend test for other trends as well (Eastman, 2015). The MK Z indicates specific levels of significance (α), "as Z = ± 2.576 refers to α = 0.01, Z = ± 1.960 refers to α = 0.05, and Z = ± 1.645 refers to α = 0.1", thus here MK Z between -1.960 and +1.960 (corresponds to $\alpha \geq 0.05$) are considered as 'no trend areas" (Schucknecht et al., 2013). Masked-out pixels due to either cloud/cloud shadow or water were not considered in trend calculations. Trends were calculated in Terraset software (Clark Labs, USA).

The TS and MK Z scores were also used on MNDWIs to monitor water trends in the delta. In MNDWI trends, positive and negative represent wetting and drying, respectively. A surface water map series was created using different thresholds of MNDWIs to evaluate the boundaries of shallow open water and rivers/streams and their annual fluctuations (hydroperiod). The trends in MNDWI were subsequently compared with the multi-year hydroperiod to verify if the trend outputs exhibit similar significant fluctuations as observed in the multi-year hydroperiod maps

2.4.2 Lidar Data Processing

All lidar point cloud data were re-projected to NAD83. Lidar point heights of the 2000 dataset were compared in overlapping areas with 2016 and 2018 datasets to correct for any system or GNSS trajectory bias. To ensure all three datasets were vertically co-registered to the most accurate data collections of 2018 and 2016, they were compared to identify any systematic offsets, and small height adjustments of between 0.3 and 0.7 m were applied to the 2000 dataset in Terrascan (Terrasolid, Finland) (Hopkinson et al., 2008). All lidar points were classified into ground and non-ground in Terrascan. Ground points were interpolated to 5 m digital elevation models (DEM) using Triangulation with Linear Interpolation. All data points were used to create a 5 m digital surface model (DSM) using a local maximum Z filter in Surfer (Golden Software Inc. USA). Finally, to create the 5 m resolution canopy height model (CHM), the DEM was subtracted from the DSM. The CHM was then aggregated to 30 m to create an index of both height and canopy cover (CC), and to make the data directly comparable with Landsat products. Masked water pixels were also removed from CHMs to enable direct CHM and NDVI comparisons. Low CHM heights of <1m were ignored in the analysis to remove the influence of seasonal vegetation phenology variations across years. To detect changes in canopy heights >1m, year 2000 CHMs for the four lidar areas were subtracted from 2016 and 2018 CHMs.

To investigate if relationships exist between CHM changes and NDVI trends, the CHM 90th percentile (PCT90) was calculated using a 9x9 5m pixel moving window on each CHM. This was to determine the maximum canopy height change within localized areas represented by the moving window and to assess the changes relative to NDVI trends. By focusing on the largest CHM changes within moving windows, correlations between these canopy height changes and variations in vegetation greenness associated with NDVI can be determined. The utilization of moving

windows accounts for spatial variability within pixels. To determine how vegetation height changes occur in ecotonal areas characterised by shorter (<5 m) and taller (>5 m) vegetation, PCT90 CHM values were first classified into two ecotones using Natural Breaks histograms. A categorical change detection analysis was then performed to illustrate the changes occurring within each ecotone. This quantifies changes within each ecotone separately, enabling a more detailed understanding of changes occurring across canopy height ranges. The average ecotonal change rate (m/yr) in lateral direction was measured and calculated manually in ArcGISPro.

2.4.3 Statistics

The 2017 DUC's landcover map was used to stratify 2016 and 2018 CHM and NDVI comparison results using a random sampling approach because it has high resolution and accuracy given the development of novel machine learning methods. As major landcover classes have different spatial coverage, and to avoid bias, 2000 random points were selected based on the proportional area coverage of classes (excluding outliers). Shapiro-Wilk normality test (Royston, 1992) was done and since the p-values obtained from the normality test are zero, we can infer that the data does not adhere to a normal distribution (Appendix A2). Because of the non-normal distribution and the apparent nonlinear relationship between the NDVI and CHM variables, we employed the Spearman correlation coefficient to determine the strength and direction of their monotonic relationship. Given the non-linear relationship between the NDVI and CHM variables, we utilized a nonlinear regression analysis to model and assess their connection. The equation applied was per Equation 2.3.

$$NDVI = b1 + b2 * Log(CHM) \quad \text{Equation 2.3}$$

In this equation, CHM is treated as an independent variable, and NDVI is the response variable. The goal is to estimate the values of b1 and b2 based on the available data. To evaluate

the model's ability to represent the observed data, an ANOVA analysis was conducted. The model's goodness of fit was evaluated using statistical metrics, including the F-statistic, p-value, and sum of squares. For residual analysis, we created a plot of the residuals against the fitted values. Our anticipation was that this residual plot would not reveal any noticeable patterns. All mentioned statistical assessment steps were repeated, this time focusing on the comparison of NDVI with CHM for each land cover class and also to compare NDVI trends with bitemporal CHM changes. Moreover, comparisons of the detected changes between the two distinct datasets, NDVI trends, and bitemporal CHM changes, NDVI-derived Mann-Kendall significance was employed to demonstrate the statistical strength of any discernible trends.

To compute rates of change in NDVI trends and lidar-derived canopy change, ArcGIS Pro was utilized to establish a set of arbitrary transects. These transects are spaced at equal intervals of 1.5 km, running parallel to each other. These transects were overlaid onto the observed greening and browning regions to calculate average change rates.

2.5 Results

2.5.1 Landsat-Derived NDVI vs. Lidar-Derived Canopy Height

Figure 2.3a shows the 2000, 2016, and 2018 CHMs over the lidar survey areas classified into four canopy height classes. Trees associated with CHM >10 m, are located on terraces and higher-elevated levees. Figure 2.3 also shows the area coverage of each canopy height class within survey polygons. From 2000 to 2018, there was a general increase in all categories of canopy height. Among tested Landsat composite approaches, Median produced higher quality annual composites [Appendix A1]. Figure 3b shows 30m Median derived-NDVIs. Despite the short stature of the canopy, NDVI exhibits high values. While there were instances where the NDVI had high values

for taller canopies, high NDVI values are also found in areas with shorter canopies, and therefore, are somewhat insensitive to canopy height.

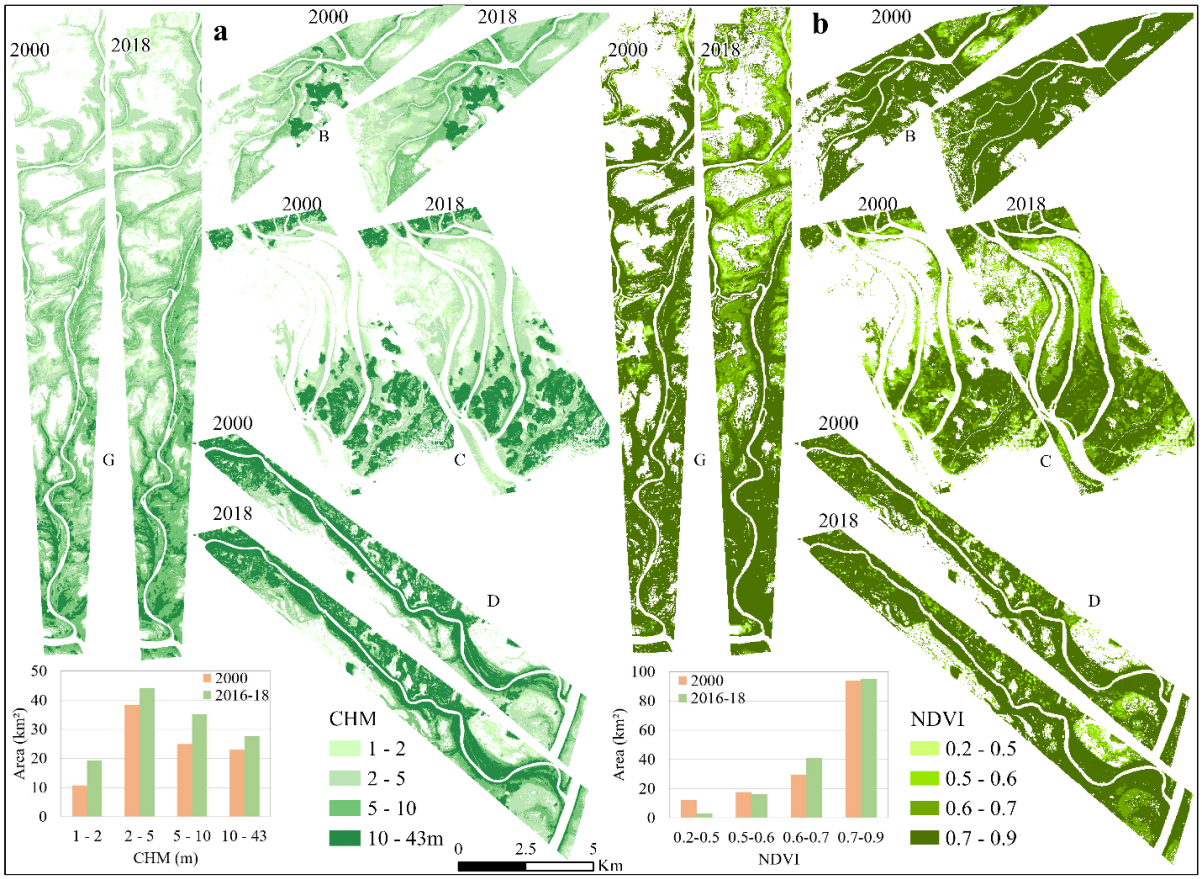

Figure 2.3. a) Canopy Height Models (CHM) (5m pixel size), b) NDVIs (30 m pixel size). 'White' areas within each sample region, represent CHM <1m or NDVI <0.2.

Table 2.2. Two-tailed Spearman correlation coefficient between NDVI and CHM of 2016/18.

		NDVI
Spearman's rho	Correlation Coefficient	0.59**
CHM	Sig. (2-tailed)	0.000
	N	1883

The results of the Spearman correlation coefficient between NDVI of 2016/18 and CHM of 2016/18 are presented in Table 2.2 [see Appendix A2 for tests of normality]. The Spearman correlation coefficient of 0.59 reveals a significant positive monotonic relationship between the variables NDVI and CHM (P-value <0.001). Table 2.3 shows the coefficients of nonlinear regression analysis.

Table 2.3. The nonlinear regression coefficients.

	Unstandardized Coefficients		Standardized Coefficients		
	B	Std. Error	Beta	t	Sig.
ln(CHM)	0.062	0.002	0.556	28.98	0.000
(Constant)	0.639	0.004		174.40	0.000

The p-value (<0.001) of the F-test displayed in Table 2.4 indicates that our regression model provides a significantly better fit to the dataset compared to a model without any predictor variables. $R^2 = 0.309$ shows the regression model fits our observations.

Table 2.4. ANOVA results and model summary of nonlinear regression analysis.

ANOVA[a]

Model		Sum of Squares	df	Mean Square	F	Sig.
1	Regression	4.90	1	4.90	839.98	0.000[b]
	Residual	10.98	1881	0.006		
	Total	15.88	1882			

a. Dependent Variable: NDVI

b. Predictors: (Constant), log_chm

Model Summary[b]

R	R Square	Adjusted R Square	Std. Error of the Estimate
0.56[a]	0.31	0.31	0.076

a. Predictors: (Constant), log_chm

b. Dependent Variable: NDVI

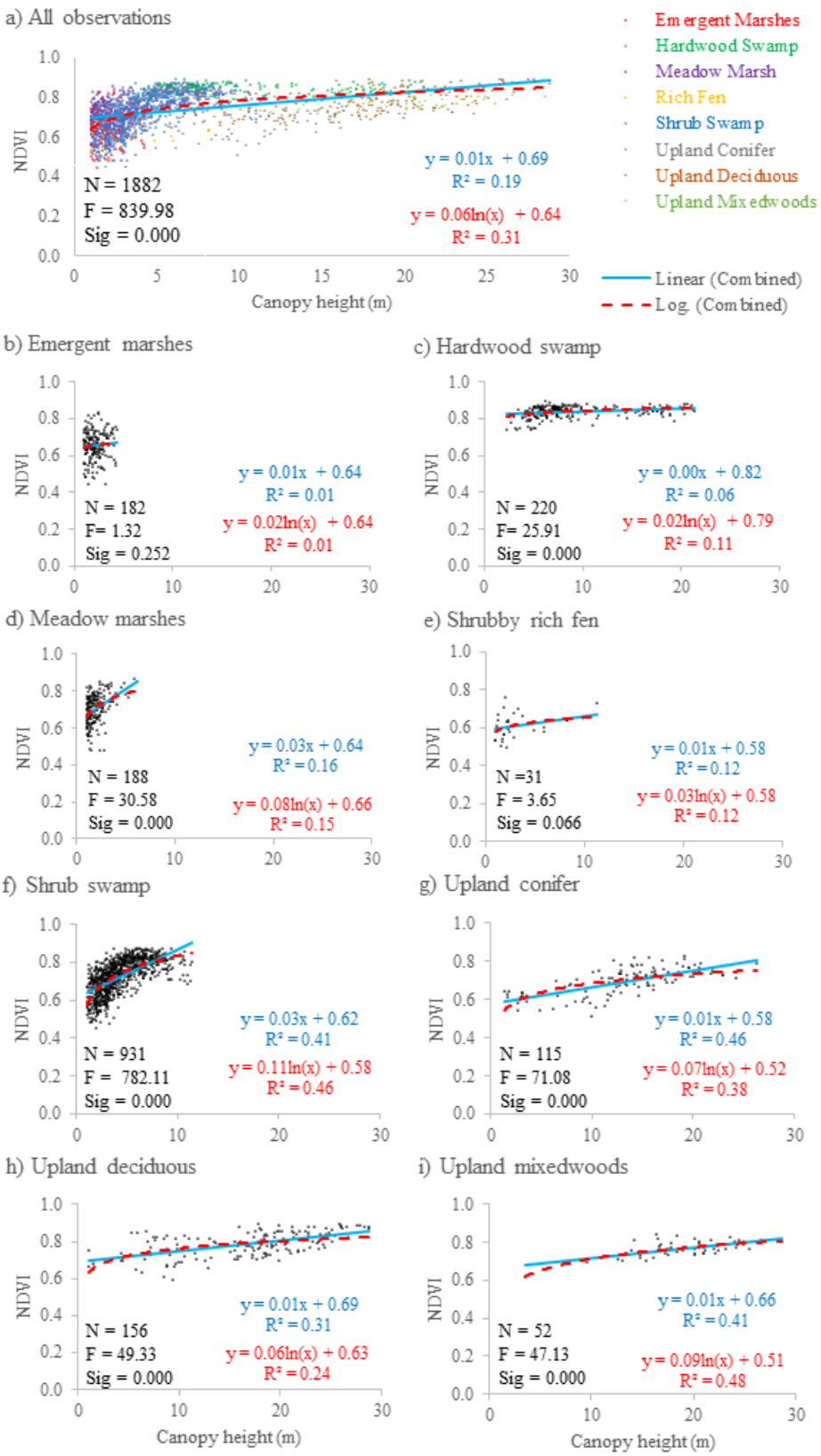

Figure 2.4. The scatter plots between Median-derived NDVI of 2016/18 and CHM of 2016/18, overall and per landcover classes. (ANOVA results of log models are only shown).

Figure 2.4 illustrates relationships between 2016/18 CHM and NDVI from random sample points for major land covers (p-values < 0.001). Two trendlines, linear and logarithmic are used to describe the relationship for coincident CHM/NDVI data points with a modest improvement of R^2 (from 0.19 to 0.31) using a logarithmic trend. In this figure, several land covers (emergent marsh, hardwood swamp, meadow marsh, and shrubby rich fen), exhibited R^2 <0.15, indicating a negligible correspondence between NDVI and canopy height. However, shrub swamp, upland conifer, and mixedwood comparisons between height and NDVI resulted in higher R^2 values (0.38, 0.46, and 0.48, respectively), suggesting a moderate level of association between the NDVI and canopy height within these land cover classes.

Figure 2.5 illustrates the distribution of CHMs and NDVIs across different land covers in the PAD. Meadow marshes, despite exhibiting a lower range of canopy heights, displayed a similar range of NDVI values compared with vegetation with taller canopies. In contrast, the hardwood swamp land cover exhibited a broader range of CHM values, however, the NDVI range was comparatively narrow, with a median value of 0.84. These observations are different from what is observed for upland conifer, deciduous, and mixedwood land cover types. In these upland habitats, tree cover ranges from 25% to 100% of the total area, with each type characterized by distinct tree species dominance, where either conifer or deciduous species make up over 75% of the tree cover.

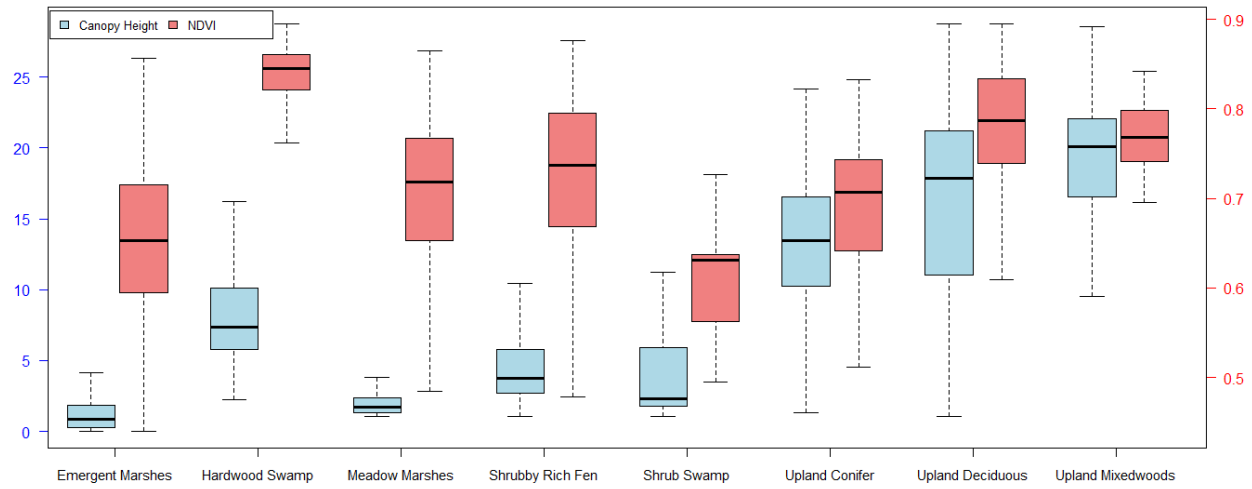

Figure 2.5. Comparison box plot random point distributions between canopy height and NDVI in 2016/2018 for major land cover classes found in the PAD.

2.5.2 CHM Bitemporal Changes vs NDVI/MNDWI Trends

Figure 2.6 shows NDVI and MNDWI trends over the study period for the lidar survey area 'G' as an example (Figure 2.1), with areas B, C, and D found in Appendix A3. OLS trend analysis can be influenced by noise or other sources of variability. In Figure 2.6a, OLS exhibited browning (negative NDVI trends) around some ponds, however, TS did not show similar browning patterns. Consequently, OLS was excluded from the remaining analyses in this study. MK demonstrated similar greening trends to other methods, indicating trend consistency. Use of the MKz statistic reveals that around 39% of pixels exhibit statistically significant greening (positive NDVI trend) change. This demonstrates that an increase in NDVI trend over the ~ two decades in the PAD is not a result of random variations in vegetation response, rather this represents a quantitative change in vegetation trajectory. Overall, all NDVI trends using the various statistical methods displayed similar change patterns over time (Figure 2.6 and Appendix A3).

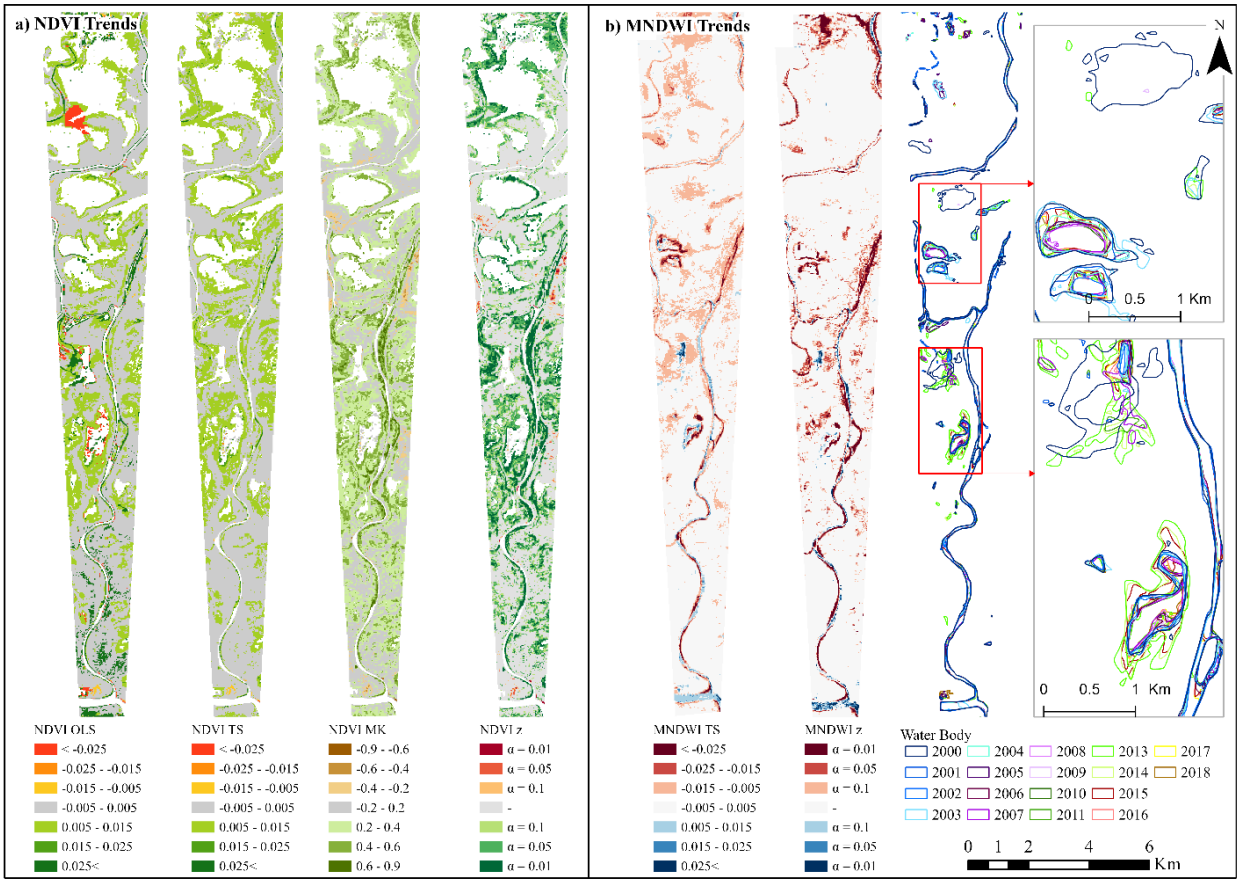

Figure 2.6. a) The NDVI and b) MNDWI trends over plot G as a case study example.

MNDWI TS indicates areas within the PAD that were undergoing drying or surface water reduction trends (Figure 2.6 and Appendix A3), while MNDWI MKz identified those areas where drying trends were statistically significant (α=0.1, α=0.05, α=0.01). To improve understanding of MNDWI trends, annual water body maps are presented alongside the MNDWI trend results (Figure 2.6b). MNDWI trend analysis reveals that significant drying trends align with annual hydroperiod fluctuations for shallow open water and rivers/streams. Large areas of shallow open water (e.g. survey area B, Figure A3 in Appendix A3) in 2000 are non-existent in more recent Landsat image collections. Overall, the MNDWI trends reveal substantial drying in study areas indicated by a reduction of areas of open water, particularly in the riparian buffers, which often experience fluctuating hydroperiods adjacent to ponds. MNDWI trends also exhibit significant

shifts in river channels over time. The analysis also reveals notable changes in river meandering associated with fluvial geomorphic processes, indicating alterations in their spatial distribution or channel morphology (Figure 2.6 and Appendix A3).

Examples of bitemporal ΔCHM are illustrated with trends in NDVI TS, NDVI MKz, and MNDWI MKz for lidar survey areas (Figure 2.7). Large increases in CHM (>5 m) over almost two decades were observed, mostly on upraised levees. Overall, the comparisons between bitemporal ΔCHM and NDVI trends reveal few similarities between the two datasets, where trend patterns and variations in ΔCHM differ significantly from NDVI trends, especially for taller canopies. Weak correspondence between CHM changes and NDVI trends is shown in Table 2.5.

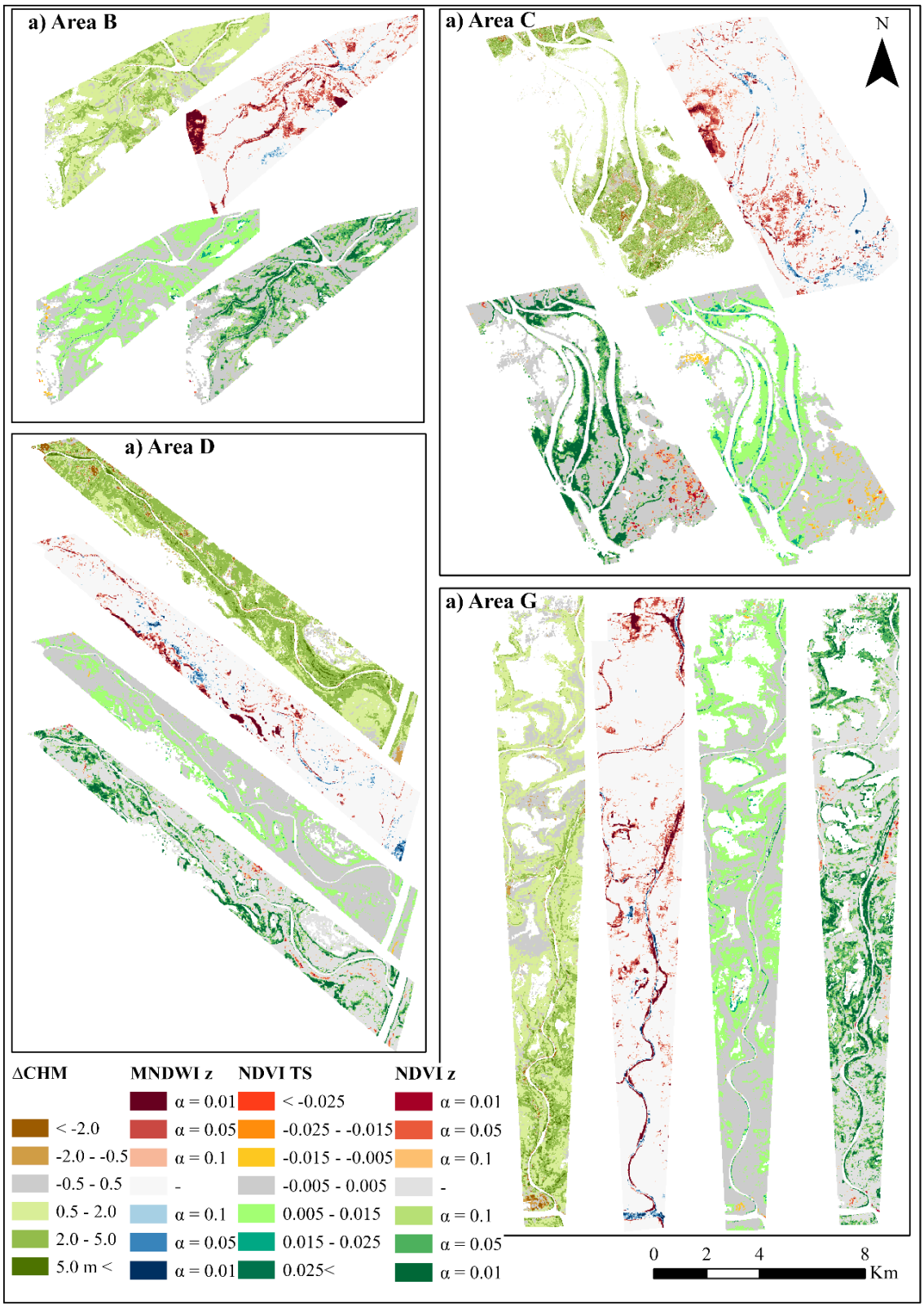

Figure 2.7. The bitemporal ΔCHM, MNDWI MKz, NDVI TS, and NDVI MKz. (Legends are based on the orders: left to right, up to bottom for areas A and B, up to bottom for area D; and left to right for area G).

Table 2.5. The Spearman's correlation between ΔCHM and NDVI trends.

	R	Sig.	N
ΔCHM vs. OLS	-0.11	0.000	
ΔCHM vs. TS	-0.13	0.000	1806
ΔCHM vs. MK	-0.05	0.037	
ΔCHM vs. MKz	-0.06	0.016	

2.5.3 Ecotonal Change vs NDVI/MNDWI Trends

Figure 2.8*a* shows the proportion of PCT90 ΔCHM area (km^2) of the total proportional area represented by the four lidar survey areas over the last almost two decades, while Figure 2.8*b* illustrates the average expansion rate of ecotones (m/yr). Approximately 90% of the study area exhibited no significant changes during the study period. Furthermore, the analysis of the three Peace Delta sector surveys (survey areas B, C, and D) showed consistently high expansion rates between 2.4 and 2.9 m/yr. This indicates substantial and rapid changes and expansions occurring within the study area during the specified period. However, in contrast, the Athabasca Delta survey area (area G) displayed a lower expansion rate of only 1.5 meters per year. The mean rate of NDVI greening in MK z (minus browning) is 3 m/yr.

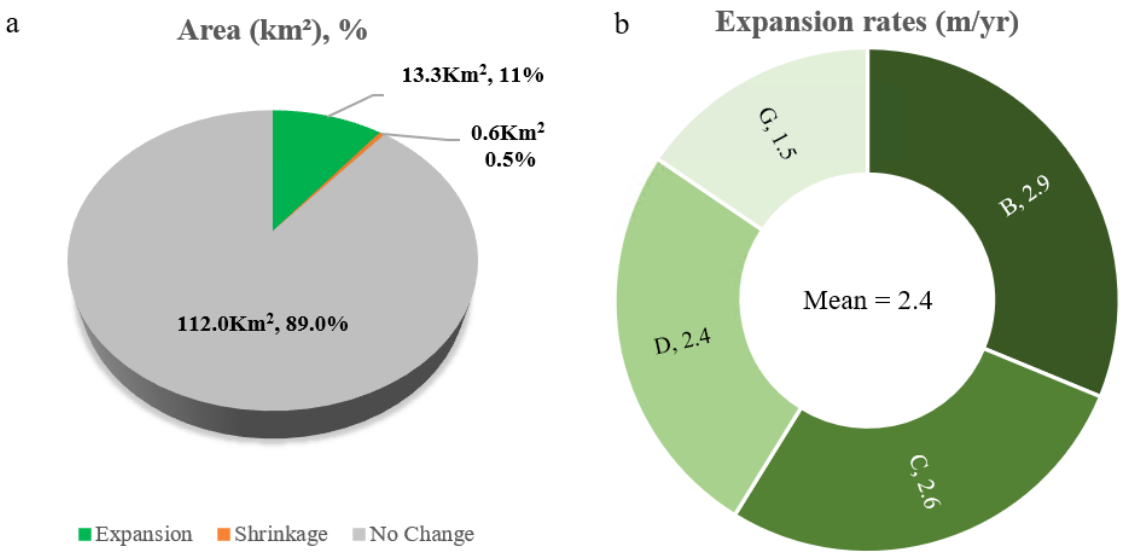

Figure 2.8. a) The PCT90 ΔCHM area (km^2) of the total proportional area represented by the four lidar survey areas and %. b) The average ecotonal expansion rate (m/yr.) in lateral direction.

Figure 2.9 provides example changes observed using PCT90 ΔCHM, ΔCHM, CHM2000, NDVI MKz, MNDWI MKz, water fluctuations, and the aerial RGB image (for context) from 2016/2018. Despite non-correspondence between the ΔCHM and the NDVI trends, positive NDVI trends correspond with ecotonal expansion patterns observed in PCT90 ΔCHM. This indicates that while vertical changes in CHM may not exhibit a clear relationship with the NDVI trends, there is a consistent pattern of positive NDVI trends and ecotonal expansion observed in the PCT90 ΔCHM and the NDVI (Figure 2.9).

In Figure 2.9c, there are areas where NDVI trends are negative, while PCT90 ΔCHM does not exhibit a corresponding decrease in canopy height. Further, MNDWI MK z analysis did not reveal moisture-related trends over the shallow open water area. Longer-term hydrological trends would provide additional insights into changes occurring in these areas. In Figure 2.9b, positive NDVI trends correspond with a similar pattern of expansion in PCT90 ΔCHM. However, the area of positive NDVI trends is highly variable, where positive trends are wider in some areas and narrower in others relative to the ecotonal expansion observed in PCT90 ΔCHM. The MNDWI analysis revealed significant drying in upland areas and levees, which are also associated with positive NDVI trends and ecotonal expansion.

In the Athabasca Delta example (Figure 2.9d), narrower expansions than the Peace Delta survey areas were observed, with these areas exhibiting more or less the same greening trends in NDVI. However, the NDVI greening appeared to cover a larger area than the PCT90 ΔCHM expansion. In the MNDWI trends, a consistent pattern of significant drying can be observed in almost all ponds. In the MNDWI analysis, a larger pond was observed and captured in the 2000 image, but it did not appear in subsequent years, indicating that the pond had disappeared or dried out (as noted above).

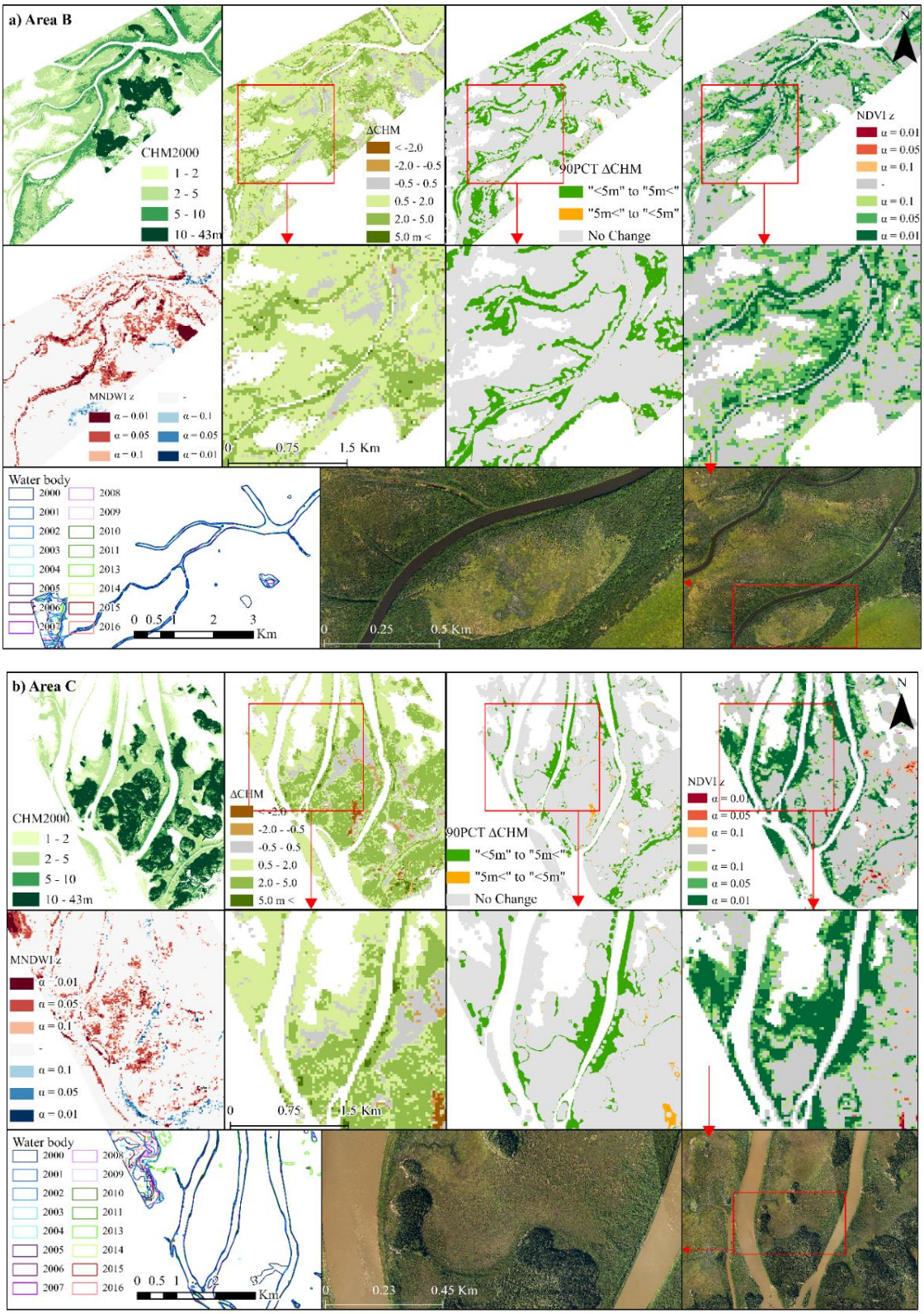

Figure 2.9. The CHM2000, ΔCHM, PCT90 ΔCHM, NDVI MKz, MNDWI MKz, water fluctuations, and zoomed-in aerial photos of 2016 over a) survey area B, b) survey area C, c) survey area D, d) survey area G.

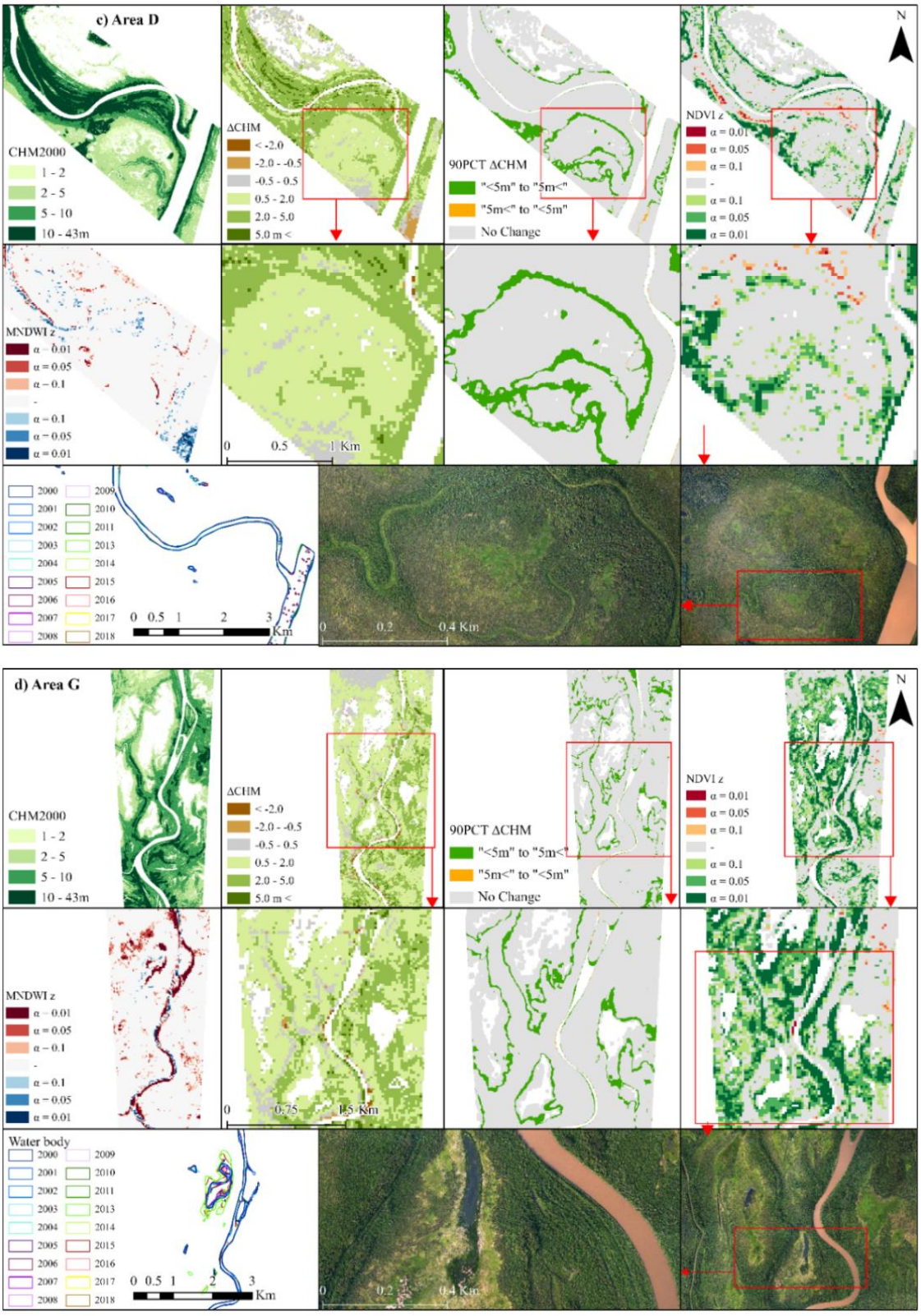

Figure 2.10. (Continued) The CHM2000, ΔCHM, PCT90 ΔCHM, NDVI MKz, MNDWI MKz, water fluctuations, and zoomed-in aerial photos of 2016 over a) survey area B, b) survey area C, c) survey area D, d) survey area G.

Comparing the PCT90 ΔCHM with the DUC landcover map (Figure 2.1) pointed out that CHM expansion occurs predominantly along the edge of shrub swamps (Figure 2.10). In some cases, shrubs also extend into marshes from adjacent swamps. The analysis of NDVI trends indicates consistent patterns with the PCT90 ΔCHM, though extents vary. In most cases, NDVI trends demonstrate significant positive trends, particularly along river banks. Positive trends are also observed in ΔCHM. NDVI time series also indicate positive trends in areas where no expansion is evident in PCT90 ΔCHM determined from bi-temporal airborne lidar data. Conversely, while some area's canopy height reduction of PCT90 ΔCHM corresponds with NDVI browning, the majority of these instances are observed as positive NDVI trends.

Table 2.6 presents the descriptive statistics, including the mean, standard deviation (STD), and median, to investigate potential differences in the distribution, variability, and central tendency of the NDVI trends across the 90PCT ΔCHM classes. The NDVI trends in all four analyses demonstrated higher mean and median values over the expanded areas compared to the no change.

Table 2.6. Mean, Standard Deviation, and Median of NDVI trend slope across the 90PCT ΔCHM “expansion” and “no change” classes. (NDVI trend slopes are dimensionless).

Ecotonal changes	**OLS**		
	Mean	STD	Median
<5m to >5m	1.313	7.606	0.006
No Change	1.243	7.079	0.003
	TS		
<5m to >5m	0.041	1.540	0.006
No Change	0.030	1.375	0.003
	MK		
<5m to >5m	0.340	0.208	0.346
No Change	0.199	0.225	0.216
	MK z		
<5m to >5m	1.864	1.139	1.894
No Change	1.101	1.238	1.136

Comparison with DUC land cover classes revealed that approximately 65% of the expansion, equivalent to around 5% of the total survey area, occurred in shrub swamps (Figure 2.10). Another land cover class, hardwood swamp, accounted for approximately 1% of the total expansion in the area.

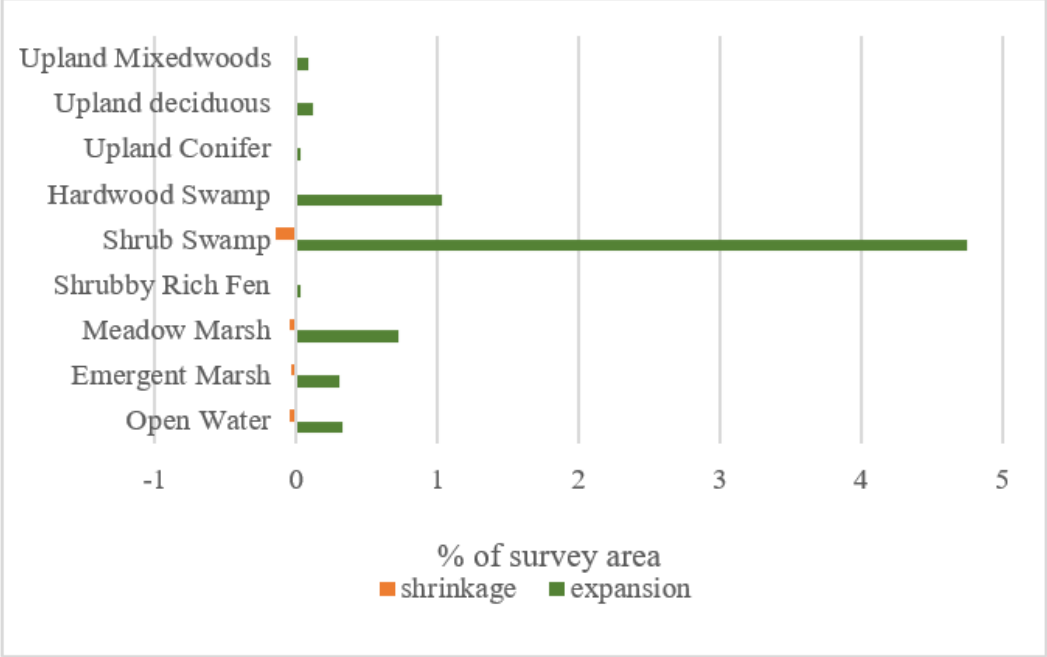

Figure 2.11. The percentage of expansion and shrinkage occurred in the survey areas.

2.6 Discussion

2.6.1 Comparing NDVI with CHM

NDVI showed low to moderate correlations with the lidar-derived CHM. There may be several reasons for this. NDVI is sensitive to sensor factors, soil, pixel components, atmosphere, moisture, biomass volume, etc. (Huang et al., 2021). The spectral response to these factors is not equivalent across Red and NIR bands, thus various environmental and atmospheric influences can complicate or alter NDVI. For example, Huang et al. (2021) found that NDVI for a mature deciduous forest can be similar to golf course grass.

To asses the first hypothesis, that there would be a relationship between NDVI and CHM over DUC landcover classes, we found that NDVI and CHM corresponded moderately (R^2 between 0.38 and 0.48, Figure 2.4) in land covers that contained taller vegetation versus other land covers found in the PAD. These included shrub swamps, upland conifer, and mixedwood. Taller vegetation also typically includes higher foliage cover (Rijkers et al., 2000), which alters the amount of green vegetation when viewed planimetrically. Taller, more heterogeneous, dense, and clumped canopies may exhibit increased greenness and reflectance as these structural complexity characteristics are known to be associated with improved light capture and higher forest productivity (LaRue et al., 2018). Conversely, canopies that are more homogeneous or less dense may appear darker, a phenomenon linked to their ability to scatter a larger portion of incoming light (LaRue et al., 2018). In the specific case of shrub landcovers, correlations may have been higher because these are the landcovers that are expanding, with open areas and gaps gradually replaced with canopy.

In this study, shorter vegetation types were not well correlated with Landsat NDVI (Figure 2.4) which can be due to lower canopy cover combined with more influences from the soil, moisture, etc. Landsat NDVI and NDVI time series analyses could provide a more accurate representation of vegetation changes in areas characterized by taller vegetation with partially open canopies, as these areas are less prone to NDVI saturation issues.

2.6.2 MNDWI Trends

In this study, MNDWI was used to map surface water in the study area. The commonly adopted approach for monitoring surface water changes over multiple years is to generate surface water maps for each year and to compare changes in water extent (multi-year hydroperiod) (Tetteh & Schönert, 2015; Vinayaraj et al., 2018; Ward et al., 2014). Here, surface water maps were created

using MNDWI thresholds (Figure 2.6 and Appendix A3). In MNDWI, threshold values distinguish water areas with positive values (greater than zero) from vegetation areas with negative values (Xu, 2006). To enhance water extraction effectiveness, it is crucial to establish a suitable threshold for MNDWI.

Deoli et al. (2023) used the same analysis with TS and MK Z and found significant drying trends in Bhopal, India. Kumar (2021) observed a decrease in water area in Naukuchiatal Lake during summer using the MK test and the Water Ratios index (WRI). Classification of water using MNDWI in 2000 depicted the presence of several areas of shallow open water (Figure A3 in Appendix A3), which were not observed in more recent years. Open water areas observed in 1-2 early years were not included in the significance of the drying trend because these areas were dry for the majority of the time series. A longer time series would enable quantification of typical vs abnormal surface water. Therefore, utilizing a longer-term time series of MNDWI is likely a more effective approach when evaluating hydrological trends. The visual comparison between the drying trends in MNDWI and the vegetation expansion observed around the drying areas suggests a potential ecological response to changes in water availability (Figure 2.6 and Appendix A3). As water availability decreases, certain vegetation types may exhibit an expansion or encroachment into the drying areas. This expansion can be attributed to the competitive advantage of certain vegetation species or their ability to adapt to changing hydrological conditions (Timoney, 2009).

2.6.3 NDVI Trends vs. Bitemporal CHM Changes

Among tested NDVI trends in this study, the TS trend produced a smoother representation of the trends, while the OLS was visually similar to the MKz result in terms of the observed significant trends, despite having some data gaps. Also, as can be observed in Figure 2.7, MKz exhibits a higher degree of similarity with the patterns revealed by CHM changes.

Although some correlation between NDVI trends and CHM changes was expected, it was found that there is only a weak correlation for the survey areas examined. The second hypothesis that there would be a significant greening trend or expansion of shrubs and trees over the PAD between 2000 and 2018 was largely supported. Bitemporal CHM changes did indicate shrubification and tree growth in many areas, with no changes over more than half of each survey area. While a positive greening trend in NDVI was observed over time, its significance was notable in the transition from marshlands to areas with taller canopy heights and increased shrubification. Forest cover did not show significant greening. Forests within the Delta are primarily found on elevated levees and terraces, experiencing fewer flooding-drawdown cycles compared to other vegetation (Timoney, 2008b). Timoney (2008b) studied rates and directions of vegetation changes from 1945 to 2001 in the PAD using historical aerial photography. He reported that the lowest changes in vegetation occurred within the Forest landcover class and the greatest changes in vegetation occurred in marshes. He also found that the succession between aquatic marsh vegetation to willow spp. Shrubs (especially after 2000) and between areas of open water and marsh vegetation succession were common.

2.6.4 NDVI Trend vs. Ecotonal Expansion

The consistent patterns observed between NDVI and PCT90 ΔCHM suggest a close relationship between vegetation greenness and changes in average canopy height (Figure 2.9). Considering the difference in ecotonal expansion between the Peace and Athabasca Delta sectors (Athabasca sector is an active delta and Peace sectors are inactive delta), this indicates different underlying processes. Indeed, we should not infer average rates of ecotonal expansion across the whole PAD, as such processes have locally variable driving mechanisms in addition to regional climate influences that impact runoff, flooding and evaporation over the two systems.

The discrepancy between the extent of greening observed in the NDVI and the expansion indicated by the PCT90 ΔCHM suggests that the NDVI captures a spatially broader range of vegetation response, including shorter stature vegetation, compared to that captured in the CHM-based analysis. Moreover, larger areas of NDVI greening may be influenced by the sensitivity of the NDVI index to changes in vegetation types, limitations of the NDVI calculation and saturations, or differences in spatial resolution between Landsat and lidar-derived products. Other studies have reported an overestimation in NDVI greening trends, which could be unrelated to *in situ* vegetation structural properties. Gao et al. (2022) attributed NDVI overestimation/ underestimation to the spatial resolution of data (250 m MODIS and 8km GIMMS). Vicente-Serrano et al. (2020) also found an overestimation of positive NDVI trends (greening) when using NDVI to detect vegetation change at 1 km resolution. Therefore, it is important to consider the magnitude and extent of the observed greening in the NDVI, taking into account the potential for overestimation. The NDVI is derived through a nonlinear transformation, which can lead to the overestimation of NDVI values in areas with low vegetation coverage and underestimation in areas with high vegetation coverage (Huete et al., 1997). It can be assumed that any systematic overestimation in NDVI would persist throughout the entire study period, suggesting that temporal variations in NDVI should be minimally impacted (Luo et al., 2022).

Further analysis and validation using ground truth data or alternative vegetation indices would improve confidence in the reliability of NDVI trend observations and would provide a more comprehensive understanding of the relationship between vegetation dynamics and canopy height-cover and NDVI changes in the study area.

2.7 Conclusion

In this study, lidar-derived CHM and ΔCHM collected over two decades were used to assist in understanding NDVI trends for some landcovers. The lidar analysis reveals an overall growth and filling-in of vegetation canopy, resulting in increased canopy heights across lidar surveyed areas. Ecotonal vegetation expansion into wetlands in the PAD was largely constrained to marsh riparian areas and river banks/levees that were mostly found adjacent to shrub swamps. These changes are indicative of patterns of shrubification due to drying of wetlands. While in situ soil moisture/ground water levels were not examined in this study, remote sensing data were used to observe drying patterns based on shallow open water MNDWI trends. The disappearance of some ponds after 2000 and the shrinkage of many small shallow open water areas were observed. The NDVI TS and MK z results presented greening patterns indicative of ecotonal expansion, though in most cases, the NDVI trends illustrated larger areas or faster rates of greening (~3.1 m/yr) than was observed in CHM-based ecotonal canopy advance (~2.4 m/yr). While the interpretation of NDVI trends should be approached with caution, this is likely due, at least in some part, to the NDVI response being more sensitive to early or leading edge changes in ecotones than ΔCHM-based approaches. Nonetheless, the spatial correspondence and similarity between the average annual rate of NDVI greening in MK z and ΔCHM-based ecotonal expansion does suggest a high proportion of the observed greening is due to shrubification processes.

NDVI trends showed small but systematic browning over some mature upland forest areas, despite not seeing a significant change in canopy height, which could be a sign of tree mortality, thinning, and/or changes in foliar spectral properties. In addition to enhancing the understanding of NDVI trends and patterns in northern delta systems, the findings of this study also provide preliminary insights into the vegetation dynamics of the PAD, highlighting the varying rates of

vegetation change and ecotonal expansion over two decades. Understanding these patterns is essential for assessing landscape dynamics, identifying areas of significant change, and informing further analysis and decision-making processes. Consequently, the results of this study represent a starting point for further research into the underlying causes of the observed trends and changes across the PAD. Assigning causes and effects to changes in complex deltaic ecosystems is challenging, as by their nature, deltas are in a state of constant spatio-temporal flux with multiple driving mechanisms, feedbacks, and variable response times, all transposed onto a long term changing climate signal.

Chapter 3: 40 Years of NDVI Trends Indicate Vegetation Threshold Response to Hydroclimatic Drivers Across the Peace Athabasca Delta

Abstract

The Peace Athabasca Delta (PAD) in western Canada is one of the world's largest inland freshwater deltas, designated a RAMSAR wetland of global importance in 1982, and situated within the UNESCO-listed Wood Buffalo National Park. It is vital to the traditional activities of the Athabasca-Chipewyan, Mikisew Cree, and Métis Indigenous communities. In this study, we analyzed Landsat trends of NDVI and MNDWI from 1984 to 2022 to determine the change in vegetation and surface water over the past four decades. NDVI trend analysis revealed positive and negative NDVI trends (greening and browning) primarily concentrated near the peripheries of perched basins, each covering around 20% of the entire PAD. The MNDWI trends also showed a wetting (20%) and drying pattern (10%) between 1984 and 2022. However, dividing the time series into smaller timeframes indicated that between 1984 to 1998, the delta exhibited a noticeable wetting trend encompassing Lake Claire, Mamawi Creek, and the lower Embarras River. Subsequently, a marked drying phase occurred between 1999 and 2003, significantly altering the conditions within the PAD. The drying trends persisted until 2017, followed by a resurgence of wet conditions from 2018 to 2022. The primary land cover classes observed across the "spectrally greened perched basins" include shrub swamps and marshes suggesting a pattern of "shrubification" associated with the drying of wetlands in the PAD (11% greening post 1999-2003 vs 5% in pre-1999-2003). The overall average greening rates pre and post 1999-2003 were 2.1 m/yr. and 3.1 m/yr., respectively. Our comparison between temperature and precipitation highlighted prolonged warmer and dryer periods between 1998 and 2002 likely due to the intense El Niño /Southern Oscillation atmospheric teleconnection pattern of 1998. While flooding events

are expected to continue to be a regular feature of this landscape, the extent to which the PAD can return to its historically large areas of persistent inundation remains uncertain.

Keywords Boreal, Landsat Trend Analysis, NDVI, MNDWI, Shrubification, Ramsar, Climate Change

3.1 Introduction

Over the last century, changes in climate, land use, water utilization, and modifications to in-stream flow patterns driven by development have collectively influenced the volume and temporal distribution of water within North American rivers (Prowse et al., 2006b). Rapid climate change and anthropogenic disturbances in western Canada are altering the hydrology of natural ecosystems. For example Hood and Bayley (2008) projected diminished groundwater recharge and wetland loss in the prairie pothole and western boreal regions, attributing these changes to decreased precipitation and elevated temperatures.

Minor fluctuations in precipitation, evaporation, or transpiration, can result in significant changes in surface or groundwater levels (Burkett & Kusler, 2000). These changes can lead to the contraction or expansion of wetlands, the transformation of some wetlands into dry land, or the transition of one wetland type to another (Burkett & Kusler, 2000). Moreover, elevated temperatures during the spring and early summer months may trigger premature snowmelt, extended growing season, heightened evaporation rates, and soil desiccation, particularly if total precipitation does not increase, leading to more frequent and prolonged droughts (Kilpeläinen et al., 2010) and increased fire seasons (Stralberg et al., 2020).

This can potentially transform conifer-dominated boreal forests into deciduous forests, shrublands, or grasslands (Stralberg et al., 2020; Wang et al., 2020). Moreover, elevated

temperatures and more frequent drought events are contributing to the desiccation and reduction in the size of wetlands and shallow open water (Klein et al., 2005; Stralberg et al., 2020). Boreal regions of eastern Canada receive more precipitation and are more resilient to climate change. These forests may transition to temperate mixedwood forests within the southern part of the eastern boreal biome (Stralberg et al., 2020). Along the southern zone of sporadic to discontinuous permafrost, increasing air temperatures have led to widespread thawing, with associated ground subsidence, or thermokarst, which is further exacerbated by wildfires (Gibson et al., 2018). Thermokarst is driving various ecosystem changes, including the conversion of forests into open wetlands, increased drought stress, and declines in lake levels (Stralberg et al., 2020).

Vegetation affects aquifers by directly extracting groundwater from saturated layers while canopy interception reduces the proportion of rainfall or snowmelt available for aquifer recharge (Le Maitre et al., 1999). This suggests that increases in vegetation cover in drying wetlands can further enhance drying and deplete aquifers (Hokanson et al., 2020). Due to their distinct climate, soil, and stand structure characteristics, Canada's Boreal forests are sensitive to drought compared to other forest ecosystems, such that even low-intensity drought events can lead to changes in ecosystem character and functions (Liu et al., 2023; Michaelian et al., 2011; Webster et al., 2015). Hence, it can be inferred that small shifts in available water resources, such as due to climate change, water usage, avulsion events, etc., can significantly affect boreal vegetation and wetlands.

In western Canada, the Peace Athabasca Delta (PAD) is one of the globe's largest and most productive inland freshwater deltas. It includes habitats for thriving communities of various avian species, waterfowl, fish, muskrats, beaver, bison, and moose (Timoney, 2013). In recognition of its significance, the PAD was accorded the status of a Ramsar wetland of global importance in 1982. Moreover, 80% of its expanse falls within the boundaries of the Wood Buffalo National

Park, which has been designated a UNESCO World Heritage Site since 1983. The region also serves as the ancestral land of the Athabasca-Chipewyan, Mikisew Cree, and Métis Indigenous communities, who maintain a deep connection to the PAD ecosystem for their time-honored pursuits of hunting, fishing, trapping, and cultural practices (Wang et al., 2023).

Historically, according to Timoney (2008a), the PAD experienced dry periods, notably from 1845–1848 and 1885–1895, with low water levels, decreased muskrat harvests, and cold conditions. Throughout the last century, dry spells occurred in 1944–1946, 1953–1955, 1980–1985, and 1998–2006 (Timoney, 2008a). While the PAD experienced dry conditions in the past, the current situation is unparalleled in terms of heat and dryness (Timoney, 2008a; Timoney, 2013). Additionally, the presence of a large oil sands industry upstream is a new factor. During the drying periods since the mid-1970s, local inhabitants have observed significant disruptions to both wildlife and vegetation within the delta ecosystem (Wang et al., 2023), including but not limited to heightened delta dynamics resulting from river cutoff, uncertain trends in shrub encroachment, meadow loss, diminished mudflats, fluctuations in the populations of bison, muskrat, and fish in the delta, elevated minimum water levels, and alterations in the frequency of ice-jam floods in the Peace River (Timoney, 2002).

The delta is divided into two major sectors, the Peace and the Athabasca (Figure 3.1). Previous research linked the prolonged periods of dryness in the Peace sector to a decrease in ice-jam flooding along the lower Peace River (Beltaos, 2023; Wolfe et al., 2006a). According to Beltaos (2023), the pattern of drying corresponds with the timing of the Peace River's regulation, initiated through the building of the W.A.C. Bennett hydroelectric dam in British Columbia. This process encompassed the construction (1968), the filling of the reservoir (1968–1971), and the ongoing

operation that commenced in 1972. The dam is positioned approximately 1200 km upstream from the PAD.

Basins situated within the Athabasca sector are primarily refilled through inundation resulting from flooding events along the Athabasca River and its associated distributaries. The Athabasca River itself is not subject to regulation (Beltaos, 2023), although upstream land-use changes have occurred, including agricultural expansion, oil and gas extraction, and forest harvesting (Peters et al., 2022). Pulp mills line the river, and oil sand mining near Fort McMurray started in the late 1960s. Oil sands industry withdrawals constitute the bulk of less than 5% of the annual river flow allocated for water use (Peters et al., 2022). Moreover, its morphology in the vicinity of the Athabasca–Embarras confluence underwent significant alteration due to human intervention in 1972 (excavated a cutoff channel across the neck of a sizable 180-degree meander) and a natural avulsion in 1982 (Beltaos, 2023). The myriad natural and anthropogenic pressures outlined earlier have likely played a significant role in altering the conditions within the PAD. Understanding these dynamics requires a comprehensive study of the evolving state of the PAD over time.

Unlike traditional mapping methods, remote sensing allows for efficient monitoring of large and remote areas, capturing dynamic changes in vegetation, hydrology, and other landscape features (Lillesand et al., 2015). Additionally, it enables the acquisition of data at different spatial and temporal scales, facilitating a more detailed and accurate understanding of the evolving conditions in the PAD. To study changes in the PAD, Timoney and Lee (2016) focused on two deltas on the Athabasca River and one on Birch River (southwest of Lake Claire, Figure 3.1) to evaluate how these deltas expanded through time using aerial photographs, Landsat imagery, and a boundary delineation approach. They used the 1950-derived map as the base map to study the changes. They reported an increase in the area (0.7 km) of the Athabasca sector from 1992 to 2012.

In the case of the Cree Creek Delta, consistent with the historical avulsion pattern, the delta's area remained relatively stable from 1951 to the 1980s. Noteworthy expansion in the Cree Creek Delta's area wasn't observed until after 1992. Subsequently, between 1992 and 2012, the Cree Creek delta significantly expanded in size (Timoney & Lee, 2016).

Timoney and Lee (2016) also suggested that the similar temporal spatial growth pattern observed in Athabasca, Birch, and Cree Creek deltas highlights the expression of a climatic signal across both the Athabasca and Birch watersheds. Climate change has been associated with alterations in hydrology and vegetation (Ström et al., 2011). Warmer climates are expected to change precipitation patterns, with more rain and less snowfall in high northern latitudes, thus altering the hydrology of rivers and streams (Solomon, 2007). As a result of a warmer climate, an increase in winter discharge in boreal rivers is anticipated, as more precipitation is likely to fall as rain. Earlier snowmelt will further lead to earlier and less intense spring floods (Ström et al., 2011). Additionally, the thawing of permafrost due to warming trends impacts the hydrology of the northern boreal zone (Bridgham et al., 1995; Chasmer & Hopkinson, 2017).

These shifts in hydrology are likely to influence riverine vegetation, given their reliance on understanding water flow fluctuations. The arrangement of riparian plant communities is determined by variations in the hydrologic niches occupied by different species (Nilsson & Svedmark, 2002). Substantial shifts in riparian vegetation may occur even in the absence of changes to the mean annual flow, as alterations in both minimum and maximum flows can significantly impact riparian plant communities (Auble et al., 1994). Along boreal rivers, the arrangement of riparian vegetation follows a vertical zoning pattern based on flood tolerance and moisture needs (Nilsson & Svedmark, 2002), and where floods can lead to stress and disturbance

of riparian plants (Auble et al., 1994; Johansson & Nilsson, 2002; Vervuren et al., 2003), thus compromising key physiological processes (Renöfält et al., 2005; Vervuren et al., 2003).

A growing body of research has used passive optical NDVI (Tucker, 1979) derived from satellite imagery to monitor changes in biomass and vegetation productivity in the Arctic and northern areas (Elmendorf et al., 2012; Forbes et al., 2010; Fraser et al., 2011; Ju & Masek, 2016; Olthof et al., 2008; Raynolds et al., 2012). This index is sensitive to the chlorophyll content and canopy structure of plants, making it a useful indicator of photosynthetic activity and overall vegetation health (Tucker, 1979). The positive trend in NDVI or other vegetation indices (VIs) known as 'greening', has been linked with climate warming in high northern latitudes (Berner et al., 2020; Myers-Smith et al., 2020). This prolonged greening or positive trend has been associated with vegetation encroachment (expansion) and increased vegetation growth due to air temperature rise (McManus et al., 2012), as well as correlated with alterations in vegetation cover (Elmendorf et al., 2012), biomass and productivity (Berner et al., 2020; Forbes et al., 2010), and extended plant growing season (Park et al., 2016). Similar positive trends have been observed in northwestern Canada and Alaska by Wang and Friedl (2019). There is also evidence that spectral greening and browning (a negative trend in vegetation indices) co-occur in high-latitude regions with the presence of water bodies (Li et al., 2021a).

Utilizing the Landsat image archive and trend analysis, this study addresses the following questions: 1) What spatiotemporal changes to wetlands and vegetation occurred within the PAD between 1984 and 2022? 2) Which landcovers (woody vegetation or non-woody vegetation) have undergone the greatest changes? 3) Is there a discernible abrupt change to the spatial changes during the time series that suggests either a disturbance or system threshold in the behaviour of the PAD? 4) Whether any abrupt changes have led to altered trend patterns in space or time over the

PAD. Our hypotheses are as follows: H1 - there was a substantial increase in vegetation (greening) within the region; H2 - any change in climate or hydrology will cause an increase or decrease in the NDVI trend observed using remotely sensed data.

3.2 Study Area

Situated at the confluence of the Peace and Athabasca River Deltas (Figure 3.1), along with several smaller deltas at the western terminus of Lake Athabasca, the PAD constitutes a complex deltaic formation (Timoney & Lee, 2016), including open-drainage, restricted-drainage, and isolated basins based on their level of hydraulic connection with the primary flow system. Within the open-drainage basins, alterations in water levels rapidly propagate to nearby lakes or channels. In restricted drainage basins, hydraulic constraints like levees, high-closure channels, or subsurface flow systems lead to a time delay in the basin water level response. Localized aquifer recharge in isolated basins occurs via overland flooding, while declines in water levels are predominantly governed by evapotranspiration (Beltaos, 2023).

The PAD consistently receives substantial inflows of water and sediment from the Athabasca River. On occasion, during ice-jam floods and instances of extreme flow, it also receives water from the Peace River. Moreover, the presence of beaver dams, higher-than-usual precipitation, wind seiches, and the occurrence of spring and summer floods all contribute to the replenishment of water within the floodplain basins (Timoney, 2021).

The delta encompasses three distinct ecosystem types: open water, uplands, and wetlands. Shallow waters less than 2 meters deep are classified as shallow water wetlands rather than aquatic systems (Timoney, 2002; Timoney, 2013). Three of the four largest lakes in the delta, Mamawi, Richardson, and Baril, have mean depths less than 2 meters (Timoney, 2002). *Picea glauca* (Moench) Voss and *Populus balsamifera* L. forests exist on alluvial terraces and elevated levees.

Precambrian bedrock landforms above the delta plain support diverse tree, shrub, and grass communities. The delta proper is further characterized by perched basins, shores, and plains (Timoney, 2002)

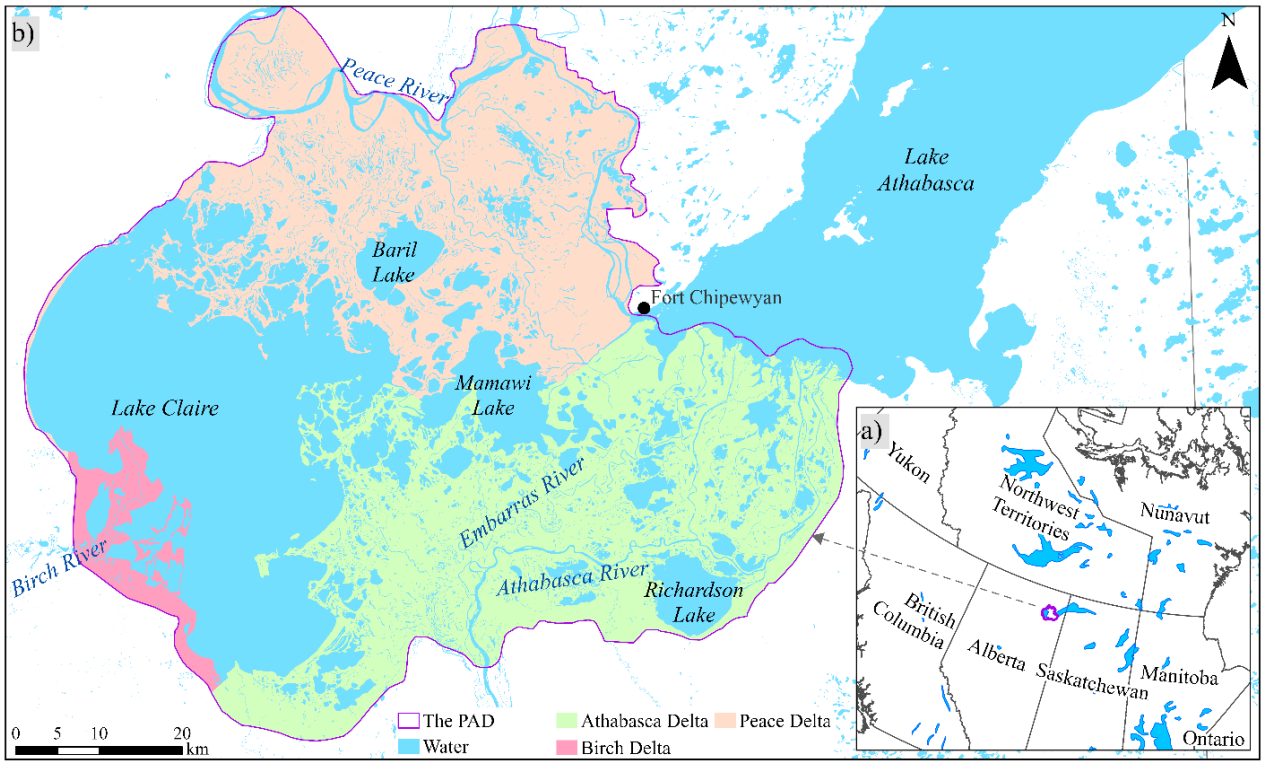

Figure 3.1. a) Location of the Peace Athabasca Delta (PAD) in Canada, b) The PAD and its main sectors, Athabasca Delta, Peace Delta, and Birch Delta. The PAD and its sectors boundaries adapted from Timoney (2013). Water areas adapted from CanVec[1], 2023.

3.3 Data

3.3.1 Climatological Data

To contextualize the study, climate data from climate stations in Fort Chipewyan (Climatedata.ca) were utilized. Specifically, mean temperature and total precipitation measurements spanning the period from 1980 to 2022 were analyzed to discern any significant

[1] Topographic Data of Canada - CanVec Series - Open Government Portal

changes or abrupt shifts in their respective trends. The analysis was based on the water year (October to September), warm season (April to October), and cold season (November to March) assuming these are representative of the climate (Chasmer & Hopkinson, 2017).

3.3.2 Ducks Unlimited Canada (DUC) Landcover

The Wetland Classification provided by Ducks Unlimited Canada (DUC) in the Wood Buffalo National Park was used in this study. The classification conducted using Sentinel-2 imagery from August 2017 and field data. The resulting land cover map boasts a resolution of 10 meters and demonstrates an overall accuracy exceeding 79% (Ducks Unlimited Canada, 2020). According to the map (Figure 3.2), approximately 30% of the PAD is characterized by open water. The next most prominent land cover types include shrub swamp, accounting for around 22.5%, followed by meadow marshes at approximately 17%, and emergent marshes at around 8%. In total, swamp areas encompass 30% of the PAD, while all upland covers collectively constitute approximately 10%.

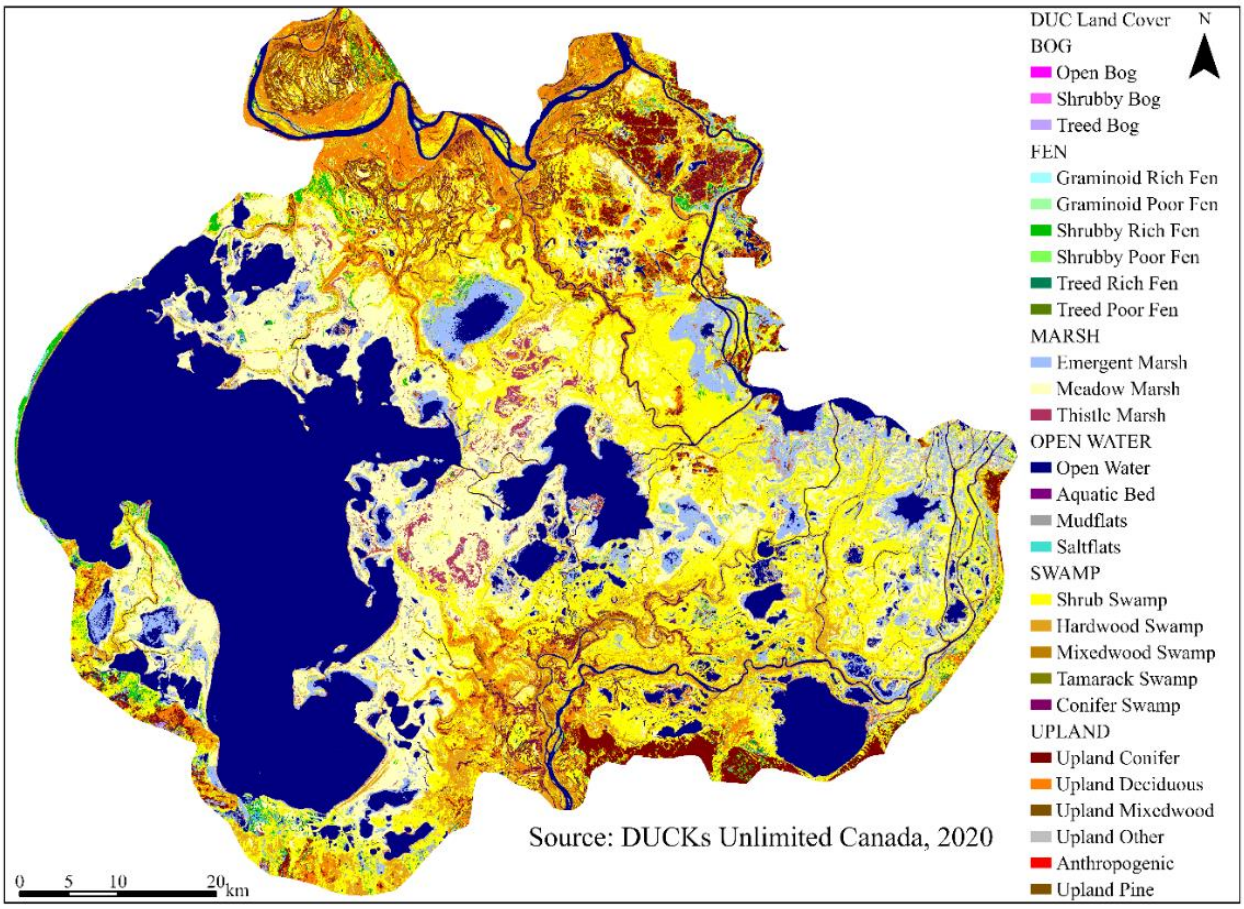

Figure 3.2. DUCKs Unlimited Canada (DUC) land cover map over the Peace Athabasca Delta (Ducks Unlimited Canada, 2020.

3.3.3 Landsat Data

Atmospherically corrected surface level Reflectance Landsat image data (Collection 2, level 2) acquired between 1984 to 2022 (U.S. Geological Survey, 2023) were used as the basis for trend analyses. According to the documentation (USGS, 2021), all Landsat sensors and therefore data processed for Collection 2 undergo inter-calibration to minimize between-sensor differences. To mitigate the Scan Line Corrector (SLC)-off problems of Enhanced Thematic Mapper Plus (ETM+) data, Landsat 5 Thematic Mapper (TM) images were used between 1984 and 1999 and from 2001 to 2011. For 2000 there were no quality TM images so ETM+ images were used (this year does

not have SLC problems). Landsat 8 Operational Land Imager (OLI) image data were used for 2013 to 2022. There were no available cloud-free images for the years 1986, 1995, 2002, and 2012. To minimize the effect of vegetation phenology, only summer season imagery (mid-June to early September) was used to create the annual composites. All composites were reprojected to the NAD83 datum.

3.4 Methods

Time series analysis has proven valuable in various fields, including environmental monitoring, land-use planning, agriculture, disaster management, and ecosystem studies (Asokan & Anitha, 2019). However, it is crucial to emphasize the significance of obtaining cloud-free images to ensure the accuracy and continuity of the time series data. Given the often extensive cloud cover over the PAD, the only viable option was to employ the annual composite technique to generate composite images for each year. Based on the assessment of optimal methods in Chapter 2, the median method (Gumma et al., 2020) of compositing was found to be the most efficient over the PAD, so this was chosen to create annual composites. Before creating annual composites, the QA-RADSAT pixel tags were used to identify and remove saturated pixels (Hemati et al., 2021). Clouds and cloud shadows were removed using QA-PIXEL tags (Crego et al., 2022). Figure 3.3 illustrates the processing framework, and the following sections provide further detail.

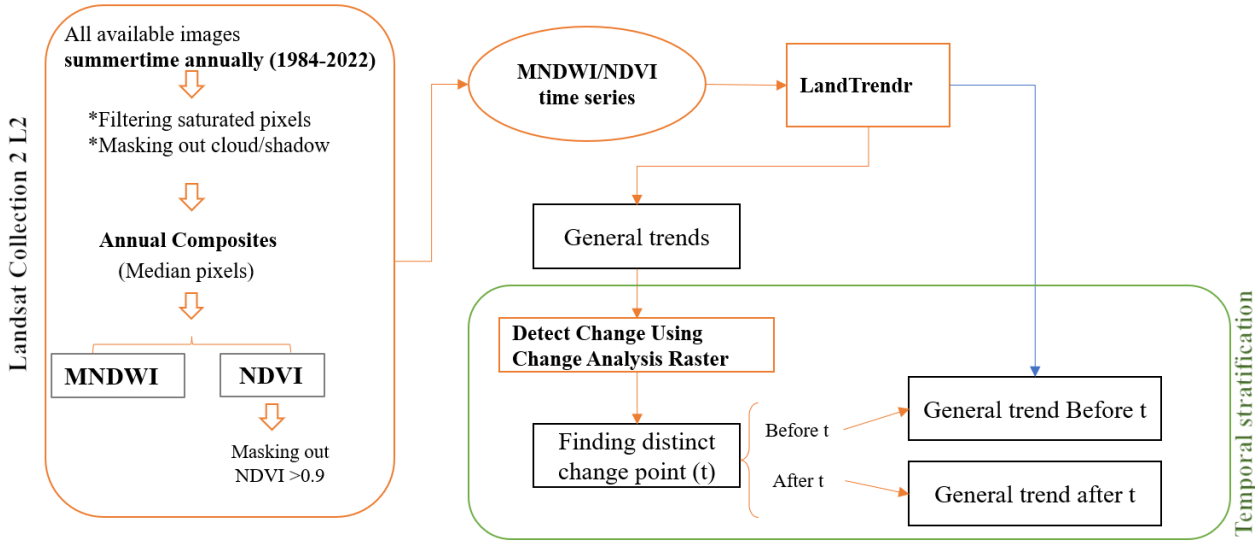

Figure 3.3. The workflow of the study. L2 (Level 2); NDVI (Normalized Difference Vegetation Index); MNDWI (Modified Normalized Difference Index).

The NDVI of each annual summer-time Landsat image was created using red and near-infrared bands [Equation 3.1]. Given the PAD consists of many shallow ponds and lakes (Timoney, 2002), the analysis of surface water trends involved the exploration of various spectral water indices. The goal was to assess their effectiveness in mitigating the impact of sediments and the shallow depth of water bodies on the analysis. After using different thresholds of different water indices, the Modified Normalized Difference Water Index (MNDWI) was used to analyze trends in surface water. This index uses green and short wave infrared (SWIR) bands [Equation 3.2; bands 2 and 5 in TM/ETM+ and Bands 3 and 6 in OLI] (Xu, 2006). All preprocessing of Landsat data was carried out using Google Earth Engine (Gorelick et al., 2017).

$$NDVI = (Near\ Infrared - Red) / (Near\ Infrared + Red) \quad \text{Equation 3.1}$$

$$MNDWI = (Green - SWIR) / (Green + SWIR) \quad \text{Equation 3.2}$$

The Landsat-based detection of trends in disturbance and recovery (LandTrendr) algorithm, a robust technique designed to detect changes in pixel values over time (Kennedy et al., 2010), was used to assess the NDVI and MNDWI trends. By analyzing patterns in time-series data, it can identify and characterize variations in landscapes, offering valuable insights into the dynamics of land cover changes. The LandTrendr algorithm involves extracting the temporal trajectory of each pixel over time, utilizing the pixel values from a specific spectral band or spectral index. This trajectory is subsequently segmented to identify phases of stability, change, and recovery following a change event (Kennedy et al., 2010).

To initiate the LandTrendr algorithm, four primary parameters must be defined. Firstly, the "maximum segments" parameter sets a cap on the number of trend segments allowed during the fitting process. Secondly, the "de-spiking" parameter controls the extent to which single outliers influence the result, with higher values leading to less smoothing but also less effective spike elimination. Thirdly, a "recovery threshold" is established to set the maximum duration of segments that indicate a positive trend. Lastly, LandTrendr necessitates the specification of the "p-of-F value", determining the goodness-of-fit (Dara et al., 2018; Kennedy et al., 2010). Xiao et al. (2020) used LandTrendr for NDVI trend analysis, experimenting with various parameters and ultimately concluding that the default settings were optimal. Another parameter that needs to be set is the Best Model Proportion. During the model selection process, the tool will calculate the p-value for each model and identify the model with the most vertices while maintaining the smallest (most significant) p-value based on the proportion value. A value of 1 signifies that the model has the lowest p-value but may not have a high number of vertices. The default value is 1.25. Contrary to the default setting of 1.25 for the Best Model Proportion parameter, some research studies have found that using a value of 0.75 yields better output results (De Marzo et al., 2021; Esri-

LandTrendr, Accessed in 2022; Hislop et al., 2019; Kennedy et al., 2018; Mugiraneza et al., 2020; Pasquarella et al., 2022) and some used the default (Xiao et al., 2020). All studies cited above opted to use a P-value threshold of 0.05, deviating from the default setting. Several studies opted for varying values of the Maximum Number of Segments, including 6 (De Marzo et al., 2021; Kennedy et al., 2018), 7 (Hislop et al., 2019), and 8 (Mugiraneza et al., 2020), depending on the specific needs of their research. In this study, we assessed different values for these parameters and identified the optimal combination through visual comparison between the individual NDVI values and the LandTrendr results. Table 3.1 provides an overview of the parameter values utilized for LandTrendr parametrization. LandTrendr was implemented within ArcGIS Pro (version 3.0.4).

Table 3.1. The parameter values used for LandTrendr parametrization.

Parameter	Max no. segments	Overshoot threshold	Spike threshold	Recovery threshold	Min observation	Best model proportion	P-value threshold
Value	7	3	0.9 (default)	0.25 (default)	6 (default)	1.25 (default)	0.05

In addition to LandTrendr direct outputs, including magnitude and slope, the multidimensional raster output was used to create the greatest gain and loss maps in both NDVI and MNDWI time series using the Change Analysis raster tool in ArcGIS Pro. For improved observation of changes and accurate calculation of change rates, permanent lakes (Lake Claire, Mamawi Lake, and Richardson Lake) were masked out. The boundaries of the three lakes were established by combining the 1984 shoreline data with the water class information from the DUC land cover map. To assess notable changes in the lake edges, a 200-meter buffer was applied to the lake boundaries. This buffer retained the edges of the lakes while excluding permanent waters from the analysis.

To compute rates of change from NDVI and MNDWI trends, ArcGIS Pro was utilized to establish a set of arbitrary transects. These transects are spaced at equal intervals of 2 km, running parallel to each other. These transects were overlaid onto areas of observed greening or browning for all landcovers to calculate the average rate of change.

3.5 Results

The long-term residual of total precipitation and mean temperature between 1980 to 2022 over water year, warm and cold seasons are shown in Figure 3.4. Overall, regardless of the season, total precipitation has decreased over the PAD. During the warm season, mean temperature has been increasing. Moreover, a prolonged warming period between 1998 and 2001 can be clearly seen in Figure 3.4 *a* and *c*.

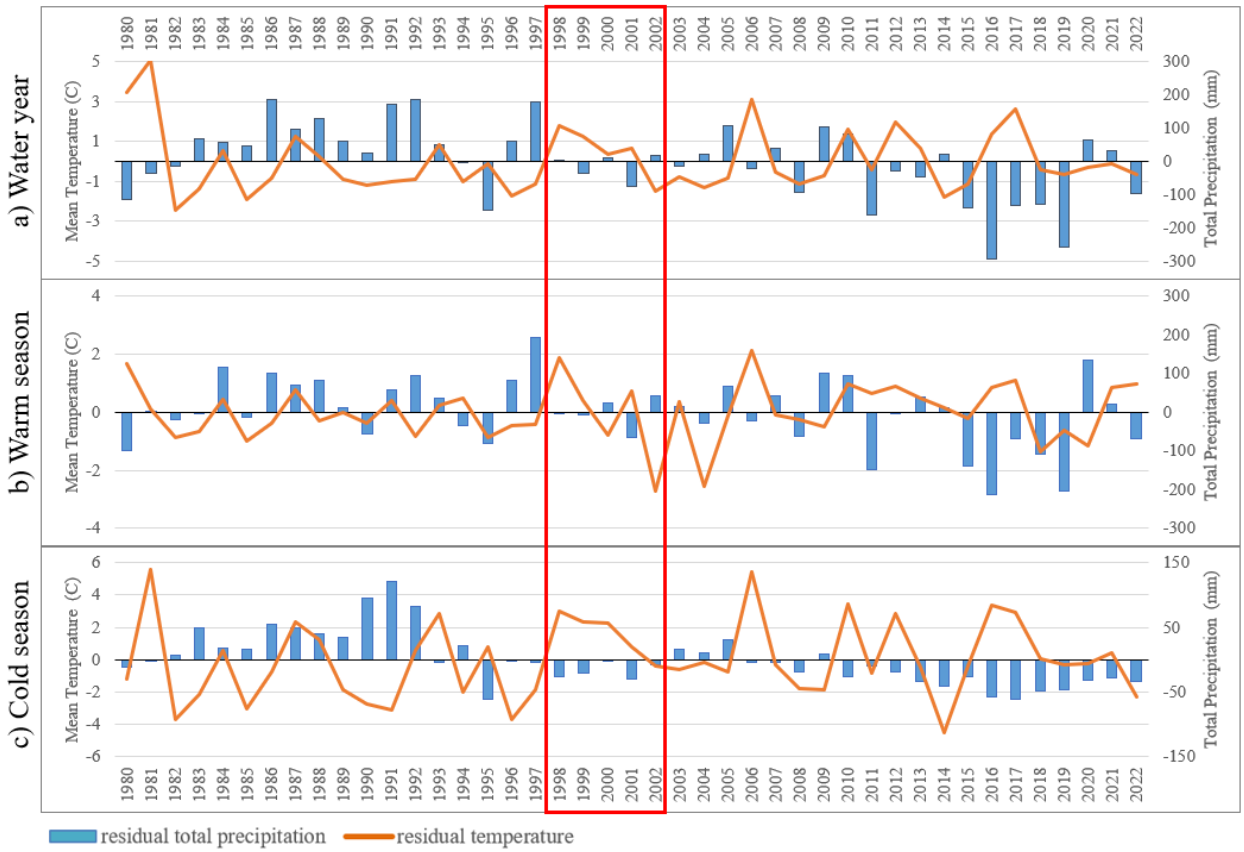

Figure 3.4. Total precipitation and mean temperature between 1980 to 2022 over: a) full water year, b) warm, and c) cold seasons.

The NDVI and MNDWI general trend change magnitudes between 1984 and 2022 are shown in Figure 3.5. The NDVI trend showed slightly positive NDVI or greening mostly near the edges or inside of ponds and lakes. At the same time, the MNDWI trend shows drying trends over some ponds and lakes. There are also some cases (e.g. Otter Lake, southeastern Lake Clair, and south of Mamawi Lake), where NDVI showed a negative or browning trend, and MNDWI trends showed a wetting trend. Both trends indicate that similar areas have witnessed both greening and browning from 1984 to 2022, while also exhibiting an overall wetting trend.

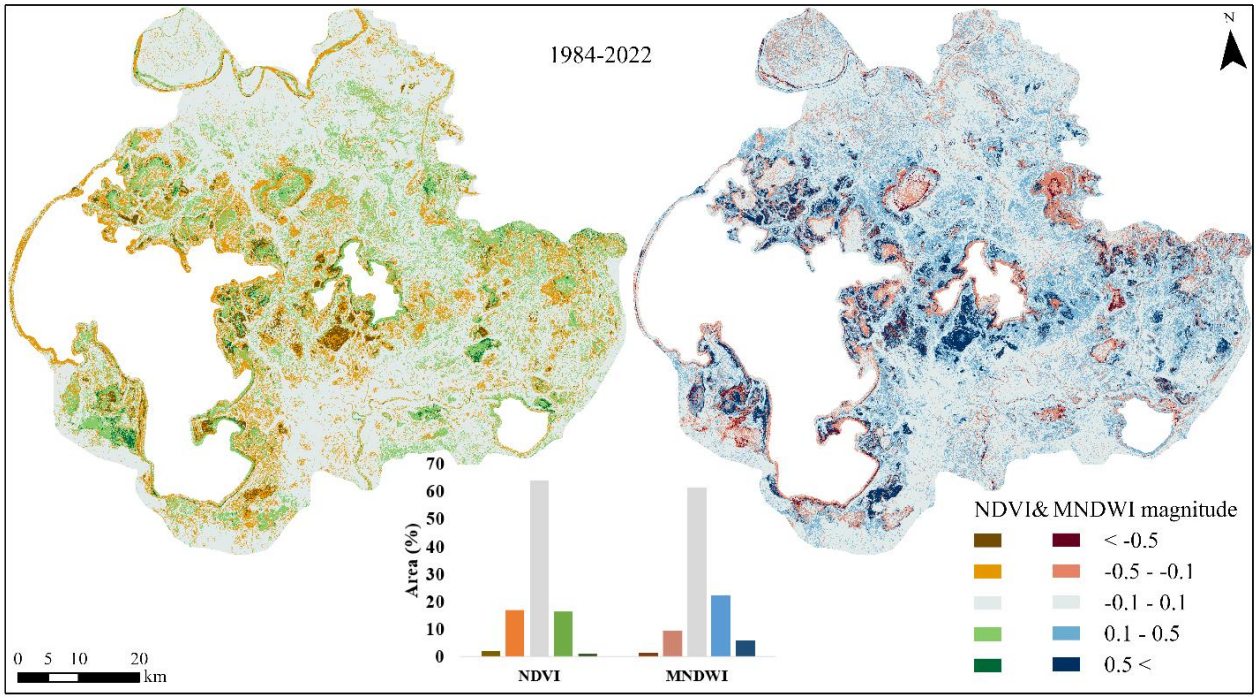

Figure 3.5. Magnitude of NDVI and MNDWI time series trend change between 1984-2022 (permanent lakes, Lake Claire, Mamawi Lake, and Richardson Lake, are masked out). On the left, the magnitude of NDVI trends indicates the degree of greening and browning, represented by green and brown colors. On the right, the magnitude of MNDWI illustrates the extent of wetting and drying trends, denoted by blue and red colors, respectively.

Following the work of Wang et al. (2023) over the PAD, defining seven different periods, including 1984-1988; 1988-1993, 1993-1998, 1998-2002, 2002-2008, 2008-2015, and 2015-2021,

we defined eight time frames with more equal temporal periods of approximately 4 years each that considered the availability of Landsat images, to show NDVI and MNDWI trends over shorter time periods. Those are 1984-1988 (no image for 1986), 1989-1993, 1994-1998 (no image for 1995), 1999-(no image for 2002) 2003, 2004-2008, 2009-(no image for 2012) 2013, 2014-2017, 2018-2022.

As seen in Figure 3.6, a significant drying and greening event occurred from 1999-2003. For example, the entire Baril Lake dried out during this period. Significant drying occurred all around Lake Athabasca and Lake Claire. While in all three periods before 1999-2003, the PAD showed similar trends, with a combination of wetting and drying mainly in the central part of the delta. After 2003, despite not having that significant trend, the PAD started to become greener and dryer.

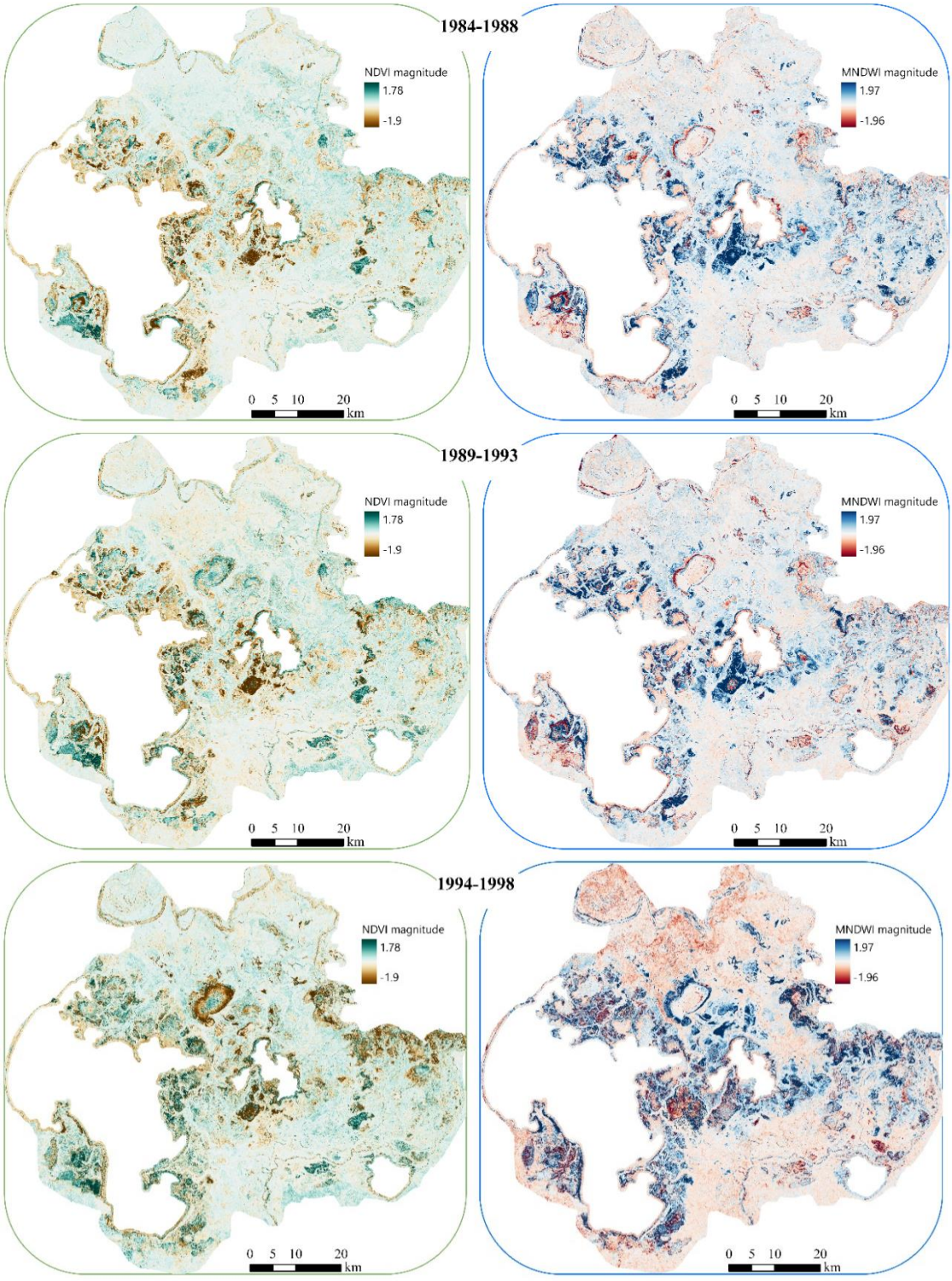
1984-1988
NDVI magnitude
1.78
-1.9
0 5 10 20
km
MNDWI magnitude
1.97
-1.96
0 5 10 20
km
1989-1993
NDVI magnitude
1.78
-1.9
0 5 10 20
km
MNDWI magnitude
1.97
-1.96
0 5 10 20
km
1994-1998
NDVI magnitude
1.78
-1.9
0 5 10 20
km
MNDWI magnitude
1.97
-1.96
0 5 10 20
km

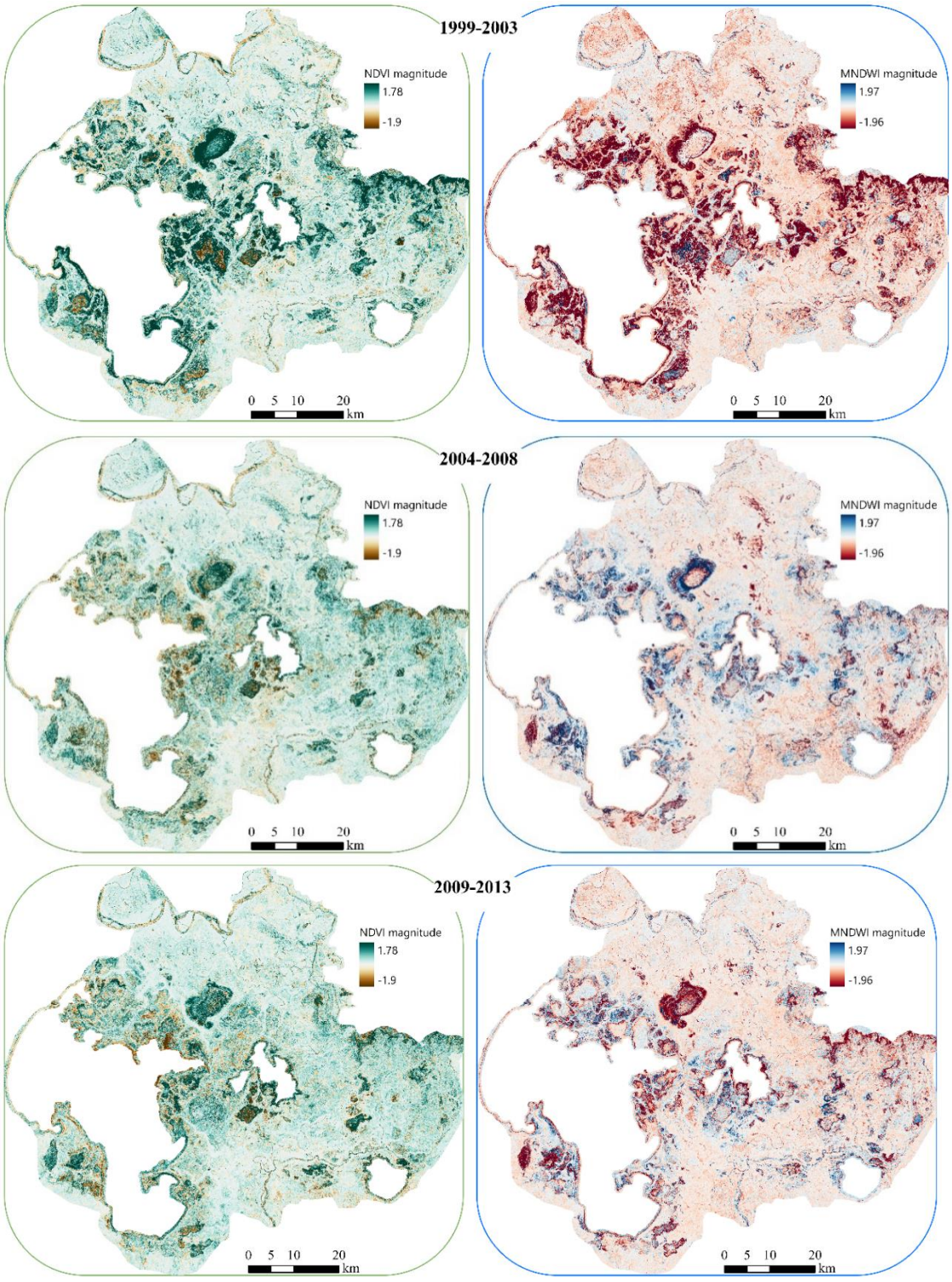
1999-2003
NDVI magnitude
1.78
-1.9
MNDWI magnitude
1.97
-1.96
0 5 10 20
km
2004-2008
NDVI magnitude
1.78
-1.9
MNDWI magnitude
1.97
-1.96
0 5 10 20
km
2009-2013
NDVI magnitude
1.78
-1.9
MNDWI magnitude
1.97
-1.96
0 5 10 20
km

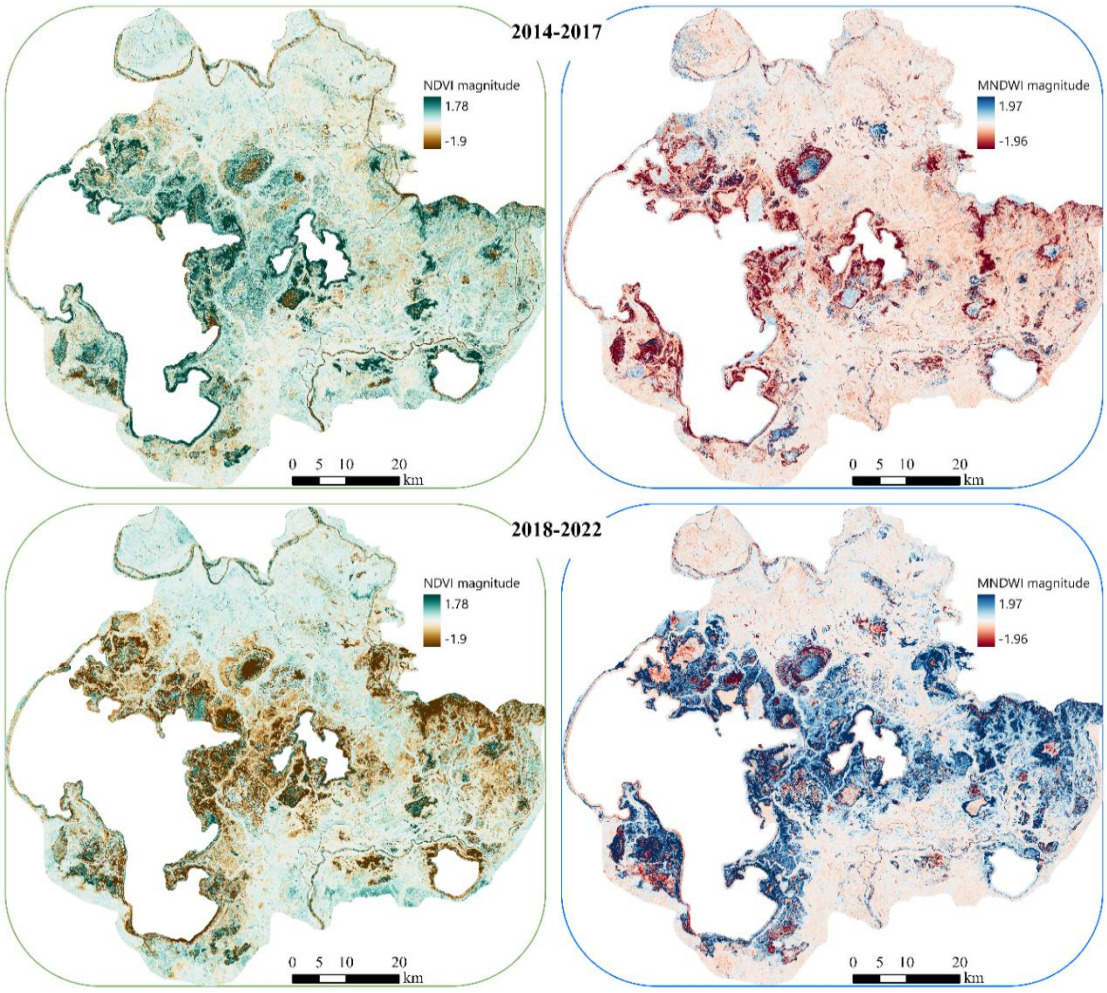

Figure 3.6 (including 2 previous pages). NDVI (left) and MNDWI (right) trend over the study time frames.

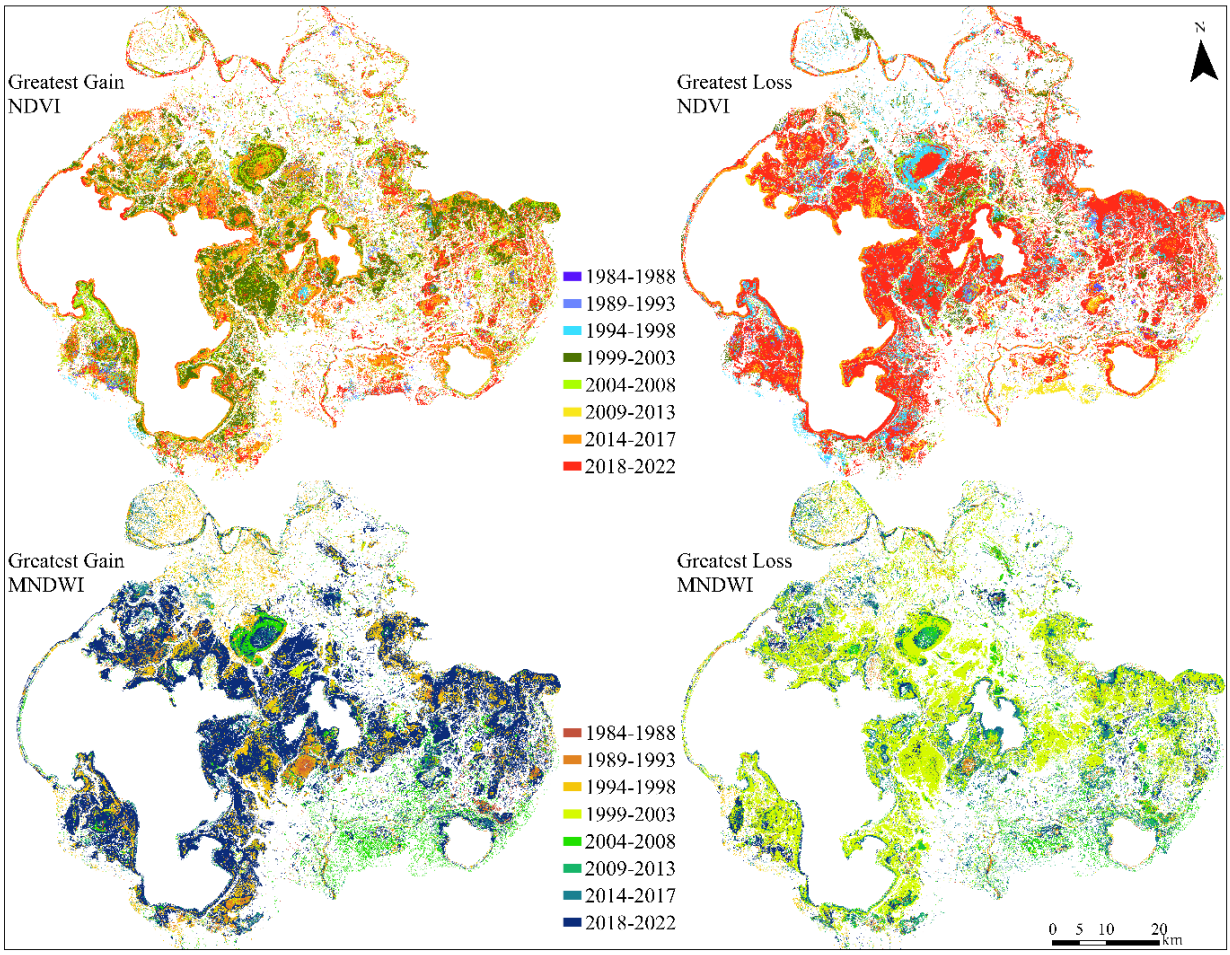

Figure 3.7. The period of greatest gain (increase) and loss (decrease) in NDVI and MNDWI.

To assess whether the apparent shift in the trend was correctly identified using the chosen time periods and LandTrendr, another approach was used by creating change analysis rasters to detect the greatest gain (increase) or loss (decrease) in NDVI and MNDWI. As shown in Figure 3.7, the greatest areal loss in MNDWI occurred during 1999-2003, confirming a significant drying event or interval. Meanwhile, one of the greatest areal gains in NDVI also occurred during 1999-2003, suggesting this was a period of significant concurrent drying and greening. Moreover, the greatest loss in NDVI occurred after 2018 when the MNDWI's greatest gain was detected. Figure 3.8 shows the area of the greatest changes in NDVI and MNDWI magnitudes relative to the time

increments in Figure 3.7. It also shows a significant browning and wetting trend in 2018-2022. Therefore, we identified the 1999-2003 period as one of the significant drying time frames. Figure 3.9 shows the trends magnitudes before (1984–1998) and after (2004–2022), with zoomed-in examples. It also supports greater greening and drying trends after 1999-2003 timeframe.

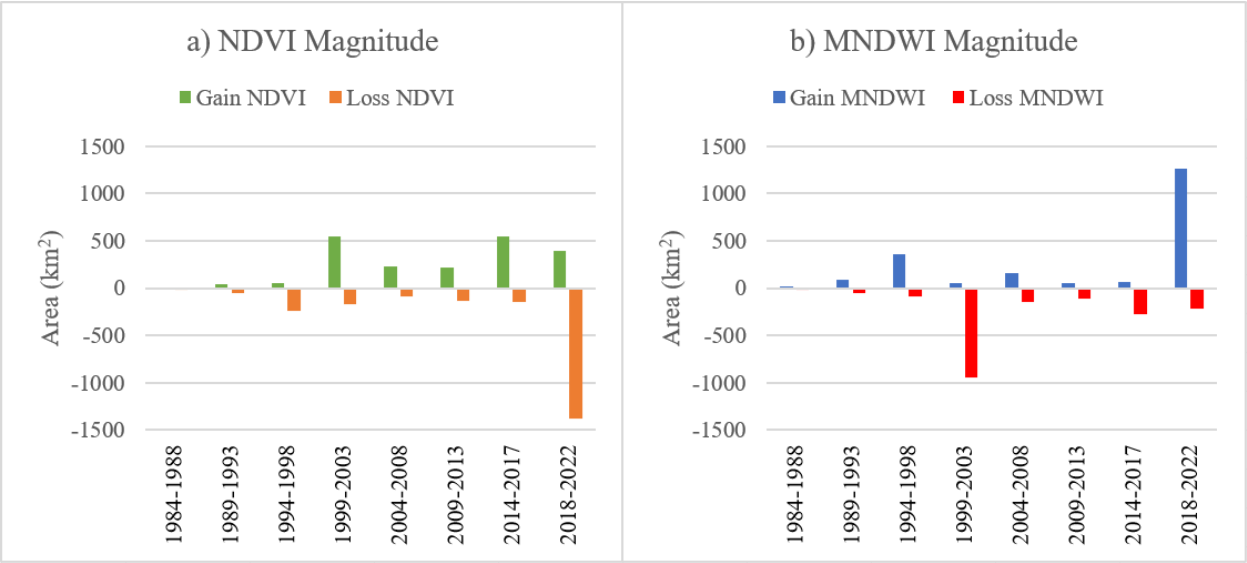

Figure 3.8. The area of a) the greatest gain and loss in NDVI, and b) the greatest gain and loss in MNDWI relative to the time increments in Figure 3.7.

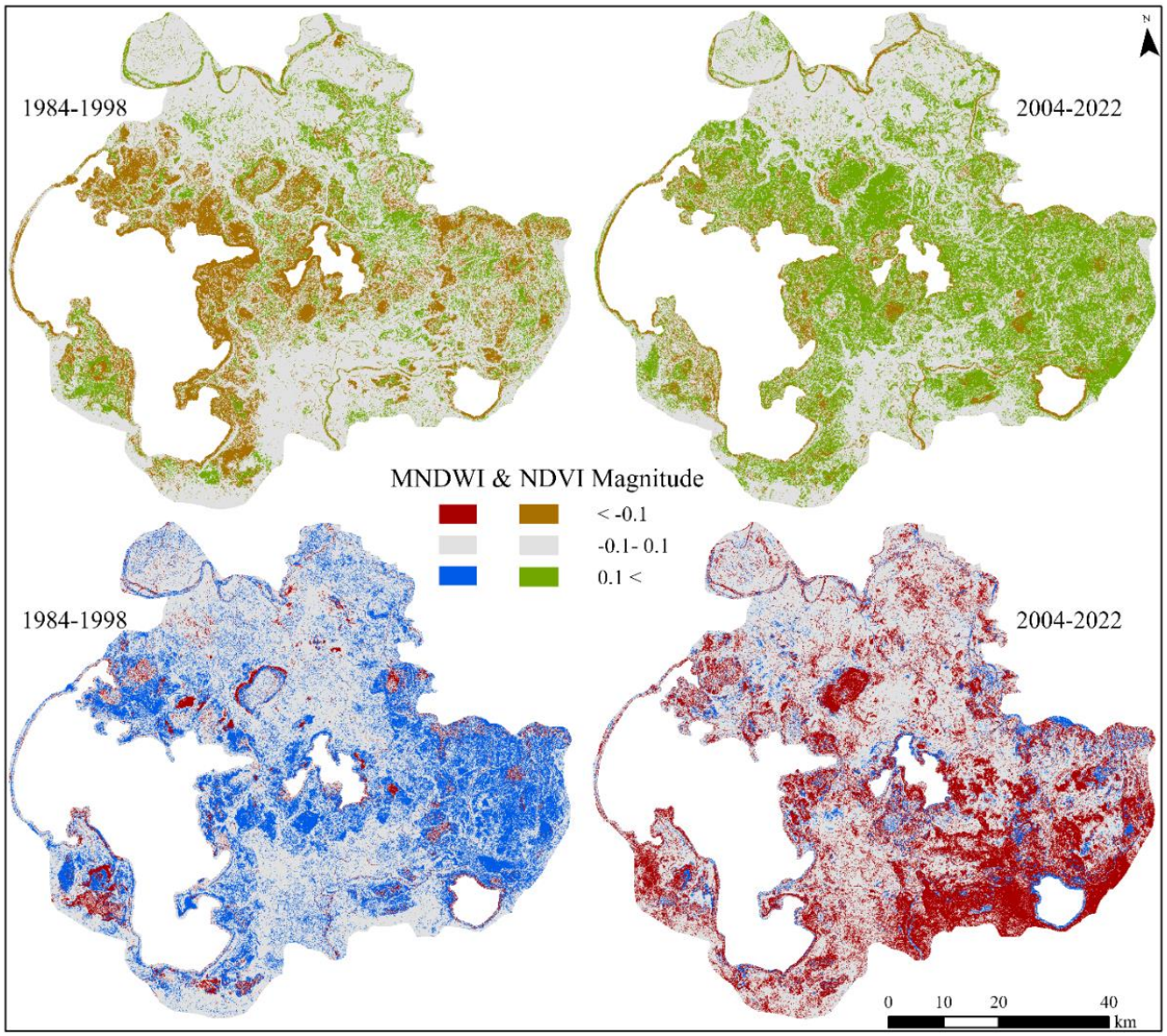

Figure 3.9. NDVI and MNDWI trend magnitudes pre (1984 – 1998) and post (2004 – 2022) the significant drying.

Moreover, Figure 3.10 compares the magnitude differences before and after the observed drying period (1999 to 2003). NDVI magnitude in Figure 3.10 showed a higher increase magnitude in the 2004-2022 period, while showed higher decrease magnitude in the 1984-1998 period. On the other hand, MNDWI magnitude showed significantly higher increase rate in the pre-1999-2003 period and higher decrease in post-1999-2003 period (Figure 3.10).

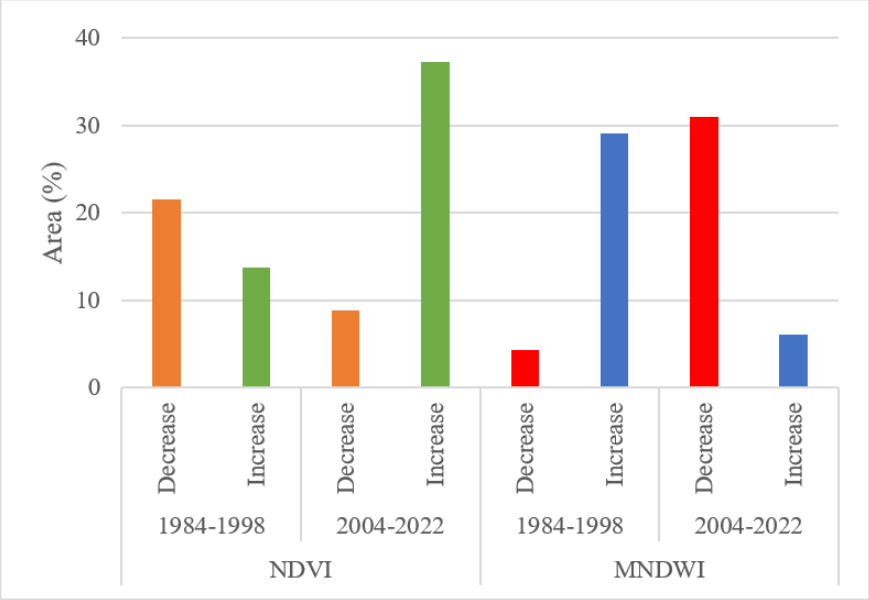

Figure 3.10. NDVI and MNDWI trend change magnitude presented by the relative increase or decrease in area (%).

To gain a more comprehensive understanding of the spatial distribution and extent of observed changes in NDVI and MNDWI trends between pre and post 1999-2002 period, a comparative analysis was conducted across various land cover classes, as illustrated in Figure 3.11. The highest positive NDVI magnitudes were observed over open water, marshes, and shrub swamps, post 1999-2002 period, covering around 10% of the NDVI greening over the PAD (Figure 3.11a). The magnitude of MNDWI before 1999-2002 exhibited a broader spatial coverage of wetting trends compared to the period after 1999-2002 (Figure 3.11b). Comparing these two graphs emphasizes that the most significant NDVI and MNDWI changes occurred over marshes, swamps and open water.

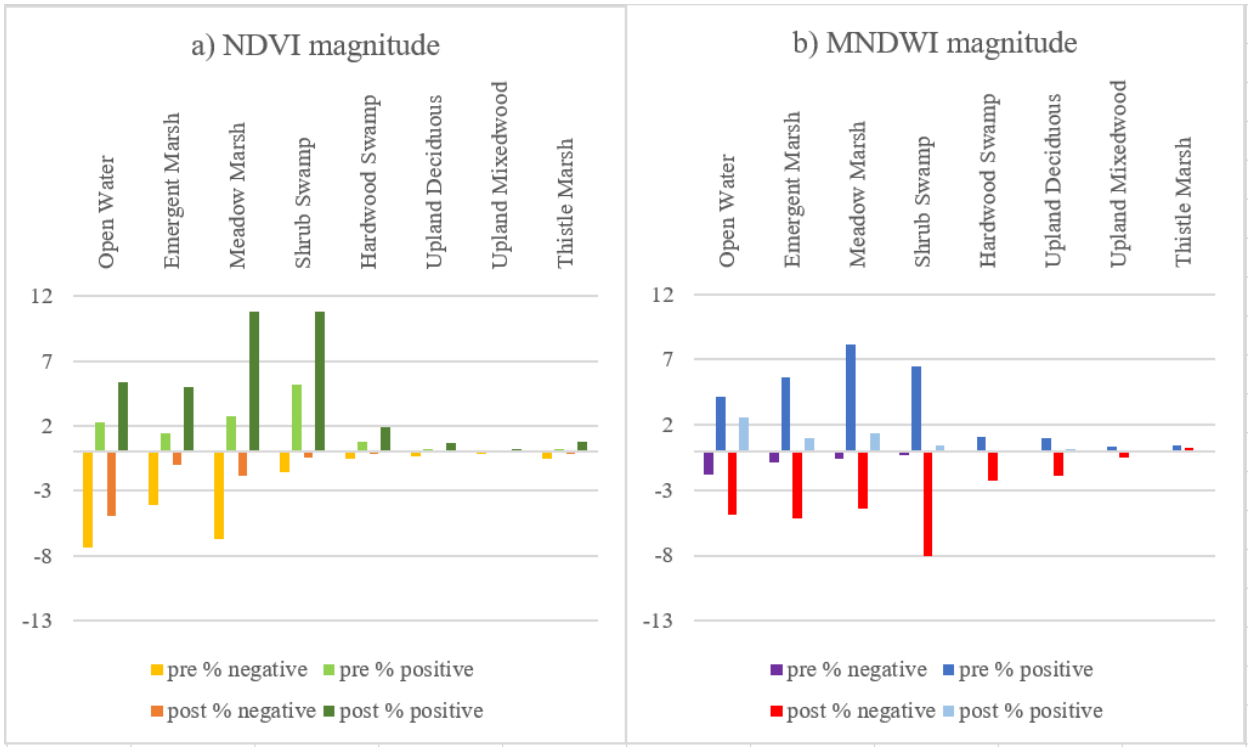

Figure 3.11. Trend magnitudes in: a) NDVI and b) MNDWI over the main landcovers pre and post 1999-2003 period.

Among the landcovers undergoing discernible changes in both NDVI and MNDWI, shrub swamps generally demonstrated the greatest changes. Figure 3.12 shows the magnitude of NDVI trend over shrub swamps pre and post 1999-2003. The average greening rates pre and post 1999-2003 are 2.1 and 3.1 m /year, respectively.

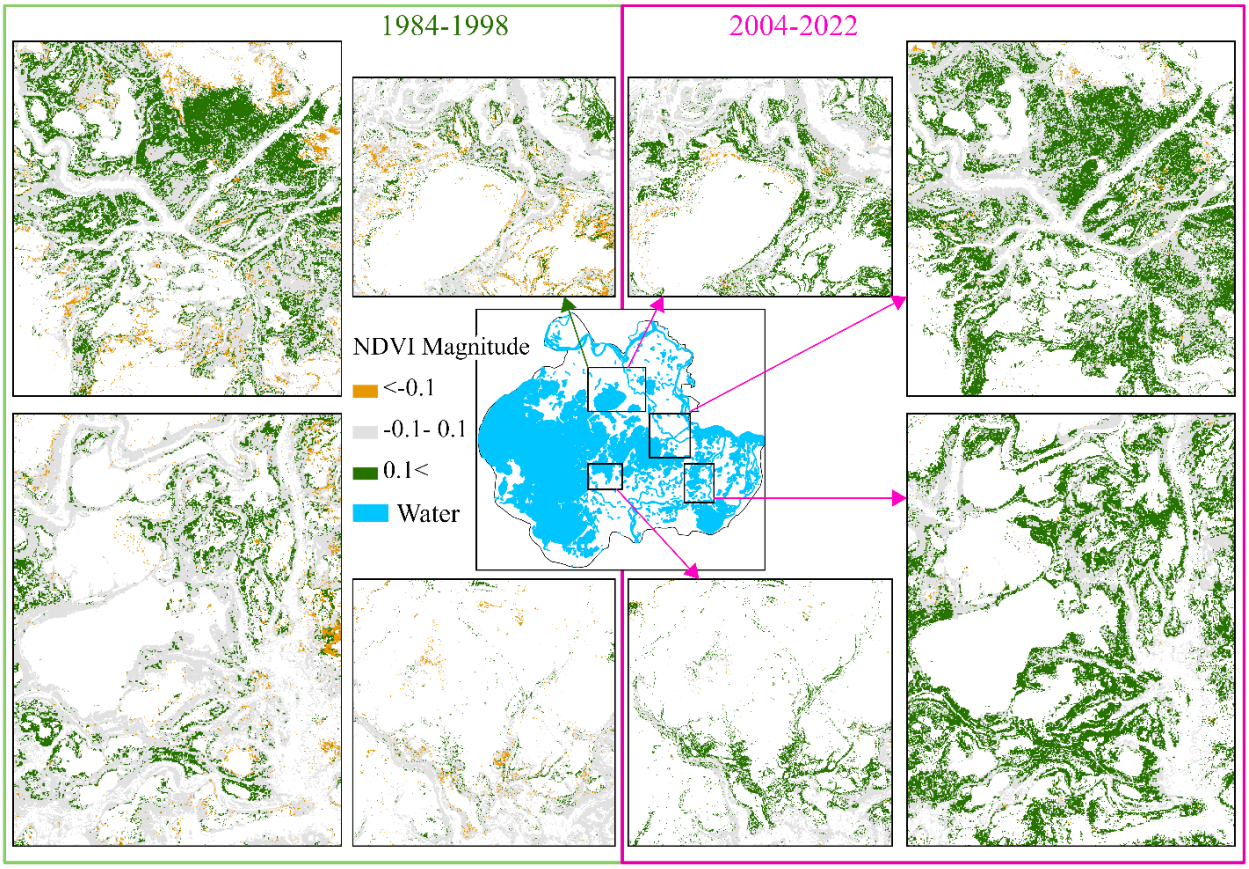

Figure 3.12. Zoomed in examples illustrating NDVI trend magnitudes pre (1984-1998) and post (2004-2022) over shrub swamps. Water in the central map adapted from CanVec, 2023.

3.6 Discussion

Our trend analysis over the PAD has provided valuable insights into the dynamic changes in both vegetation and water over the last four decades. The NDVI trend analysis between 1984 and 2022 reveals a positive NDVI trend or greening, primarily concentrated near the peripheries of perched basins where the MNDWI trends also showed a notable drying pattern. Notably, in specific regions such as Otter Lake, the southeastern area of Lake Clair, and the southern section of Mamawi Lake, we detected instances where NDVI exhibited a negative or browning trend, while the MNDWI indicated a simultaneous wetting trend (Figure 3.5). The primary land cover classes observed across the "spectrally greened perched basins" include shrub swamps and marshes

(Ducks Unlimited Canada, 2020), which is aligned with observations in the smaller sample regions studied in Chapter 2. These shifts suggest a pattern of "shrubification" associated with the drying of wetlands in the PAD. Rodrigues et al. (2023) also reported increases in shrubs in the Upper Columbia River Valley, Canada. In our investigation, a similar phenomenon of shrubification was observed around nearly all ponds and perched basins, with the exception of the regions to the south and southeast of Mamawi Creek.

The same drying and wetting trends were also reported by Wang et al. (2023) who indicated that the Athabasca River is currently undergoing a gradual shift in its course due to the 1982 avulsion in adjacent Mamawi Creek. Similarly, in line with our research (Figure 3.5), previous studies have documented corresponding drying trends in the lower Embarras River and the lower Athabasca River. Moreover, notable drying has been reported in the vicinity of the Peace River, particularly northwest of Mamawi Lake (Wang et al., 2023). Additionally, they observed a significant yet marginal increase in inundation along the Athabasca-Embarras avulsion course (Wang et al., 2023). Our findings revealed similar patterns of wetting trends in those areas, albeit more extensive and encompassing a larger geographical area (Figure 3.5). Kay et al. (2019) in their paleo-hydrological study also documented an escalation of flooding in the Mamawi Creek region, along with diminished flooding along the lower Athabasca River, attributing these variations to the 1982 avulsion. Our findings corroborate their assertions and additionally show that the lower Embarras River experienced a wetting trend between 1984 and 2022.

The calculation of the greatest gains and losses in NDVI and MNDWI observed in our study (Figure 3.7) is consistent with the findings of Wang et al. (2023). Segmenting the study period into sub-periods provided interesting insights. The investigation of the spectral indices has enabled us to identify significant trends, particularly shedding light on the occurrence of a noteworthy drying

event from 1999 to 2003 that is in line with the findings of Wang et al. (2023) demonstrating significant expansions in the Athabasca and Mamawi deltas. Hopkinson et al. (2020) also showed a shift in hydroperiod inundation regime after 2002 in the Upper Columbia wetlands, Canada, using Landsat-derived NDVI and MNDWI between 1984 and 2019. Our finding showed that between 1984 to 1998, the delta exhibited a noticeable wetting trend encompassing Lake Claire, Mamawi Creek, and the lower Embarras River. Subsequently, a marked drying phase occurred between 1999 and 2003, thus altering the conditions within the PAD. The drying trends persisted up to 2017, followed by a resurgence of wet conditions from 2018 to 2022 (Figure 3.6).

Additionally, our study did not identify any divergent trends in NDVI or MNDWI across the Peace and Athabasca sectors. Both sectors exhibited similar greening trends, except for the Mamawi Creek section. Previous studies have reported declining ice-jam flooding on the lower Peace river which is an important reason for the drying in the Peace delta since the 1970s (Beltaos et al., 2006; Töyrä et al., 2002). Wang et al. (2023) observations indicated that besides the effects of reduced ice-jam flooding in the northern PAD, the inundation patterns in the southern PAD have also impacted regions that were not traditionally affected by ice-jam floods. Timoney and Lee (2016) through the construction of river discharge and sediment histories to examine alterations in the subaerial extents of the Cree Creek and Athabasca River Deltas (both located on the Athabasca River system) as well as the Birch River Delta from 1950 to 2014 found that temporal growth patterns displayed similarities across the deltas suggesting a common prevalent climatic signal. Their results showed limited or negligible areal growth from 1950 to 1968, followed by moderate growth between 1968 and the early to mid-1980s, and significant rapid growth from 1992 to 2012 (Timoney & Lee, 2016). Our study found that the rapid growth actually occurred during the dry period from 1999 to 2003.

Our comparison between temperature and precipitation highlighted prolonged warmer and dryer periods between 1998 and 2002 (Figure 3.4). Chasmer and Hopkinson (2017) also underscored notable alterations in air temperature, precipitation, runoff, and a reduction in the duration of the snow-covered season post-1997 within a southern Taiga Plains watershed in the Northwest Territories, Canada (<3 degrees of latitude north of the PAD). This was attributed to the combined impact of the warm phase of the Pacific Decadal Oscillation (PDO), frequent warming modes of the North Atlantic Oscillation (NAO), increased Southern Oscillation prevalence (the atmospheric aspect of El Niño, ENSO). When considered alongside the North Atlantic Oscillation, the ENSO accounted for nearly 50% of the air temperature variability in the Northern Hemisphere during the winter, including warmer and fewer cold periods (Chasmer & Hopkinson, 2017). Furthermore, Timoney (2009) emphasized the year 1998 as a warm year with the lowest winter snowfall (79 cm below average). Figure 3.4 showed that 1998 to 2001 was a period of prolonged higher mean temperatures and lower total precipitation than the long-term mean. It was also reported that 1999 experienced elevated temperatures and the third-lowest winter snowfall (66 cm below average) (Timoney, 2009). The period 2005-2006 is recorded as the warmest in Canada since record-keeping began in 1948 (Timoney, 2009). The Fort Chipewyan climate data highlighted 2006 as having the highest summer season temperature between 1984 and 2022. Peters et al. (2013) reported the highest mean air temperature and low precipitation in the Athabasca River in 1998.

In a multi-scale hydroclimatic study of runoff generation in the Athabasca River mainstream by Peters et al. (2013), an extended period of reduced annual runoff was observed between 1998 and 2002 (Figure 2d in Peters et al. (2013)). Based on Timoney (2021), the Athabasca and Peace Rivers both encountered a rapid decline in mean annual flow in 1998, after a notable increase in

1996 and 1997. However, both rivers experienced an extended period of reduced flow from 1998 to 2003 (Timoney, 2021), which aligns with the period identified in our study as the driest. Timoney (2021) reported notable spring flood events in 2014, 2018, and 2020 and Figure 3.7 shows the greatest gain in MNDWI after 2018 possibly due to the flood in 2020 (Desrochers et al., 2023).

ENSO produces interannual variations in the tropical thermal circulation, influencing atmospheric circulation and causing regional climate impacts beyond the tropics, including North America, through teleconnection effects that alter normal precipitation and temperature patterns (Li & Kafatos, 2000). Consequently, such events can impact entire ecosystems and contribute to disastrous weather events by changing key climatic factors (Zhao et al., 2020). Numerous studies have explored the connection between NDVI and ENSO in core impact regions like Africa (Anyamba et al., 2001; Propastin et al., 2010), the Amazon (Nagai et al., 2007), Indonesia (Erasmi et al., 2009) and China (Zhao et al., 2020). Lü et al. (2012) noted that vegetation response to El Niño events varied across different ecosystems in China, with grasslands and shrubs identified as the most sensitive areas. In the PAD, the most notable changed land cover occurred over swamps, marshes, and shallow open water.

Based on our observations, there is some evidence to suggest that the long-term systemic hydro-ecological behaviour of the delta was disrupted following the 1998/1999 El Niño. The prolonged intense dry period may have moved parts of the PAD into a threshold or tipping point state where the long-term interactions between wetland hydroperiod and surrounding vegetation were altered and an accelerated ‘greening’ phase initiated. A threshold is characterized as a juncture at which there is a sudden and significant alteration in ecosystem features or processes (such as

productivity, structure, or composition), or where minor shifts in critical environmental factors result in substantial changes within an ecosystem (Carter Johnson et al., 2016).

The water regime (water level change, timing, groundwater depletion, damming, water table depth, flood duration, and frequency, shift in surface flow from permanent to intermittent, etc.) serves as the primary controlling factor in regulating wetlands, frequently acting as the principal driver of threshold behaviors and state shifts (Carter Johnson et al., 2016; Larsen & Alp, 2015). Moreover, sediment supply, climate-driven changes in the phenology and distribution of important riparian species are also inter-related factors (Larsen & Alp, 2015).

Prior to 1998, the combination of a declining precipitation trend, potential influences of flow regulation or upstream resource extraction activities, and gradually increasing growth of woody vegetation, is thought likely to have resulted in lowered the groundwater tables. The warm dry year of 1998, would then likely result in heightened evapotranspiration, diminished soil moisture, and greater demands on groundwater, therefore drying out many wetlands (Carter Johnson et al., 2016). Combined with already diminished local water tables and surface water, the length of the dry period allowed woody vegetation to grow and spread at a faster rate than in the earlier time frame. This resulted in the observed pronounced greening trends post-2003.

We suggest that an accelerating encroachment of woody vegetation is both indicative of and due to a systematic lowering in water tables within the PAD. A decline in water table enhances the potential water storage capacity for future floods, while the expansion of woody biomass ecotones accelerates evaporative fluxes to the atmosphere. These systemic alterations in hydro-ecological behaviour are therefore expected to lead to reduced flood persistence and associated wetland hydroperiods.

Alterations in water table levels and the rate of water flux may impact the availability of water resources for local populations. Therefore, residents in the PAD or nearby may need to adapt to shifting water patterns, requiring community planners to develop strategies for managing water resources, enhancing flood resilience, and ensuring sustainable living conditions. Altered water levels and vegetation dynamics in the PAD can shift habitat suitability, impacting species distribution and interactions. Changes in flooding patterns may affect breeding and nesting sites, influencing predator-prey relationships. Disruptions to migratory corridors can alter seasonal movements of certain species. Altered vegetation and water dynamics may affect ecological processes, influencing services like water purification and flood regulation. Biodiversity faces challenges in adapting to rapid changes, placing less adaptable species at risk. Continuous research and monitoring are crucial for informed conservation strategies within the PAD.

3.7 Conclusion

The PAD is an intricate and interconnected ecosystem, displaying variability across a range of spatial and temporal scales, from less than an hour to thousands of years. Although it may be natural to observe the delta within the context of human experience, this perspective prevents a comprehensive understanding of its intricate dynamics in space and through time (Timoney, 2009). In this study, we leveraged the longest accessible and consistent satellite image archive over the PAD to gain insights into the delta's transformations over the last four decades. We observed that the PAD has undergone significant spectral greening, particularly following an intense drying period after 1998, which may be associated with the El Niño phenomenon. The main land cover categories identified within the "spectrally greened perched basins" encompass shrub swamps and marshes, which had the highest changes in MNDWI trends as well, emphasizing shrubification.

We propose that the initiation of the El Niño event in 1998, followed by the warm dry period up to 2001, initiated a shift in the hydro-ecological system dynamics. This shift is marked by a tendency for accelerated loss of landscape moisture, an extended growing season, and the expansion of woody ecotones into areas that were previously frequently inundated. It is important to note that this suggested change in system behavior doesn't contradict the cyclic nature of annual or periodic flooding and gradual drainage. Instead, it suggests that the period since 2003 may have been characterized by more rapid surface water losses through infiltration, evaporation and evapotranspiration from standing water bodies, wetlands, and expanding vegetated ecotones across the PAD. We conclude that in the future the delta may experience an overall decrease in moisture levels, and an increase in vegetation canopy and shrubs, while specific areas, such as the southern region of Mamawi Lake, could become wetter and show signs of spectral browning. While large-scale flood events are expected to continue, the extent to which the PAD can return to historical levels of persistent inundation remains uncertain and requires further assessment and long term simulation.

Chapter 4: Conclusion

4.1 Introduction

In the past century, climate shifts, land use changes, water use variations, and alterations to in-stream flow patterns from development have collectively impacted the volume and timing of water in North American rivers (Prowse et al., 2006). Monitoring vegetation changes in boreal wetlands is crucial for understanding the intricate dynamics of these ecosystems and their critical role in global biodiversity and climate regulation. In Western Canada, the Peace Athabasca Delta (PAD) is one of the world's largest and most productive inland freshwater deltas consisting of lakes, wetlands, and upland forests. The PAD is also home to Indigenous people who depend heavily on the resources provided by these wetlands for their cultural and economic sustenance (Hylton, 2023). Changes in vegetation patterns can impact traditional practices such as hunting, gathering, and cultural activities, thus affecting the overall social fabric and livelihoods of these communities. Understanding shifts in vegetation cover and any potential impacts on the ecosystem services these wetlands provide is crucial for developing sustainable management strategies and ensuring the preservation of indigenous cultures (Ford et al., 2020).

Previous research has highlighted the critical importance of monitoring vegetation changes in boreal wetlands generally, and over the PAD, in particular. Recent studies, such as by Wang et al. (2023) and Timoney (2021), have emphasized the significance of tracking ecological shifts in these delicate ecosystems, underlining the complex interplay between vegetation dynamics, climate change, and the well-being of indigenous communities. Monitoring and understanding these changes is key to preserving the ecological integrity and cultural heritage of these vital northern regions. Nevertheless, the absence of extensive field observation data has constrained our ability to conduct comprehensive spatially continuous analyses of vegetation trends across the PAD.

While the Landsat image archive from 1984 onwards provides an opportunity to evaluate vegetation distributions and trends, the lack of spatial or temporal representation in ground truth data limits confidence in achievable assessments. Therefore, in this study, efforts were made to extract and understand observed landscape change trends over the PAD using airborne lidar and the Landsat image archive.

Landsat imagery encompasses the longest continuous archive on Earth for monitoring land surface change. One of the most common methodologies for studying vegetation trends with Landsat involves the application of spectral indices, with NDVI being the most widely utilized. Positive NDVI trends are commonly interpreted as 'greening', however, the relationship between NDVI values and trends and changes in biomass or growth conditions across different boreal wetland land covers (e.g., marshes, shrubs, forests) is unclear. Thus, the initial phase in analyzing trends across the PAD involved gaining a deeper understanding of NDVI derived from Landsat data. Here, the first two objectives focused on exploring the correlation (or lack thereof) between NDVI and canopy height over lidar survey sample areas to aid in interpreting NDVI and any trends across boreal deltaic wetlands and similar northern landscapes.

4.2 Objective Outcomes

4.2.1 Objective 1 – NDVI vs CHM

Objective 1 of this study was to determine if, by how much and where spatial variations in NDVI correspond with spatial variations in canopy height. The hypothesis posited that there was a relationship between NDVI and CHM (which at low resolution is also an index of canopy cover) across land cover classes. Only over a few land covers, including shrub swamp, upland conifer, and mixed wood, did comparisons between height and NDVI result in elevated and meaningful R^2 values (0.38, 0.46 and 0.48, respectively), suggesting a moderate level of covariance between

NDVI and CHM. To some degree, taller vegetation generally corresponds with increased foliage cover (Rijkers et al., 2000), leading to increases in the quantity of green vegetation observed from above.

The observed weak correlation between Landsat NDVI and shorter vegetation types is likely attributable to diminished canopy cover and increased influences from soil, moisture, and other factors (Piedallu et al., 2019). These two distinct datasets exhibited a weak correlation over upland deciduous areas (characterized by tall forest vegetation), potentially due to lower crown density or a greater capacity to scatter a larger portion of incoming light, resulting in a darker (less 'green') appearance (LaRue et al., 2018).

4.2.2 Objective 2 - NDVI Trends vs CHM Change

Objective 2 was to evaluate how changes in canopy height manifest in NDVI trends. The hypothesis was to see a significant greening trend in shrubs and taller canopy over the PAD between 2000 and 2018, which is supported in the study. Despite the lack of *in situ* data or vegetation validation plots, our conclusion, drawn solely from CHM changes in various strata, indicates occurrences of both shrubification and tree growth in many areas. Additionally, over more than half of each surveyed area, no changes were observed. Significant positive greening in NDVI was notable in the transition from marshlands to shrub swamps or levees, suggestive of shrubification, which corroborates results of Timoney (2008b), who highlighted the greatest changes in vegetation occurred in marshes between 1945 to 2001. However, the comparisons between bitemporal ΔCHM and NDVI trends reveal few similarities between the two datasets.

Given the identified moderate correlation between NDVI and CHM over shrub swamps, observed similarities between bitemporal ΔCHM and NDVI trends, and the enhanced visibility of NDVI trends over shrub swamps through visual comparison, a more detailed examination into

lidar-derived ecotonal expansions was pursued. Despite non-correspondence between the ΔCHM and the NDVI trends, positive NDVI trends correspond with ecotonal expansion patterns observed in PCT90 ΔCHM. The lateral expansion of ecotonal vegetation into wetlands within the PAD was found to be limited to specific areas such as marsh riparian zones and river banks/levees. Comparing ecotonal expansion areas over landcover classes pointed out that 65% of the ecotonal expansions occurred along the edge of shrub swamps or into marshes from adjacent swamps, equivalent to around 5% of the total survey area. The average rate of greening and expansion per year in both NDVI trends and PCT90 ΔCHM were close at 3 m/yr. and 2.4 m/yr., respectively. Additionally, the disappearance of several ponds after 2000 and a noticeable shrinkage of numerous small shallow open water bodies were documented after analyzing MNDWI-derived water maps and trends, mostly synchronous to areas of greening, thus demonstrating the area is undergoing a process of drying out. All these findings provided sufficient grounds to posit that NDVI trends indicate a process of shrubification due to the desiccation of wetlands across the PAD. This knowledge can be extended to not only the region of the PAD but also similar landscapes.

When comparing NDVI trends with CHM-derived ecotonal changes, care must be exercised interpreting the changing patterns of NDVI in space and time. Proximal or regional influences, beyond those that are directly associated with wetland–upland ecotones, need to also be considered as potential contributors to broader greening trends.

On the other hand, in certain mature upland forest areas, negative NDVI trends indicated a subtle yet consistent browning effect. This change in vegetation coloration was observed despite the absence of any significant alterations in canopy height. The browning effect might signify various influences, including potential tree mortality, canopy thinning, or shifts in foliar spectral

properties, which warrant further investigation to better understand the underlying ecological processes at play in these specific forested regions. In this case, it is hypothesized that upland canopy mortality in areas of lowering water table is a likely factor but this needs to be tested.

4.2.3 Objective 3 - NDVI/MNDWI Trends 1984- 2022

Upon gaining a better understanding of NDVI through objectives 1 and 2, objective 3 was to analyze NDVI and MNDWI trends across the entire PAD to study general patterns over the four-decade period. The NDVI trend analysis between 1984 and 2022 reveals an overall positive NDVI trend or greening, primarily concentrated near the peripheries of, or ecotones surrounding, perched basins where the MNDWI trends also showed a notable drying pattern. This was interpreted as evidence of shrubification. In some places, we detected instances where the NDVI exhibited a negative or browning trend, while the MNDWI indicated a simultaneous wetting trend. However, an examination of the spatial extent (area) of greening and browning observed across the entirety of the delta revealed that an equivalent proportion of the landscape (20% of the entire delta, excluding the main lakes) has tended to naturally cycle between greening and browning periods from 1984 to 2022.

4.2.4 Objective 4 - Abrupt Change in NDVI and MNDWI Trends

Objective 4 was to identify any potential abrupt change between 1984 and 2022. This was evaluated through examination of LandTrendr outputs. This allowed us to detect a significant period of extensive drying spanning 1999 to 2003, corroborating the findings of Wang et al. (2023). A comparison between temperature and precipitation highlighted prolonged warmer and dryer periods between 1998 and 2002, which point to a combined influence of the warm phase of the Pacific Decadal Oscillation (PDO), frequent warming modes of the North Atlantic Oscillation

(NAO), increased Southern Oscillation prevalence (the atmospheric aspect of El Niño, ENSO) (Chasmer & Hopkinson, 2017).

The greening trends after 2004 became greater in magnitude up to 2017, then 2018-2022 showed an increased wetting tendency. The observed severe drying period during 1998-2002 appears to have altered the trajectory of vegetation patterns across delta post-2003. According to David Phillips, senior climatologist at Environment Canada, "The world is a different place now since we last had the super El Niño." (Mortillaro, 2015). Presently, we are experiencing the effects of the 2023-24 El Niño, which may lead to further dry and warmer conditions across the PAD. Among the land covers under the highest changes in both NDVI and MNDWI, shrub swamps showed the highest change. The overall average greening rates pre and post-1999-2003 were 2.1 and 3.1 m/yr., respectively. Given the trajectory of recent observations, particularly the trends of shrubification and wetland drying, it is reasonable to speculate that these trajectories may continue or even amplify, with further drying and shrubification following the El Niño event this year. Nevertheless, as demonstrated in this study, while flooding events are expected to continue to be a regular feature of this landscape, the extent to which the PAD can return to its historically large areas of persistent inundation remains uncertain and requires further investigation.

4.3 Take-Home Messages

The PAD, characterized by intricate dynamics spanning various spatial and temporal scales, from less than an hour to thousands of years, challenges a comprehensive understanding when solely viewed through the lens of human experience (Timoney, 2009). Based on our observations, there is evidence that the long-term systemic hydro-ecological behaviour of the delta was disrupted following the 1998/1999 El Niño, possibly exhibiting a threshold or shift in the long term hydroperiod and vegetation response to primary hydroclimatic drivers. We posit that the onset of

the 1998 El Niño event, coupled with subsequent arid phases from 1999 to 2003, served as catalysts for a transition into a new system dynamic characterised by a tendency for more rapid landscape moisture loss, an increased growing season length and expansion of woody ecotones into previously frequently inundated areas. Such a postulated transition in system behaviour does not contradict the cyclical nature of annual or periodic flooding and slow drainage. However, it does suggest that the period since 2003 has been characterised by more rapid fluxes of water out of the PAD's standing water bodies and wetlands.

Our findings suggest that the delta is likely to undergo a general reduction in moisture levels and an increase in vegetation canopy and shrub cover in the future. However, certain regions, such as the southern area of Mamawi Lake, may experience increased wetness and exhibit some spectral browning. We propose that the increasing encroachment of woody vegetation is indicative of a systematic lowering in the regional water table. This decline enhances potential water storage capacity for future floods, while the expansion of woody biomass ecotones accelerates evaporative fluxes to the atmosphere. Such systemic alterations in behaviour are thought unlikely to severely alter inundation-inducing overbank flooding events, however, increased floodplain storage combined with enhanced evaporative fluxes is expected to reduce flood persistence and associated wetland hydroperiods.

4.4 The Future Landscape: Implications, Challenges, and Opportunities

Changes in water levels and vegetation dynamics within the PAD can modify habitat suitability and influence the distribution and interactions of species (e.g., it may impact breeding, nesting sites, predator-prey relationships, migratory corridors, etc.) and services like water purification and flood regulation. Biodiversity encounters challenges in adapting to swift changes, putting less adaptable species at risk. Therefore, residents in and adjacent to the PAD may need to

adapt to shifting water patterns and hydroperiods, requiring community planners to develop strategies for managing water resources, enhancing flood resilience, and ensuring sustainable living conditions. Decreasing water levels in rivers and lakes have already led to elevated levels of toxic contaminants stemming from industrial activities upstream, further exacerbating the already high rates of disease prevalent in the Fort Chipewyan region (Timoney, 2009).

Based on this and many other studies, such as Timoney (2021), the PAD is at risk of becoming drier, potentially leading to declining fish, waterfowl, and aquatic mammal populations. Reductions in water availability for the Fort Chipewyan communities have resulted in a scarcity of muskrats (Hylton, 2023). Also based on an interview by Hylton (2023), the government has indicated that the fishing industry in Fort Chipewyan is no longer sustainable. We suggest that the situation has the potential to deteriorate further based on the evidence for a shift in the PAD's hydro-ecological system behaviour over the last two decades.

In the boreal forest, numerous tree species have lifespans that extend to 250-300 years, and with gradual warming, they might endure these changes even if growth conditions become suboptimal. Nevertheless, the more probable scenario involves the influence of extreme climatic events, coupled with insect outbreaks and forest fires, which will lead to the replacement of existing stands and significantly impact the composition of the new forest (Wein & Wein, 1995). Additionally, in a drier environment, wildfires potentially occur later in the season, be more intense, and cover greater areas (Wein & Wein, 1995). The anticipated expansion of the burn area has already begun (Tymstra et al., 2020). The recent catastrophic wildfire season of 2023 in the vicinity of the PAD and Wood Buffalo National Park underscores the pressing need to address the escalating wildfire threat. As the region experiences increasing aridity, the heightened risk of wildfires due to buildup of combustible material, poses a significant challenge, necessitating urgent

and proactive measures to safeguard the vulnerable ecosystems and the well-being of the residents. The future landscape is anticipated to be predominantly populated by early succession stages of forests, characterized by an increased prevalence of broad-leaved trees, notably aspen, over needle-leaved varieties. The transition to broad-leaved trees is expected to have implications for the wildlife population, favoring early succession species such as deer, moose, bear, and sharp-tailed grouse. As a result, the success of hunting activities in northern regions may depend on gradual re-alignment with these ecological shifts (Wein & Wein, 1995). Continuous research and monitoring are crucial for informed conservation strategies within the PAD.

The principal obstacle in monitoring regions such as the PAD arises from the lack of vegetation validation plots, a complication further compounded by the remote characteristics of the study area. Therefore, the utilization of cutting-edge technologies in remote sensing and data processing stands as a pivotal solution. Despite the absence of vegetation data, the incorporation of gauge data, particularly in situ soil moisture and groundwater levels, would have greatly enhanced our understanding of the observed patterns in vegetation change. This is particularly relevant considering the reciprocal influences between woody vegetation and groundwater levels.

Consequently, I recommend that future spatially explicit remote sensing-based research incorporates in situ measurements of soil moisture and groundwater levels. Specifically, to test the hypothesis that due to the coupling of plant root zone access and local water table, the spatial variations in soil water levels are the primary control on changing surface vegetation type and observed ecotonal extents across the PAD.

Furthermore, the ecotonal expansions and greening trends identified in this study, interpreted as shrubification indicators, highlight the influence of changing hydro-climatic conditions on the ecological composition of large wetland complexes. This underscores the need for continued

research into the underlying environmental drivers of landcover change and/or the rates of such changes. As discussed, while flooding events are expected to persist, the extent to which the PAD can return to historical levels of persistent inundation remains uncertain and requires further assessment and long-term simulation.

References

Abib, T. H., Chasmer, L., Hopkinson, C., Mahoney, C., & Rodriguez, L. C. E. (2019). Seismic line impacts on proximal boreal forest and wetland environments in Alberta. *Science of The Total Environment, 658*, 1601-1613. doi:https://doi.org/10.1016/j.scitotenv.2018.12.244

Anyamba, A., Tucker, C., & Eastman, J. (2001). NDVI anomaly patterns over Africa during the 1997/98 ENSO warm event. *International Journal of Remote Sensing, 22*(10), 1847-1860.

Asokan, A., & Anitha, J. (2019). Change detection techniques for remote sensing applications: a survey. *Earth Science Informatics, 12*(2), 143-160. doi:10.1007/s12145-019-00380-5

Auble, G. T., Friedman, J. M., & Scott, M. L. (1994). Relating riparian vegetation to present and future streamflows. *Ecological Applications, 4*(3), 544-554.

Baird, R. A., Verbyla, D., & Hollingsworth, T. N. (2012). Browning of the landscape of interior Alaska based on 1986-2009 Landsat sensor NDVI. *Canadian Journal of Forest Research, 42*(7), 1371-1382.

Baltsavias, E. P. (1999). Airborne laser scanning: existing systems and firms and other resources. *ISPRS Journal of Photogrammetry and Remote Sensing, 54*(2-3), 164-198.

Beltaos, S. (2023). The Drying Peace–Athabasca Delta, Canada: Review and Synthesis of Cryo-Hydrologic Controls and Projections to Future Climatic Conditions. *Sustainability, 15*(3), 2103.

Beltaos, S., & Peters, D. L. (2023). Effects of regulation on open-water flows in the lower Peace River, Canada, and implications for the recharge of Peace-Athabasca Delta basins. *River Research and Applications*.

Beltaos, S., Prowse, T. D., & Carter, T. (2006). Ice regime of the lower Peace River and ice-jam flooding of the Peace-Athabasca Delta. *Hydrological Processes: An International Journal, 20*(19), 4009-4029.

Berner, L. T., & Goetz, S. J. (2022). Satellite observations document trends consistent with a boreal forest biome shift. *Global Change Biology, 28*(10), 3275-3292.

Berner, L. T., Massey, R., Jantz, P., Forbes, B. C., Macias-Fauria, M., Myers-Smith, I., . . . Goetz, S. J. (2020). Summer warming explains widespread but not uniform greening in the Arctic tundra biome. *Nature Communications, 11*(1), 4621. doi:10.1038/s41467-020-18479-5

Bijeesh, T., & Narasimhamurthy, K. (2020). Surface water detection and delineation using remote sensing images: A review of methods and algorithms. *Sustainable Water Resources Management, 6*, 1-23.

Bolton, D. K., Coops, N. C., Hermosilla, T., Wulder, M. A., & White, J. C. (2018). Evidence of vegetation greening at alpine treeline ecotones: Three decades of Landsat spectral trends informed by lidar-derived vertical structure. *Environmental Research Letters, 13*(8), 084022.

Bolton, D. K., Tompalski, P., Coops, N. C., White, J. C., Wulder, M. A., Hermosilla, T., . . . Quist, L. (2020). Optimizing Landsat time series length for regional mapping of lidar-derived forest structure. *Remote sensing of Environment, 239*, 111645. doi:https://doi.org/10.1016/j.rse.2020.111645

Bonsal, B. R., & Kochtubajda, B. (2009). An assessment of present and future climate in the Mackenzie Delta and the near-shore Beaufort Sea region of Canada. *J International Journal of Climatology: A Journal of the Royal Meteorological Society, 29*(12), 1780-1795.

Brandt, J. P. (2009). The extent of the North American boreal zone. *Environmental Reviews, 17*(NA), 101-161. doi:10.1139/a09-004

Bridgham, S. D., Johnston, C. A., Pastor, J., & Updegraff, K. (1995). Potential Feedbacks of Northern Wetlands on Climate Change. *BioScience, 45*(4), 262-274. doi:10.2307/1312419

Burkett, V., & Kusler, J. (2000). Climate change: Potential impacts and interactions in wetlands of the untted states 1. *JAWRA Journal of the American Water Resources Association, 36*(2), 313-320.

Campbell, J. B., & Wynne, R. H. (2011). *Introduction to remote sensing*: Guilford press.

Canadell, J. G., Ciais, P., Cox, P., & Heimann, M. (2004). Quantifying, Understanding and Managing the Carbon Cycle in the Next Decades. *Climatic Change, 67*(2), 147-160. doi:10.1007/s10584-004-3765-y

Canadian Environmental Sustainability Indicators. (2016). Extent of Canada's Wetlands. Retrieved from https://www.canada.ca/content/dam/eccc/migration/main/indicateurs-indicators/69e2d25b-52a2-451e-ad87-257fb13711b9/4.0.b-20wetlands_en.pdf (accessed on 31 August 2016)

Carter Johnson, W., Werner, B., & Guntenspergen, G. R. (2016). Non-linear responses of glaciated prairie wetlands to climate warming. *Climatic Change, 134*(1), 209-223. doi:10.1007/s10584-015-1534-8

Chae, Y., Kang, S. M., Jeong, S.-J., Kim, B., & Frierson, D. M. W. (2015). Arctic greening can cause earlier seasonality of Arctic amplification. *Geophysical Research Letters, 42*(2), 536-541. doi:https://doi.org/10.1002/2014GL061841

Chapin, F. S., Peterson, G., Berkes, F., Callaghan, T., Angelstam, P., Apps, M., . . . Danell, K. (2004). Resilience and vulnerability of northern regions to social and environmental change. *AMBIO: a Journal of the Human Environment, 33*(6), 344-349.

Chapin, F. S., Sturm, M., Serreze, M. C., McFadden, J. P., Key, J. R., Lloyd, A. H., . . . Welker, J. M. (2005). Role of Land-Surface Changes in Arctic Summer Warming. *Science, 310*(5748), 657-660. doi:doi:10.1126/science.1117368

Chasmer, L., Cobbaert, D., Mahoney, C., Millard, K., Peters, D., Devito, K., . . . Niemann, O. (2020a). Remote Sensing of Boreal Wetlands 1: Data Use for Policy and Management. *Remote Sensing, 12*(8), 1320. Retrieved from https://www.mdpi.com/2072-4292/12/8/1320

Chasmer, L., & Hopkinson, C. (2017). Threshold loss of discontinuous permafrost and landscape evolution. *Global Change Biology, 23*(7), 2672-2686.

Chasmer, L., Hopkinson, C., Montgomery, J., & Petrone, R. (2016). A Physically Based Terrain Morphology and Vegetation Structural Classification for Wetlands of the Boreal Plains, Alberta, Canada. *Canadian Journal of Remote Sensing, 42*(5), 521-540. doi:10.1080/07038992.2016.1196583

Chasmer, L., Mahoney, C., Millard, K., Nelson, K., Peters, D., Merchant, M., . . . Montgomery, J. (2020b). Remote sensing of boreal wetlands 2: methods for evaluating boreal wetland ecosystem state and drivers of change. *Remote Sensing, 12*(8), 1321.

Chawla, I., Karthikeyan, L., & Mishra, A. K. (2020). A review of remote sensing applications for water security: Quantity, quality, and extremes. *Journal of Hydrology, 585*, 124826. doi:https://doi.org/10.1016/j.jhydrol.2020.124826

Chen, S., Woodcock, C. E., Bullock, E. L., Arévalo, P., Torchinava, P., Peng, S., & Olofsson, P. (2021). Monitoring temperate forest degradation on Google Earth Engine using Landsat time series analysis. *Remote sensing of Environment, 265*, 112648.

Connon, R. F., Chasmer, L., Haughton, E., Helbig, M., Hopkinson, C., Sonnentag, O., & Quinton, W. L. (2021). The implications of permafrost thaw and land cover change on snow water equivalent accumulation, melt and runoff in discontinuous permafrost peatlands. *Hydrological Processes, 35*(9), e14363.

Connon, R. F., Quinton, W. L., Craig, J. R., & Hayashi, M. (2014). Changing hydrologic connectivity due to permafrost thaw in the lower Liard River valley, NWT, Canada. *Hydrological Processes, 28*(14), 4163-4178. doi:https://doi.org/10.1002/hyp.10206

Crego, R. D., Stabach, J. A., & Connette, G. (2022). Implementation of species distribution models in Google Earth Engine. *Diversity and Distributions, 28*(5), 904-916.

Dara, A., Baumann, M., Kuemmerle, T., Pflugmacher, D., Rabe, A., Griffiths, P., . . . Hostert, P. (2018). Mapping the timing of cropland abandonment and recultivation in northern Kazakhstan using annual Landsat time series. *Remote sensing of Environment, 213*, 49-60. doi:https://doi.org/10.1016/j.rse.2018.05.005

Dassot, M., Constant, T., & Fournier, M. (2011). The use of terrestrial LiDAR technology in forest science: application fields, benefits and challenges. *Annals of forest science, 68*, 959-974.

Davidson, N. C. (2014). How much wetland has the world lost? Long-term and recent trends in global wetland area. *Marine and Freshwater Research, 65*(10), 934-941.

De Marzo, T., Pflugmacher, D., Baumann, M., Lambin, E. F., Gasparri, I., & Kuemmerle, T. (2021). Characterizing forest disturbances across the Argentine Dry Chaco based on Landsat time series. *International journal of applied earth observation and geoinformation, 98*, 102310. doi:https://doi.org/10.1016/j.jag.2021.102310

Deoli, V., Kumar, D., Shikha, D., Saw, S., & Patel, R. (2023). Mapping and Trend Analysis in Water Spread Area of Upper and Lower Lakes of Bhopal, Using Remote Sensing Technique. In *Surface and Groundwater Resources Development and Management in*

Semi-arid Region: Strategies and Solutions for Sustainable Water Management (pp. 177-189): Springer.

Desrochers, N. M., Peters, D. L., Siles, G., Cauvier Charest, E., Trudel, M., & Leconte, R. (2023). A Remote Sensing View of the 2020 Extreme Lake-Expansion Flood Event into the Peace–Athabasca Delta Floodplain—Implications for the Future SWOT Mission. *Remote Sensing, 15*(5), 1278.

Dong, P., & Chen, Q. (2017). *LiDAR remote sensing and applications*: CRC Press.

Ducks Unlimited Canada. (2020). *Wood Buffalo National Park Enhanced Wetland Classification User's Guide*. Retrieved from Edmonton, Alberta:

Dusenge, M. E., Duarte, A. G., & Way, D. A. (2019). Plant carbon metabolism and climate change: elevated CO 2 and temperature impacts on photosynthesis, photorespiration and respiration. *New Phytologist, 221*(1), 32-49.

Eastman, J. R. (2015). TerrSet: Geospatial monitoring and modeling software. *Clark Labs, Clark University*.

Eastman, J. R., Sangermano, F., Machado, E. A., Rogan, J., & Anyamba, A. (2013). Global trends in seasonality of normalized difference vegetation index (NDVI), 1982–2011. *Remote Sensing, 5*(10), 4799-4818.

Elmendorf, S. C., Henry, G. H., Hollister, R. D., Björk, R. G., Bjorkman, A. D., Callaghan, T. V., . . . Day, T. A. (2012). Global assessment of experimental climate warming on tundra vegetation: heterogeneity over space and time. *Ecology letters, 15*(2), 164-175.

Erasmi, S., Klinge, M., Dulamsuren, C., Schneider, F., & Hauck, M. (2021). Modelling the productivity of Siberian larch forests from Landsat NDVI time series in fragmented forest stands of the Mongolian forest-steppe. *Environmental monitoring and assessment, 193*(4), 1-18.

Erasmi, S., Propastin, P., Kappas, M., & Panferov, O. (2009). Spatial Patterns of NDVI Variation over Indonesia and Their Relationship to ENSO Warm Events during the Period 1982–2006. *Journal of Climate, 22*(24), 6612-6623. doi:https://doi.org/10.1175/2009JCLI2460.1

Esri-LandTrendr. (Accessed in 2022). Analyze Changes Using LandTrendr (Image Analyst). Retrieved from https://pro.arcgis.com/en/pro-app/latest/tool-reference/image-analyst/analyze-changes-using-landtrendr.htm

Evans, P., & Brown, C. D. (2017). The boreal–temperate forest ecotone response to climate change. *Environmental Reviews, 25*(4), 423-431. doi:10.1139/er-2017-0009

Field, C. B., Barros, V. R., Dokken, D. J., Mach, K. J., Mastrandrea, M. D., Bilir, T. E., & White, L. (2014). Intergovernmental Panel on Climate Change. *Climate Change 2014: Impacts, Adaptation, and Vulnerability. Part A: Global and Sectoral Aspects*.

Flood, N. (2013). Seasonal composite Landsat TM/ETM+ images using the medoid (a multi-dimensional median). *Remote Sensing, 5*(12), 6481-6500.

Foley, J. A., DeFries, R., Asner, G. P., Barford, C., Bonan, G., Carpenter, S. R., . . . Gibbs, H. K. (2005). Global consequences of land use. *Science, 309*(5734), 570-574.

Forbes, B. C., Fauria, M. M., & Zetterberg, P. (2010). Russian Arctic warming and 'greening'are closely tracked by tundra shrub willows. *Global Change Biology, 16*(5), 1542-1554.

Ford, J. D., King, N., Galappaththi, E. K., Pearce, T., McDowell, G., & Harper, S. L. (2020). The resilience of indigenous peoples to environmental change. *One Earth, 2*(6), 532-543.

Francini, S. (2021). BAP-GEE - A Google Earth Engine application for Best Available Pixel composites calculation, visualization, calibration, and download. Retrieved from https://github.com/saveriofrancini/bap. https://github.com/saveriofrancini/bap

Fraser, R., Olthof, I., Carrière, M., Deschamps, A., & Pouliot, D. (2011). Detecting long-term changes to vegetation in northern Canada using the Landsat satellite image archive. *Environmental Research Letters, 6*(4), 045502.

Fraser, R. H., Lantz, T. C., Olthof, I., Kokelj, S. V., & Sims, R. A. (2014a). Warming-induced shrub expansion and lichen decline in the Western Canadian Arctic. *Ecosystems, 17*(7), 1151-1168.

Fraser, R. H., Olthof, I., Kokelj, S. V., Lantz, T. C., Lacelle, D., Brooker, A., . . . Schwarz, S. (2014b). Detecting landscape changes in high latitude environments using landsat trend analysis: 1. Visualization. *Remote Sensing, 6*(11), 11533-11557.

Gallant, A. L. (2015). The Challenges of Remote Monitoring of Wetlands. *Remote Sensing, 7*(8), 10938-10950. Retrieved from https://www.mdpi.com/2072-4292/7/8/10938

Gao, W., Zheng, C., Liu, X., Lu, Y., Chen, Y., Wei, Y., & Ma, Y. (2022). NDVI-based vegetation dynamics and their responses to climate change and human activities from 1982 to 2020: A case study in the Mu Us Sandy Land, China. *Ecological Indicators, 137*, 108745. doi:https://doi.org/10.1016/j.ecolind.2022.108745

Gibson, C. M., Chasmer, L. E., Thompson, D. K., Quinton, W. L., Flannigan, M. D., & Olefeldt, D. (2018). Wildfire as a major driver of recent permafrost thaw in boreal peatlands. *Nature Communications, 9*(1), 3041. doi:10.1038/s41467-018-05457-1

Goldblum, D., & Rigg, L. S. (2010). The deciduous forest–boreal forest ecotone. *Geography Compass, 4*(7), 701-717.

Gorelick, N., Hancher, M., Dixon, M., Ilyushchenko, S., Thau, D., & Moore, R. (2017). Google Earth Engine: Planetary-scale geospatial analysis for everyone. *Remote sensing of Environment, 202*, 18-27.

Griffiths, P., van der Linden, S., Kuemmerle, T., & Hostert, P. (2013). A pixel-based Landsat compositing algorithm for large area land cover mapping. *IEEE Journal of Selected Topics in Applied Earth Observations and Remote Sensing, 6*(5), 2088-2101.

Gumma, M. K., Thenkabail, P. S., Teluguntla, P. G., Oliphant, A., Xiong, J., Giri, C., . . . Whitbread, A. M. (2020). Agricultural cropland extent and areas of South Asia derived using Landsat satellite 30-m time-series big-data using random forest machine learning algorithms on the Google Earth Engine cloud. *GIScience & Remote Sensing, 57*(3), 302-322.

Guo, Q., Pu, R., Li, J., & Cheng, J. (2017). A weighted normalized difference water index for water extraction using Landsat imagery. *International Journal of Remote Sensing, 38*(19), 5430-5445.

Hall, R. I., Wolfe, B. B., Wiklund, J. A., Edwards, T. W., Farwell, A. J., & Dixon, D. G. (2012). Has Alberta oil sands development altered delivery of polycyclic aromatic compounds to the Peace-Athabasca Delta? *PLoS ONE, 7(9)*, e46089. doi:doi:10.1371/journal.pone.0046089

He, Q., Chen, E., An, R., & Li, Y. (2013). Above-Ground Biomass and Biomass Components Estimation Using LiDAR Data in a Coniferous Forest. *Forests, 4*(4), 984-1002. Retrieved from https://www.mdpi.com/1999-4907/4/4/984

Hemati, M., Hasanlou, M., Mahdianpari, M., & Mohammadimanesh, F. (2021). A systematic review of landsat data for change detection applications: 50 years of monitoring the earth. *Remote Sensing, 13*(15), 2869.

Hermosilla, T., Wulder, M. A., White, J. C., Coops, N. C., & Hobart, G. W. (2018). Disturbance-informed annual land cover classification maps of Canada's forested ecosystems for a 29-year landsat time series. *Canadian Journal of Remote Sensing, 44*(1), 67-87.

Hislop, S., Jones, S., Soto-Berelov, M., Skidmore, A., Haywood, A., & Nguyen, T. H. (2019). A fusion approach to forest disturbance mapping using time series ensemble techniques. *Remote sensing of Environment, 221*, 188-197. doi:https://doi.org/10.1016/j.rse.2018.11.025

Hokanson, K., Peterson, E., Devito, K., & Mendoza, C. (2020). Forestland-peatland hydrologic connectivity in water-limited environments: hydraulic gradients often oppose topography. *Environmental Research Letters, 15*(3), 034021.

Hood, G. A., & Bayley, S. E. (2008). Beaver (Castor canadensis) mitigate the effects of climate on the area of open water in boreal wetlands in western Canada. *Biological Conservation, 141*(2), 556-567. doi:https://doi.org/10.1016/j.biocon.2007.12.003

Hope, A., Kimball, J., & Stow, D. (1993). The relationship between tussock tundra spectral reflectance properties and biomass and vegetation composition. *International Journal of Remote Sensing, 14*(10), 1861-1874.

Hopkinson, C. (2007). The influence of flying altitude, beam divergence, and pulse repetition frequency on laser pulse return intensity and canopy frequency distribution. *Canadian Journal of Remote Sensing, 33*(4), 312-324. doi:10.5589/m07-029

Hopkinson, C., & Chasmer, L. (2009). Testing LiDAR models of fractional cover across multiple forest ecozones. *Remote sensing of Environment, 113*(1), 275-288.

Hopkinson, C., Chasmer, L., Gynan, C., Mahoney, C., & Sitar, M. (2016). Multisensor and Multispectral LiDAR Characterization and Classification of a Forest Environment. *Canadian Journal of Remote Sensing, 42*(5), 501-520. doi:10.1080/07038992.2016.1196584

Hopkinson, C., Chasmer, L., & Hall, R. (2008). The uncertainty in conifer plantation growth prediction from multi-temporal lidar datasets. *Remote sensing of Environment, 112*(3), 1168-1180.

Hopkinson, C., Crasto, N., Marsh, P., Forbes, D., & Lesack, L. (2011). Investigating the spatial distribution of water levels in the Mackenzie Delta using airborne LiDAR. *Hydrological Processes, 25*(19), 2995-3011. doi:https://doi.org/10.1002/hyp.8167

Hopkinson, C., Demuth, M., Sitar, M., & Chasmer, L. (2001, 9-13 July 2001). *Applications of airborne LiDAR mapping in glacierised mountainous terrain.* Paper presented at the IGARSS 2001. Scanning the Present and Resolving the Future. Proceedings. IEEE 2001 International Geoscience and Remote Sensing Symposium (Cat. No.01CH37217).

Hopkinson, C., Fuoco, B., Grant, T., Bayley, S. E., Brisco, B., & MacDonald, R. (2020). Wetland Hydroperiod Change Along the Upper Columbia River Floodplain, Canada, 1984 to 2019. *Remote Sensing, 12*(24), 4084. Retrieved from https://www.mdpi.com/2072-4292/12/24/4084

Hopkinson, C., Sitar, M., Chasmer, L., & Treitz, P. (2004). Mapping snowpack depth beneath forest canopies using airborne lidar. *Photogrammetric Engineering & Remote Sensing, 70*(3), 323-330.

Hu, S., Niu, Z., & Chen, Y. (2017). Global wetland datasets: a review. *Wetlands, 37*(5), 807-817.

Huang, C., Peng, Y., Lang, M., Yeo, I.-Y., & McCarty, G. (2014). Wetland inundation mapping and change monitoring using Landsat and airborne LiDAR data. *Remote sensing of Environment, 141*, 231-242. doi:https://doi.org/10.1016/j.rse.2013.10.020

Huang, H., Chen, Y., Clinton, N., Wang, J., Wang, X., Liu, C., . . . Zheng, Y. (2017). Mapping major land cover dynamics in Beijing using all Landsat images in Google Earth Engine. *Remote sensing of Environment, 202*, 166-176.

Huang, S., Tang, L., Hupy, J. P., Wang, Y., & Shao, G. (2021). A commentary review on the use of normalized difference vegetation index (NDVI) in the era of popular remote sensing. *Journal of Forestry Research, 32*(1), 1-6.

Huete, A., Liu, H., Batchily, K., & Van Leeuwen, W. (1997). A comparison of vegetation indices over a global set of TM images for EOS-MODIS. *Remote sensing of Environment, 59*(3), 440-451.

Hupy, C. M., & Yansa, C. H. (2009). Late Holocene vegetation history of the forest tension zone in central Lower Michigan, USA. *Physical Geography, 30*(3), 205-235.

Hylton, S. (2023). Lifeblood: Fort Chipewyan's relationship to water. *Canadian Geography*. Retrieved from https://canadiangeographic.ca/articles/lifeblood-fort-chipewyans-relationship-to-water/

Ichii, K., Kawabata, A., & Yamaguchi, Y. (2002). Global correlation analysis for NDVI and climatic variables and NDVI trends: 1982-1990. *International Journal of Remote Sensing, 23*(18), 3873-3878.

Johansson, M., & Nilsson, C. (2002). Responses of riparian plants to flooding in free-flowing and regulated boreal rivers: an experimental study. *Journal of Applied Ecology, 39*(6), 971-986.

Ju, J., & Masek, J. G. (2016). The vegetation greenness trend in Canada and US Alaska from 1984–2012 Landsat data. *Remote sensing of Environment, 176*, 1-16.

Kay, M., Wiklund, J., Remmer, C., Neary, L., Brown, K., Ghosh, A., . . . Wesenberg, K. (2019). Bi-directional hydrological changes in perched basins of the Athabasca Delta (Canada) in recent decades caused by natural processes. *Environmental Research Communications, 1*(8), 081001.

Kelly, E. N., Schindler, D. W., Hodson, P. V., Short, J. W., Radmanovich, R., & Nielsen, C. C. (2010). Oil sands development contributes elements toxic at low concentrations to the Athabasca River and its tributaries. *Proceedings of the National Academy of Sciences, 107*(37), 16178-16183.

Kendall, M. G. (1948). *Rank correlation methods*: Griffin.

Kennedy, R. E., Yang, Z., & Cohen, W. B. (2010). Detecting trends in forest disturbance and recovery using yearly Landsat time series: 1. LandTrendr — Temporal segmentation algorithms. *Remote sensing of Environment, 114*(12), 2897-2910. doi:https://doi.org/10.1016/j.rse.2010.07.008

Kennedy, R. E., Yang, Z., Gorelick, N., Braaten, J., Cavalcante, L., Cohen, W. B., & Healey, S. (2018). Implementation of the LandTrendr Algorithm on Google Earth Engine. *Remote Sensing, 10*(5), 691. Retrieved from https://www.mdpi.com/2072-4292/10/5/691

Kilpeläinen, A., Kellomäki, S., Strandman, H., & Venäläinen, A. (2010). Climate change impacts on forest fire potential in boreal conditions in Finland. *Climatic Change, 103*, 383-398.

Klein, E., Berg, E. E., & Dial, R. (2005). Wetland drying and succession across the Kenai Peninsula Lowlands, south-central Alaska. *Canadian Journal of Forest Research, 35*(8), 1931-1941. doi:10.1139/x05-129

Kompanizare, M., Petrone, R. M., Shafii, M., Robinson, D. T., & Rooney, R. C. (2018). Effect of climate change and mining on hydrological connectivity of surficial layers in the Athabasca Oil Sands Region. *Hydrological Processes, 32*(25), 3698-3716. doi:https://doi.org/10.1002/hyp.13292

Kumar, D. (2021). *Spatio-temporal Variability of Water Spread Area of Water Bodies using LANDSAT imagery and GIS: A Case study of Naukuchia Lake, Uttarakhand India*. https://ui.adsabs.harvard.edu/abs/2021AGUFM.H55T0970K

Kumar, R., Nath, A. J., Nath, A., Sahu, N., & Pandey, R. (2022). Landsat-based multi-decadal spatio-temporal assessment of the vegetation greening and browning trend in the Eastern Indian Himalayan Region. *Remote Sensing Applications: Society and Environment, 25*, 100695. doi:https://doi.org/10.1016/j.rsase.2022.100695

Kurek, J., Kirk, J. L., Muir, D. C., Wang, X., Evans, M. S., & Smol, J. P. (2013). Legacy of a half century of Athabasca oil sands development recorded by lake ecosystems. *Proceedings of the National Academy of Sciences, 110*(5), 1761-1766.

Lamontagne, J. R., Jasek, M., & Smith, J. D. (2021). Coupling physical understanding and statistical modeling to estimate ice jam flood frequency in the northern Peace-Athabasca Delta under climate change. *Cold Regions Science and Technology, 192*, 103383.

Lang, M., McDonough, O., McCarty, G., Oesterling, R., & Wilen, B. (2012). Enhanced Detection of Wetland-Stream Connectivity Using LiDAR. *Wetlands, 32*(3), 461-473. doi:10.1007/s13157-012-0279-7

Lang, M. W., & McCarty, G. W. (2009). Lidar intensity for improved detection of inundation below the forest canopy. *Wetlands, 29*(4), 1166-1178. doi:10.1672/08-197.1

Larsen, S., & Alp, M. (2015). Ecological thresholds and riparian wetlands: an overview for environmental managers. *Limnology, 16*(1), 1-9.

LaRue, E. A., Atkins, J. W., Dahlin, K., Fahey, R., Fei, S., Gough, C., & Hardiman, B. S. (2018). Linking Landsat to terrestrial LiDAR: Vegetation metrics of forest greenness are correlated with canopy structural complexity. *International journal of applied earth observation and geoinformation, 73*, 420-427. doi:https://doi.org/10.1016/j.jag.2018.07.001

Le Maitre, D. C., Scott, D. F., & Colvin, C. (1999). Review of information on interactions between vegetation and groundwater. In.

Leemans, R., Asrar, G., Busalacchi, A., Canadell, J., Ingram, J., Larigauderie, A., . . . Young, O. (2009). Developing a common strategy for integrative global environmental change research and outreach: the Earth System Science Partnership (ESSP). *Current Opinion in Environmental Sustainability, 1*(1), 4-13. doi:https://doi.org/10.1016/j.cosust.2009.07.013

Lefsky, M. A., Cohen, W. B., Parker, G. G., & Harding, D. J. (2002). Lidar Remote Sensing for Ecosystem Studies: Lidar, an emerging remote sensing technology that directly measures the three-dimensional distribution of plant canopies, can accurately estimate vegetation structural attributes and should be of particular interest to forest, landscape, and global ecologists. *BioScience, 52*(1), 19-30. doi:10.1641/0006-3568(2002)052[0019:Lrsfes]2.0.Co;2

Lemay, M. A., Provencher-Nolet, L., Bernier, M., Lévesque, E., & Boudreau, S. (2018). Spatially explicit modeling and prediction of shrub cover increase near Umiujaq, Nunavik. *Ecological Monographs, 88*(3), 385-407.

Li, J., Holmgren, M., & Xu, C. (2021a). Greening vs browning? Surface water cover mediates how tundra and boreal ecosystems respond to climate warming. *Environmental Research Letters, 16*(10), 104004. doi:10.1088/1748-9326/ac2376

Li, X., Liu, C., Wang, Z., Xie, X., Li, D., & Xu, L. (2021b). Airborne LiDAR: state-of-the-art of system design, technology and application. *Measurement Science and Technology, 32*(3), 032002. doi:10.1088/1361-6501/abc867

Li, Z., & Kafatos, M. (2000). Interannual Variability of Vegetation in the United States and Its Relation to El Niño/Southern Oscillation. *Remote sensing of Environment, 71*(3), 239-247. doi:https://doi.org/10.1016/S0034-4257(99)00034-6

Lillesand, T., Kiefer, R. W., & Chipman, J. (2015). *Remote sensing and image interpretation*: John Wiley & Sons.

Lim, K., Hopkinson, C., & Treitz, P. (2008). Examining the effects of sampling point densities on laser canopy height and density metrics. *The Forestry Chronicle, 84*(6), 876-885.

Liu, Q., Peng, C., Schneider, R., Cyr, D., McDowell, N. G., & Kneeshaw, D. (2023). Drought-induced increase in tree mortality and corresponding decrease in the carbon sink capacity of Canada's boreal forests from 1970 to 2020. *Global Change Biology, 29*(8), 2274-2285. doi:https://doi.org/10.1111/gcb.16599

Liu, Y., Li, Y., Li, S., & Motesharrei, S. (2015). Spatial and Temporal Patterns of Global NDVI Trends: Correlations with Climate and Human Factors. *Remote Sensing, 7*(10), 13233-13250. Retrieved from https://www.mdpi.com/2072-4292/7/10/13233

Lü, A., Zhu, W., & Jia, S. (2012). Assessment of the sensitivity of vegetation to El-Niño/Southern Oscillation events over China. *Advances in Space Research, 50*(10), 1362-1373. doi:https://doi.org/10.1016/j.asr.2012.06.033

Luo, H., Zhang, L., & Zhang, X. (2022). Shifts in land-greening hotspots in the Yellow River Eco-Economic Belt during the last four decades and their connections to human activities. *Remote Sensing Applications: Society and Environment, 27*, 100783. doi:https://doi.org/10.1016/j.rsase.2022.100783

Luo, S., Wang, C., Pan, F., Xi, X., Li, G., Nie, S., & Xia, S. (2015). Estimation of wetland vegetation height and leaf area index using airborne laser scanning data. *Ecological Indicators, 48*, 550-559. doi:https://doi.org/10.1016/j.ecolind.2014.09.024

Mack, M. C., Walker, X. J., Johnstone, J. F., Alexander, H. D., Melvin, A. M., Jean, M., & Miller, S. N. (2021). Carbon loss from boreal forest wildfires offset by increased dominance of deciduous trees. *Science, 372*(6539), 280-283. doi:doi:10.1126/science.abf3903

Mann, H. B. (1945). Nonparametric tests against trend. *Econometrica: Journal of the econometric society*, 245-259.

Martinez, A. d. l. I., & Labib, S. M. (2023). Demystifying normalized difference vegetation index (NDVI) for greenness exposure assessments and policy interventions in urban greening. *Environmental Research, 220*, 115155. doi:https://doi.org/10.1016/j.envres.2022.115155

Masek, J. G., Wulder, M. A., Markham, B., McCorkel, J., Crawford, C. J., Storey, J., & Jenstrom, D. T. (2020). Landsat 9: Empowering open science and applications through continuity. *Remote sensing of Environment, 248*, 111968. doi:https://doi.org/10.1016/j.rse.2020.111968

Masson-Delmotte, V., Zhai, P., Pirani, S., Connors, C., Péan, S., Berger, N., . . . Scheel Monteiro, P. M. (2021). Ipcc, 2021: Summary for policymakers. in: Climate change 2021: The physical science basis. contribution of working group i to the sixth assessment report of the intergovernmental panel on climate change.

McManus, K. M., Morton, D. C., Masek, J. G., Wang, D., Sexton, J. O., Nagol, J. R., . . . Boudreau, S. (2012). Satellite-based evidence for shrub and graminoid tundra expansion in northern Q uebec from 1986 to 2010. *Global Change Biology, 18*(7), 2313-2323.

Mekonnen, Z. A., Riley, W. J., & Grant, R. F. (2018). Accelerated Nutrient Cycling and Increased Light Competition Will Lead to 21st Century Shrub Expansion in North American Arctic

Tundra. *Journal of Geophysical Research: Biogeosciences, 123*(5), 1683-1701. doi:10.1029/2017jg004319

Melillo, J., Callaghan, T., Woodward, F., Salati, E., & Sinha, S. (1990). Effects on ecosystems. *Climate change: The IPCC scientific assessment*, 283-310.

Michaelian, M., Hogg, E. H., Hall, R. J., & Arsenault, E. (2011). Massive mortality of aspen following severe drought along the southern edge of the Canadian boreal forest. *Global Change Biology, 17*(6), 2084-2094.

Mishra, N., Helder, D., Barsi, J., & Markham, B. (2016). Continuous calibration improvement in solar reflective bands: Landsat 5 through Landsat 8. *Remote sensing of Environment, 185*, 7-15.

Mitsch, W. J., & Gosselink, J. G. (2015). *Wetlands*: John Wiley & Sons.

Montgomery, J., Brisco, B., Chasmer, L., Devito, K., Cobbaert, D., & Hopkinson, C. (2019). SAR and LiDAR temporal data fusion approaches to boreal wetland ecosystem monitoring. *Remote Sensing, 11*(2), 161.

Morawitz, D. F., Blewett, T. M., Cohen, A., & Alberti, M. (2006). Using NDVI to Assess Vegetative Land Cover Change in Central Puget Sound. *Environmental monitoring and assessment, 114*(1), 85-106. doi:10.1007/s10661-006-1679-z

Mortillaro, N. (2015). 5 things to know about El Nino, coming to Canada this winter. *Global News*. Retrieved from https://globalnews.ca/news/2288071/5-things-to-know-about-el-nino-coming-to-canada-this-winter/

Mugiraneza, T., Nascetti, A., & Ban, Y. (2020). Continuous Monitoring of Urban Land Cover Change Trajectories with Landsat Time Series and LandTrendr-Google Earth Engine Cloud Computing. *Remote Sensing, 12*(18), 2883. Retrieved from https://www.mdpi.com/2072-4292/12/18/2883

Mwale, D., Gan, T. Y., Devito, K., Mendoza, C., Silins, U., & Petrone, R. (2009). Precipitation variability and its relationship to hydrologic variability in Alberta. *Hydrological Processes: An International Journal, 23*(21), 3040-3056.

Myers-Smith, I. H., & Hik, D. S. (2018). Climate warming as a driver of tundra shrubline advance. *Journal of Ecology, 106*(2), 547-560. doi:10.1111/1365-2745.12817

Myers-Smith, I. H., Kerby, J. T., Phoenix, G. K., Bjerke, J. W., Epstein, H. E., Assmann, J. J., . . . Wipf, S. (2020). Complexity revealed in the greening of the Arctic. *Nature Climate Change, 10*(2), 106-117. doi:10.1038/s41558-019-0688-1

Myers-Smith, I. H., & Hik, D. S. (2018). Climate warming as a driver of tundra shrubline advance. *Journal of Ecology, 106*(2), 547-560.

Nagai, S., Ichii, K., & Morimoto, H. (2007). Interannual variations in vegetation activities and climate variability caused by ENSO in tropical rainforests. *International Journal of Remote Sensing, 28*(6), 1285-1297. doi:10.1080/01431160600904972

Neeti, N., & Eastman, J. R. (2011). A contextual mann-kendall approach for the assessment of trend significance in image time series. *Transactions in GIS, 15*(5), 599-611.

Newton, B. W., Prowse, T. D., & de Rham, L. P. (2016). Hydro-climatic drivers of mid-winter break-up of river ice in western Canada and Alaska. *Hydrology Research, 48*(4), 945-956. doi:10.2166/nh.2016.358

Nilsson, C., & Svedmark, M. (2002). Basic Principles and Ecological Consequences of Changing Water Regimes: Riparian Plant Communities. *Environmental Management, 30*(4), 468-480. doi:10.1007/s00267-002-2735-2

Oliphant, A. J., Thenkabail, P. S., Teluguntla, P., Xiong, J., Gumma, M. K., Congalton, R. G., & Yadav, K. (2019). Mapping cropland extent of Southeast and Northeast Asia using multi-year time-series Landsat 30-m data using a random forest classifier on the Google Earth Engine Cloud. *International journal of applied earth observation and geoinformation, 81*, 110-124.

Olthof, I., Pouliot, D., Latifovic, R., & Chen, W. (2008). Recent (1986-2006) vegetation-specific NDVI trends in northern Canada from satellite data. *Arctic*, 381-394.

Pan, N., Feng, X., Fu, B., Wang, S., Ji, F., & Pan, S. (2018). Increasing global vegetation browning hidden in overall vegetation greening: Insights from time-varying trends. *Remote sensing of Environment, 214*, 59-72. doi:https://doi.org/10.1016/j.rse.2018.05.018

Park, T., Ganguly, S., Tømmervik, H., Euskirchen, E. S., Høgda, K.-A., Karlsen, S. R., . . . Myneni, R. B. (2016). Changes in growing season duration and productivity of northern vegetation inferred from long-term remote sensing data. *Environmental Research Letters, 11*(8), 084001.

Pasquarella, V. J., Arévalo, P., Bratley, K. H., Bullock, E. L., Gorelick, N., Yang, Z., & Kennedy, R. E. (2022). Demystifying LandTrendr and CCDC temporal segmentation. *International journal of applied earth observation and geoinformation, 110*, 102806. doi:https://doi.org/10.1016/j.jag.2022.102806

Peters, D., Niemann, K. O., & Skelly, R. (2020). Remote sensing of ecosystem structure: Fusing passive and active remotely sensed data to characterize a deltaic wetland landscape. *Remote Sensing, 12*(22), 3819.

Peters, D. L., Atkinson, D., Monk, W. A., Tenenbaum, D. E., & Baird, D. J. (2013). A multi-scale hydroclimatic analysis of runoff generation in the Athabasca River, western Canada. *Hydrological Processes, 27*(13), 1915-1934.

Peters, D. L., Niemann, K. O., & Skelly, R. (2021). Remote Sensing of Ecosystem Structure—Part 2: Initial Findings of Ecosystem Functioning through Intra-and Inter-Annual Comparisons with Earth Observation Data. *Remote Sensing, 13*(16), 3219.

Peters, D. L., & Prowse, T. D. (2001). Regulation effects on the lower Peace River, Canada. *Hydrological Processes, 15*(16), 3181-3194.

Peters, D. L., Prowse, T. D., Marsh, P., Lafleur, P. M., & Buttle, J. M. (2006a). Persistence of Water within Perched Basins of the Peace-Athabasca Delta, Northern Canada. *Wetlands Ecology and Management, 14*(3), 221-243. doi:10.1007/s11273-005-1114-1

Peters, D. L., Prowse, T. D., Pietroniro, A., & Leconte, R. (2006b). Flood hydrology of the Peace-Athabasca Delta, northern Canada. *Hydrological Processes: An International Journal, 20*(19), 4073-4096.

Peters, D. L., Watt, D., Devito, K., Monk, W. A., Shrestha, R. R., & Baird, D. J. (2022). Changes in geographical runoff generation in regions affected by climate and resource development: A case study of the Athabasca River. *Journal of Hydrology: Regional Studies, 39*, 100981. doi:https://doi.org/10.1016/j.ejrh.2021.100981

Pi, K., Bieroza, M., Brouchkov, A., Chen, W., Dufour, L. J. P., Gongalsky, K. B., . . . Cappellen, P. V. (2021). The Cold Region Critical Zone in Transition: Responses to Climate Warming and Land Use Change. *Annual Review of Environment and Resources, 46*(1), 111-134. doi:10.1146/annurev-environ-012220-125703

Piedallu, C., Chéret, V., Denux, J. P., Perez, V., Azcona, J. S., Seynave, I., & Gégout, J. C. (2019). Soil and climate differently impact NDVI patterns according to the season and the stand type. *Science of The Total Environment, 651*, 2874-2885. doi:https://doi.org/10.1016/j.scitotenv.2018.10.052

Pietroniro, A., Leconte, R., Toth, B., Peters, D. L., Kouwen, N., Conly, F. M., & Prowse, T. (2006). Modelling climate change impacts in the Peace and Athabasca catchment and delta: III—integrated model assessment. *Hydrological Processes, 20*(19), 4231-4245. doi:10.1002/hyp.6428

Potapov, P., Turubanova, S., & Hansen, M. C. (2011). Regional-scale boreal forest cover and change mapping using Landsat data composites for European Russia. *Remote sensing of Environment, 115*(2), 548-561.

Propastin, P., Fotso, L., & Kappas, M. (2010). Assessment of vegetation vulnerability to ENSO warm events over Africa. *International journal of applied earth observation and geoinformation, 12*, S83-S89. doi:https://doi.org/10.1016/j.jag.2009.10.007

Prowse, T., Beltaos, S., Gardner, J., Gibson, J., Granger, R., Leconte, R., . . . Toth, B. (2006a). Climate change, flow regulation and land-use effects on the hydrology of the Peace-Athabasca-Slave system; Findings from the Northern Rivers Ecosystem Initiative. *Environmental monitoring and assessment, 113*(1), 167-197.

Prowse, T. D., Beltaos, S., Gardner, J. T., Gibson, J. J., Granger, R. J., Leconte, R., . . . Toth, B. (2006b). Climate Change, Flow Regulation and Land-Use Effects on the Hydrology of the Peace-Athabasca-Slave System; Findings from the Northern Rivers Ecosystem Initiative. *J Environmental Monitoring Assessment, 113*(1), 167-197. doi:10.1007/s10661-005-9080-x

Qiu, S., Lin, Y., Shang, R., Zhang, J., Ma, L., & Zhu, Z. (2018). Making Landsat time series consistent: Evaluating and improving Landsat analysis ready data. *Remote Sensing, 11*(1), 51.

Qiu, S., Zhu, Z., Olofsson, P., Woodcock, C. E., & Jin, S. (2023). Evaluation of Landsat image compositing algorithms. *Remote sensing of Environment, 285*, 113375. doi:https://doi.org/10.1016/j.rse.2022.113375

Ramsar Convention. (2016). An introduction to the Ramsar Convention on Wetlands, 7th ed. (Publication no. https://www.ramsar.org/sites/default/files/documents/library/handbook1_5ed_introductiontoconvention_final_e.pdf).

Raynolds, M. K., Walker, D. A., Epstein, H. E., Pinzon, J. E., & Tucker, C. J. (2012). A new estimate of tundra-biome phytomass from trans-Arctic field data and AVHRR NDVI. *Remote Sensing Letters, 3*(5), 403-411.

Renöfält, B. M., Nilsson, C., & Jansson, R. (2005). Spatial and temporal patterns of species richness in a riparian landscape. *Journal of Biogeography, 32*(11), 2025-2037.

Riedel, S., Epstein, H., & Walker, D. (2005). Biotic controls over spectral reflectance of arctic tundra vegetation. *International Journal of Remote Sensing, 26*(11), 2391-2405.

Rijkers, T., Pons, T. L., & Bongers, F. (2000). The effect of tree height and light availability on photosynthetic leaf traits of four neotropical species differing in shade tolerance. *Functional Ecology, 14*(1), 77-86. doi:https://doi.org/10.1046/j.1365-2435.2000.00395.x

Robinson, N. P., Allred, B. W., Jones, M. O., Moreno, A., Kimball, J. S., Naugle, D. E., . . . Richardson, A. D. (2017). A dynamic Landsat derived normalized difference vegetation index (NDVI) product for the conterminous United States. *Remote Sensing, 9*(8), 863.

Rodrigues, I. S., Hopkinson, C., Chasmer, L., MacDonald, R., Bayley, S., & Brisco, B. (2023). Multi-decadal Floodplain Classification and Trend Analysis in the Upper Columbia River Valley, British Columbia. *Hydrology and Earth System Sciences Discussions, 2023*, 1-34.

Rooney, R. C., Bayley, S. E., & Schindler, D. W. (2012). Oil sands mining and reclamation cause massive loss of peatland and stored carbon. *Proceedings of the National Academy of Sciences, 109*(13), 4933-4937. doi:doi:10.1073/pnas.1117693108

Roy, D. P., Kovalskyy, V., Zhang, H., Vermote, E. F., Yan, L., Kumar, S., & Egorov, A. (2016). Characterization of Landsat-7 to Landsat-8 reflective wavelength and normalized difference vegetation index continuity. *Remote sensing of Environment, 185*, 57-70.

Royston, P. (1992). Approximating the Shapiro-Wilk W-test for non-normality. *Statistics and Computing, 2*(3), 117-119. doi:10.1007/BF01891203

Ruefenacht, B. (2016). Comparison of three Landsat TM compositing methods: a case study using modeled tree canopy cover. *Photogrammetric Engineering & Remote Sensing, 82*(3), 199-211.

Sala, O. E., Stuart Chapin, F., Armesto, J. J., Berlow, E., Bloomfield, J., Dirzo, R., . . . Kinzig, A. (2000). Global biodiversity scenarios for the year 2100. *Science, 287*(5459), 1770-1774.

Salas, E. A. L. (2021). Waveform LiDAR concepts and applications for potential vegetation phenology monitoring and modeling: a comprehensive review. *Geo-spatial Information Science, 24*(2), 179-200.

Sánchez-Pinillos, M., D'Orangeville, L., Boulanger, Y., Comeau, P., Wang, J., Taylor, A. R., & Kneeshaw, D. (2022). Sequential droughts: A silent trigger of boreal forest mortality. *Global Change Biology, 28*(2), 542-556. doi:https://doi.org/10.1111/gcb.15913

Schindler, D. W., & Donahue, W. F. (2006). An impending water crisis in Canada's western prairie provinces. *Proceedings of the National Academy of Sciences, 103*(19), 7210-7216.

Schindler, D. W., & Smol, J. P. (2006). Cumulative effects of climate warming and other human activities on freshwaters of Arctic and subarctic North America. *AMBIO: a Journal of the Human Environment, 35*(4), 160-168.

Schucknecht, A., Erasmi, S., Niemeyer, I., & Matschullat, J. (2013). Assessing vegetation variability and trends in north-eastern Brazil using AVHRR and MODIS NDVI time series. *European Journal of Remote Sensing, 46*(1), 40-59.

Sen, P. K. (1968). Estimates of the regression coefficient based on Kendall's tau. *Journal of the American statistical association, 63*(324), 1379-1389.

Sim, T. G., Swindles, G., Morris, P., Gałka, M., Mullan, D., & Galloway, J. (2019). Pathways for ecological change in Canadian High Arctic wetlands under rapid twentieth century warming. *Geophysical Research Letters, 46*(9), 4726-4737.

Smith, K., Smith, C., Forest, S., & Richard, A. (2007). A field guide to the wetlands of the boreal plains ecozone of Canada. *Ducks Unlimited Canada, Western Boreal Office: Edmonton, Alberta*.

Solomon, S. (2007). The physical science basis: Contribution of Working Group I to the fourth assessment report of the Intergovernmental Panel on Climate Change. *Intergovernmental Panel on Climate Change (IPCC), Climate change 2007, 996*.

Sonnenschein, R., Kuemmerle, T., Udelhoven, T., Stellmes, M., & Hostert, P. (2011). Differences in Landsat-based trend analyses in drylands due to the choice of vegetation estimate. *Remote sensing of Environment, 115*(6), 1408-1420.

Stamford, J. D., Vialet-Chabrand, S., Cameron, I., & Lawson, T. (2023). Development of an accurate low cost NDVI imaging system for assessing plant health. *Plant Methods, 19*(1), 9. doi:10.1186/s13007-023-00981-8

Stralberg, D., Arseneault, D., Baltzer, J. L., Barber, Q. E., Bayne, E. M., Boulanger, Y., . . . Edwards, J. (2020). Climate-change refugia in boreal North America: what, where, and for how long? *Frontiers in Ecology and the Environment, 18*(5), 261-270.

Ström, L., Jansson, R., Nilsson, C., Johansson, M. E., & Xiong, S. (2011). Hydrologic effects on riparian vegetation in a boreal river: an experiment testing climate change predictions. *Global Change Biology, 17*(1), 254-267.

Sulla-Menashe, D., Friedl, M. A., & Woodcock, C. E. (2016). Sources of bias and variability in long-term Landsat time series over Canadian boreal forests. *Remote sensing of Environment, 177*, 206-219.

Teluguntla, P., Thenkabail, P. S., Oliphant, A., Xiong, J., Gumma, M. K., Congalton, R. G., . . . Huete, A. (2018). A 30-m landsat-derived cropland extent product of Australia and China using random forest machine learning algorithm on Google Earth Engine cloud computing platform. *ISPRS Journal of Photogrammetry and Remote Sensing, 144*, 325-340.

Tetteh, G. O., & Schönert, M. (2015). Automatic generation of water masks from rapideye images. *Journal of Geoscience and Environment Protection, 3*(10), 17-23.

Theil, H. (1950). A rank-invariant method of linear and polynomial regression analysis. *Indagationes mathematicae, 12*(85), 173.

Timoney, K. (2002). A dyin delta? A case study of a wetland paradigm. *Wetlands, 22*(2), 282-300.

Timoney, K. (2006). Landscape cover change in the Peace-Athabasca Delta, 1927–2001. *Wetlands, 26*(3), 765-778.

Timoney, K. (2008a). Factors influencing wetland plant communities during a flood-drawdown cycle in the Peace-Athabasca Delta, northern Alberta, Canada. *Wetlands, 28*(2), 450-463.

Timoney, K. (2008b). Rates of vegetation change in the Peace-Athabasca Delta. *Wetlands, 28*(2), 513-520.

Timoney, K., & Lee, P. (2016). Changes in the areal extents of the Athabasca River, Birch River, and Cree Creek Deltas, 1950–2014, Peace–Athabasca Delta, Canada. *Geomorphology, 258*, 95-107. doi:https://doi.org/10.1016/j.geomorph.2016.01.011

Timoney, K. P. (2009). Three centuries of change in the Peace–Athabasca Delta, Canada. *Climatic Change, 93*(3), 485-515.

Timoney, K. P. (2013). *The Peace-Athabasca Delta: portrait of a dynamic ecosystem*: University of Alberta.

Timoney, K. P. (2021). Flooding in the Peace-Athabasca Delta: climatic and hydrologic change and variation over the past 120 years. *Climatic Change, 169*(3), 1-26. doi:10.1007/s10584-021-03257-z

Timoney, K. P., & Argus, G. (2006). Willows, water regime, and recent cover change in the Peace–Athabasca Delta. *Ecoscience, 13*(3), 308-317.

Töyrä, J., Pietroniro, A., Hopkinson, C., & Kalbfleisch, W. (2003). Assessment of airborne scanning laser altimetry (lidar) in a deltaic wetland environment. *Canadian Journal of Remote Sensing, 29*(6), 718-728.

Töyrä, J., Pietroniro, A., Martz, L. W., & Prowse, T. D. (2002). A multi-sensor approach to wetland flood monitoring. *Hydrological Processes, 16*(8), 1569-1581.

Tran, T. V., Tran, D. X., Myint, S. W., Huang, C.-y., Pham, H. V., Luu, T. H., & Vo, T. M. T. (2019). Examining spatiotemporal salinity dynamics in the Mekong River Delta using Landsat time series imagery and a spatial regression approach. *Science of The Total Environment, 687*, 1087-1097. doi:https://doi.org/10.1016/j.scitotenv.2019.06.056

Tucker, C. J. (1979). Red and photographic infrared linear combinations for monitoring vegetation. *Remote sensing of Environment, 8*(2), 127-150.

Tymstra, C., Stocks, B. J., Cai, X., & Flannigan, M. D. (2020). Wildfire management in Canada: Review, challenges and opportunities. *Progress in Disaster Science, 5*, 100045. doi:https://doi.org/10.1016/j.pdisas.2019.100045

USGS. (2021). Landsat Collection 2. Retrieved from https://pubs.usgs.gov/fs/2021/3002/fs20213002.pdf

Valk, A. G. v. d. (2005). Water-level fluctuations in North American prairie wetlands. *Hydrobiologia, 539*, 171-188.

Vervuren, P., Blom, C., & De Kroon, H. (2003). Extreme flooding events on the Rhine and the survival and distribution of riparian plant species. *Journal of Ecology, 91*(1), 135-146.

Vicente-Serrano, S. M., Martín-Hernández, N., Reig, F., Azorin-Molina, C., Zabalza, J., Beguería, S., . . . García, M. (2020). Vegetation greening in Spain detected from long term data (1981–2015). *International Journal of Remote Sensing, 41*(5), 1709-1740. doi:10.1080/01431161.2019.1674460

Vinayaraj, P., Oishi, Y., & Nakamura, R. (2018). *Development of an automatic dynamic global water mask using landsat-8 images.* Paper presented at the IGARSS 2018-2018 IEEE International Geoscience and Remote Sensing Symposium.

Wang, B., Smith, L. C., Gleason, C., Kyzivat, E. D., Fayne, J. V., Harlan, M. E., . . . Peters, D. L. (2023). Athabasca River Avulsion Underway in the Peace-Athabasca Delta, Canada. *Water Resources Research, 59*(3), e2022WR034114. doi:https://doi.org/10.1029/2022WR034114

Wang, J. A., & Friedl, M. A. (2019). The role of land cover change in Arctic-Boreal greening and browning trends. *Environmental Research Letters, 14*(12), 125007.

Wang, J. A., Sulla-Menashe, D., Woodcock, C. E., Sonnentag, O., Keeling, R. F., & Friedl, M. A. (2020). Extensive land cover change across Arctic–Boreal Northwestern North America from disturbance and climate forcing. *Global Change Biology, 26*(2), 807-822.

Wang, Y., & Fang, H. (2020). Estimation of LAI with the LiDAR Technology: A Review. *Remote Sensing, 12*(20), 3457. Retrieved from https://www.mdpi.com/2072-4292/12/20/3457

Ward, D. P., Petty, A., Setterfield, S. A., Douglas, M. M., Ferdinands, K., Hamilton, S. K., & Phinn, S. (2014). Floodplain inundation and vegetation dynamics in the Alligator Rivers region (Kakadu) of northern Australia assessed using optical and radar remote sensing. *Remote sensing of Environment, 147*, 43-55. doi:https://doi.org/10.1016/j.rse.2014.02.009

Warner, B. G., & Rubec, C. D. (1997). *The Canadian wetlands classification system*: Wetlands Research Centre, University of Waterloo.

Webster, K. L., Beall, F. D., Creed, I. F., & Kreutzweiser, D. P. (2015). Impacts and prognosis of natural resource development on water and wetlands in Canada's boreal zone. *Environmental Reviews, 23*(1), 78-131. doi:10.1139/er-2014-0063

Wehr, A., & Lohr, U. (1999). Airborne laser scanning—an introduction and overview. *ISPRS Journal of Photogrammetry and Remote Sensing, 54*(2), 68-82. doi:https://doi.org/10.1016/S0924-2716(99)00011-8

Wein, E. E., & Wein, R. W. (1995). Predictions of global warming influences on aboriginal food-use patterns in Northwestern Canada. *Northern Review*(14).

White, J. C., Wulder, M., Hobart, G., Luther, J., Hermosilla, T., Griffiths, P., . . . Dyk, A. (2014). Pixel-based image compositing for large-area dense time series applications and science. *Canadian Journal of Remote Sensing, 40*(3), 192-212.

White, L., Brisco, B., Dabboor, M., Schmitt, A., & Pratt, A. (2015). A Collection of SAR Methodologies for Monitoring Wetlands. *Remote Sensing, 7*(6), 7615-7645. Retrieved from https://www.mdpi.com/2072-4292/7/6/7615

Wickware, G. M., & Howarth, P. J. (1981). Change detection in the Peace—Athabasca delta using digital Landsat data. *Remote sensing of Environment, 11*, 9-25.

Wickware, M. G. (1979). *Wetland classification and environmental monitoring in the Peace-Athabasca Delta using Landsat digital data.*

Wolfe, B. B., Hall, R. I., Last, W. M., Edwards, T. W., English, M. C., Karst-Riddoch, T. L., . . . Palmini, R. (2006a). Reconstruction of multi-century flood histories from oxbow lake sediments, Peace-Athabasca Delta, Canada. *Hydrological Processes: An International Journal, 20*(19), 4131-4153.

Wolfe, B. B., Hall, R. I., Last, W. M., Edwards, T. W. D., English, M. C., Karst-Riddoch, T. L., . . . Palmini, R. (2006b). Reconstruction of multi-century flood histories from oxbow lake sediments, Peace-Athabasca Delta, Canada. *Hydrological Processes, 20*(19), 4131-4153. doi:10.1002/hyp.6423

Wulder, M. A., Li, Z., Campbell, E. M., White, J. C., Hobart, G., Hermosilla, T., & Coops, N. C. (2018). A National Assessment of Wetland Status and Trends for Canada's Forested Ecosystems Using 33 Years of Earth Observation Satellite Data. *Remote Sensing, 10*(10), 1623. Retrieved from https://www.mdpi.com/2072-4292/10/10/1623

Xiao, W., Deng, X., He, T., & Chen, W. (2020). Mapping Annual Land Disturbance and Reclamation in a Surface Coal Mining Region Using Google Earth Engine and the LandTrendr Algorithm: A Case Study of the Shengli Coalfield in Inner Mongolia, China. *Remote Sensing, 12*(10), 1612. Retrieved from https://www.mdpi.com/2072-4292/12/10/1612

Xu, H. (2006). Modification of normalised difference water index (NDWI) to enhance open water features in remotely sensed imagery. *International Journal of Remote Sensing, 27*(14), 3025-3033.

Xu, R. (2021). Mapping rural settlements from landsat and sentinel time series by integrating pixel- and object-based methods. *Land, 10*(3), 244.

Yang, Y., Wu, T., Wang, S., Li, J., & Muhanmmad, F. (2019). The NDVI-CV method for mapping evergreen trees in complex urban areas using reconstructed landsat 8 time-series data. *Forests, 10*(2), 139.

Yoder, B. J., & Waring, R. H. (1994). The normalized difference vegetation index of small Douglas-fir canopies with varying chlorophyll concentrations. *Remote sensing of Environment, 49*(1), 81-91. doi:https://doi.org/10.1016/0034-4257(94)90061-2

Zhao, Q., Ma, X., Yao, W., Liu, Y., & Yao, Y. (2020). Anomaly Variation of Vegetation and Its Influencing Factors in Mainland China During ENSO Period. *IEEE Access, 8*, 721-734. doi:10.1109/ACCESS.2019.2962787

Zhou, G., & Yin, X. (2014). Relationship of cotton nitrogen and yield with Normalized Difference Vegetation Index and plant height. *Nutrient Cycling in Agroecosystems, 100*(2), 147-160. doi:10.1007/s10705-014-9640-y

Appendix

Section A1- Landsat-Derived NDVI vs. Lidar-Derived Canopy Height

Robinson et al. (2017) used the mean pixel approach to create a time series NDVI for the United States. However, Flood (2013) suggested that simple approaches such as the mean of all observations are likely not ideal due to outliers from atmospheric effects and bi-directional reflectance distribution function adjustments, as well as imperfections in cloud/shadow masking procedures. The univariate median represents a potential improvement over the mean due to its resistance to outliers (Oliphant et al., 2019; Ruefenacht, 2016). The Medoid approach, which selects the point that minimizes the sum of the distances to all other points, has the outlier resistance characteristics of the univariate median and can be applied to multi-variate data such as reflective bands of Landsat (Flood, 2013). In the Maximum NDVI method, the maximum NDVI for all scenes is determined and then the pixel with all its bands from the corresponding scene is included in the final composite (Ruefenacht, 2016). Flood (2013) suggests that using the maximum NDVI provides a time series that favors vegetation conditions with high greenness, and this might not be appropriate for all applications; e.g. this approach has the potential to reduce the contrast between trees and grasslands. However, several studies have successfully used this approach (Erasmi et al., 2021; Huang et al., 2017; Xu, 2021; Yang et al., 2019). Another approach uses a score-based system of four scores for each pixel, including sensor score, day-of-year score, cloud/cloud shadow or distance to cloud score, and opacity score (Griffiths et al., 2013). The total scores for each pixel are summed, and the image composite chooses the pixel with the highest score (White et al., 2014). To the best of the authors' knowledge, the only studies that have thus far compared the relative performance of the above-noted approaches are (Ruefenacht, 2016) and (Qiu et al., 2023). Qiu et al. (2023) indicate that each composite algorithm possesses unique characteristics, and no single algorithm can surpass all others in terms of performance across all locations and composite periods. Therefore, the most appropriate best available pixel compositing algorithm is likely somewhat location- and application-dependent, thus requiring some initial investigative work to choose the approach most suited to the study.

Trend analysis using Landsat imagery can be subject to various sources of bias, including atmospheric effects radiometric differences between sensors, and different view angles (Sulla-Menashe et al., 2016). In this study, the impact of biases was minimized by utilizing Landsat Collection 2 data. In this study, various methods of compositing were employed. To assess the effectiveness of composite approaches because there were no coincident measurements of spectral response for different land cover types, composites were visually compared for outliers/noises and similarity.

In contrast to numerous applications of the BAP approach (Bolton et al., 2020; Qiu et al., 2023), this study encountered challenges producing high-quality composites using the BAP approach, particularly over marshes, mudflats, and shallow open water and rivers/streams where this approached resulted in circular artifacts. This may be attributed to the limited availability of high-quality images over the study area or differences between sensors that persist in collection 2. Qiu et al. (2023) reported that although the BAP approach demonstrated superior performance in regions with low cloud cover, it produced spatial artifacts in areas with moderate to high cloud cover due to the selection of observations from different dates.

The Mean approach created a relatively smooth result with lower localized variability in NDVI but with many blurred areas (Figure A1a). Median and Medoid methods had similar results, but Medoid resulted in a lower quality where certain pixels exhibited significant differences from their neighboring pixels (Figure A1b and A1c). The max NDVI composite approach led highest NDVI values approaching 0.99. Moreover, this approach resulted in a pixelated image, many null pixels, and slightly different NDVI values between two Landsat scenes, resulting in a line or breakpoint between them (Figure A1d). Based on this comparison, we determined that the Median composite approach was an optimal compositing method because fine-scale features can be identified while reducing the influence of high spectral variance pixels found with other compositing procedures. The efficiency of this compositing approach was also demonstrated in a study by Ruefenacht (2016), where the Median approach was compared with the Max NDVI approach. This was used to create the NDVI and MNDWI time series from 2000 to 2018.

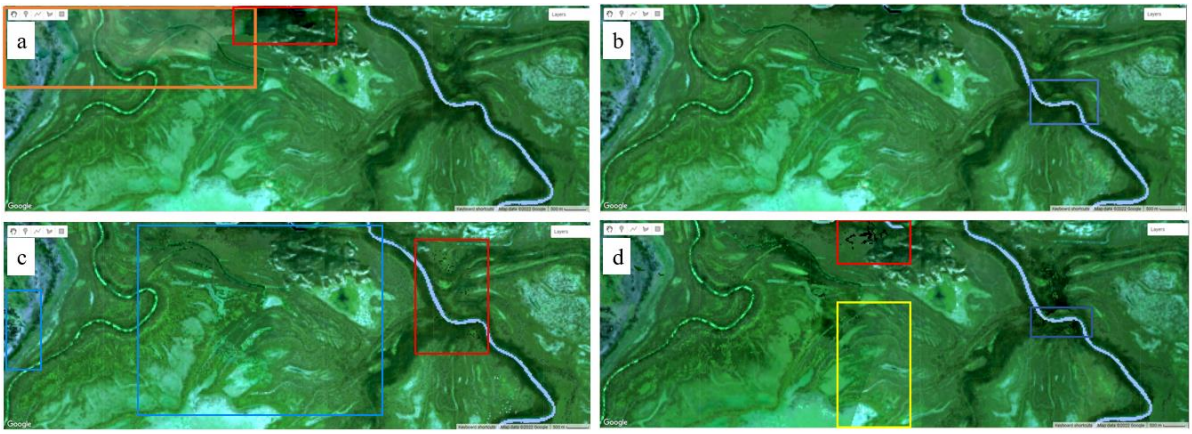

Figure A1. Close-up comparison between composite approaches, a) Mean, b) Median, c) Medoid, and d) MaxNDVI (RGB 234, Landsat 8, 2018). The orange box outlines blurred pixels. The blue box outlines slightly different pixel values than nearby pixels. The red box outlines null pixels. The yellow box outlines distinct zonal boundaries between scenes. Medoid and MaxNDVI are highly pixelated here.

Section A2- Statistical Comparison between NDVI and CHM

As the p-values in the normality test (Shapiro-Wilk) are zero (Table A1), we can conclude that the data (CHM versus NDVI) does not follow a normal distribution.

Table A1. Tests of Normality.

	Kolmogorov-Smirnov[a]			Shapiro-Wilk		
	Statistic	df	Sig.	Statistic	df	Sig.
CHM	.18	1883	.000	.79	1883	.000
NDVI	.05	1883	.000	.97	1883	.000

a. Lilliefors Significance Correction

To conduct residual analysis, we plotted the residuals against the fitted values. As shown in Figure A2, we observed a random pattern, suggesting a good fit for the linear log model.

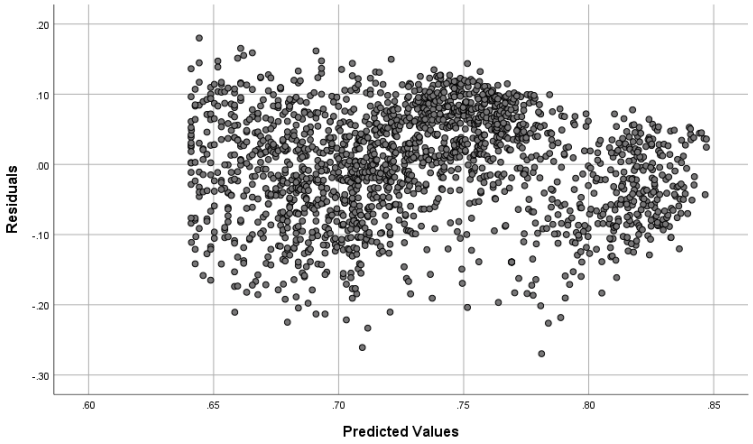

Figure A2. The residual analysis.

Section A3- NDVI and MNDWI Trends

Figures A3 to A5 show NDVI and MNDWI trends over the study period for the lidar survey area: 'B', 'C', and 'D'. Overall, all NDVI trends using the various statistical methods displayed similar change patterns over time.

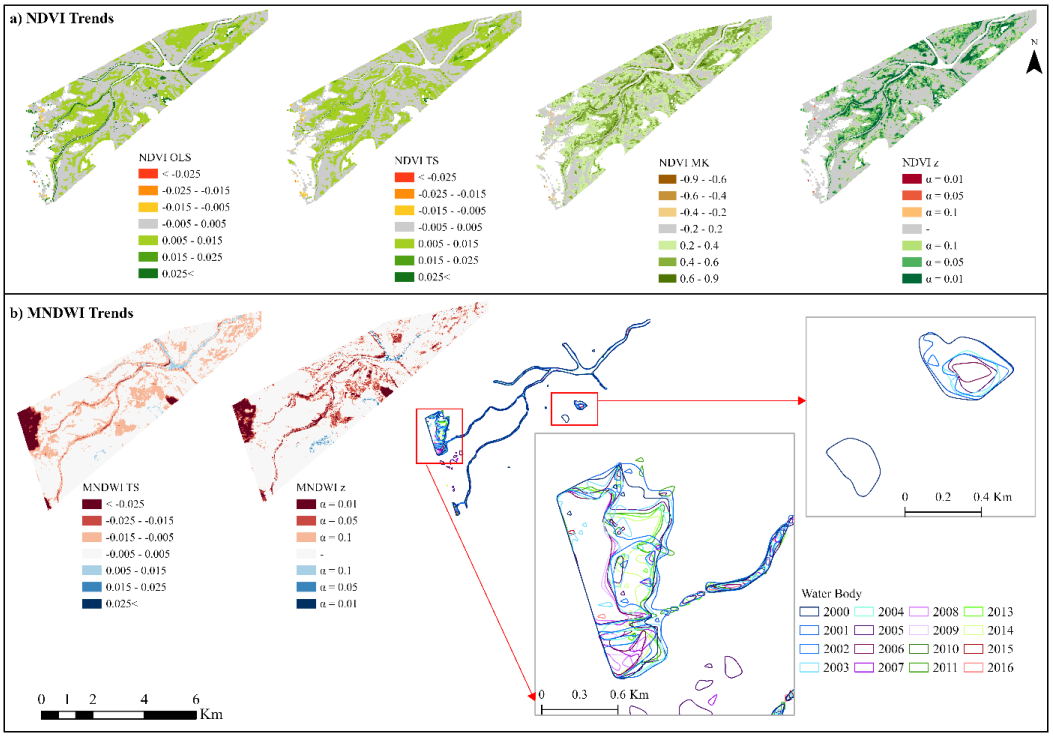

Figure A3. a) NDVI trends; b) MNDWI trends over survey area B.

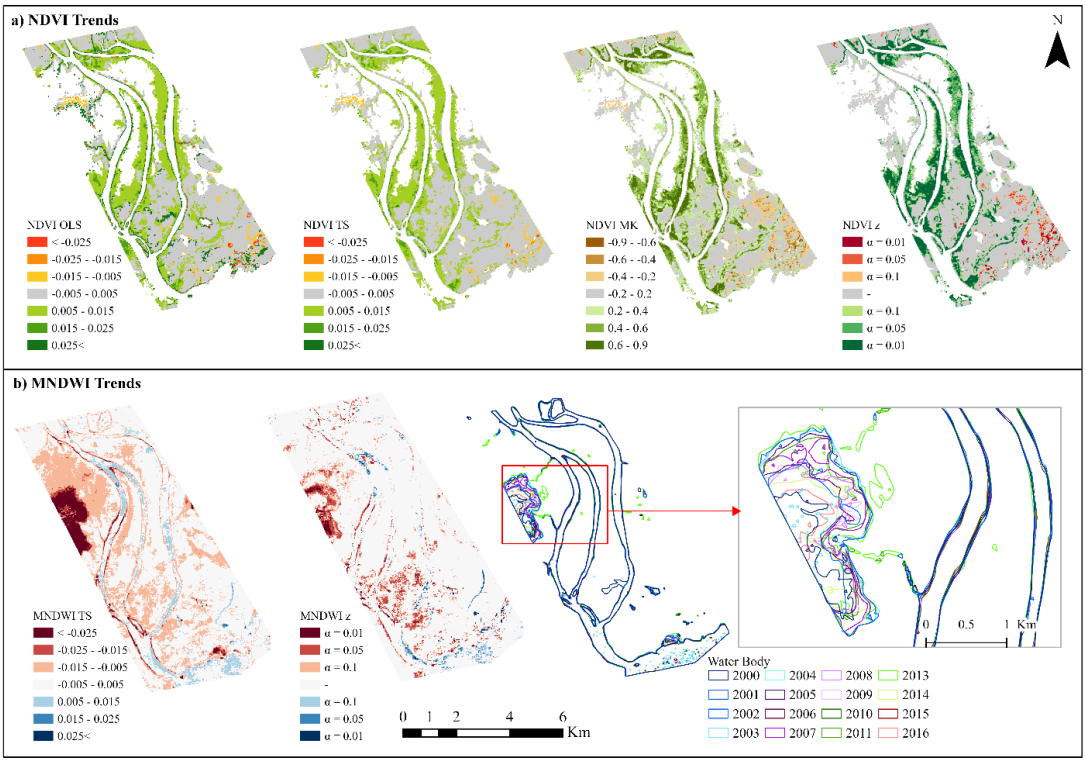

Figure A4. a) NDVI trends; b) MNDWI trends over survey area C.

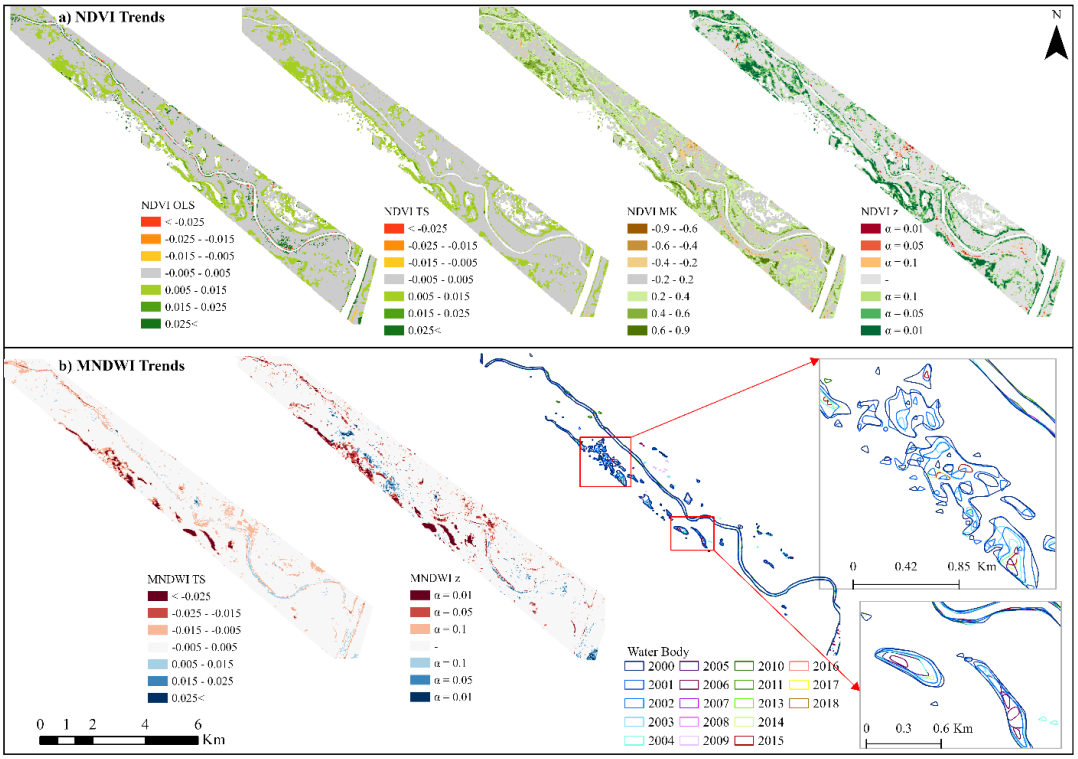

Figure A5. a) NDVI trends; b) MNDWI trends over survey area D.